

MICROCOPY RESOLUTION TEST CHART
NATIONAL BUREAU OF STANDARDS-1963-A

000 92 6 08

(11)

LEVEL

NUSC Technical Report 8807



Computer Models of Underwater Acoustic Propagation

Frederick R. DiNapoli
Roy L. Deavenport
Special Projects Department

ADA 082380

DTIC
ELECTE
S MAR 27 1980 D

21 January 1980

A
NUSC

Naval Underwater Systems Center
Newport, Rhode Island • New London, Connecticut

Approved for public release; distribution unlimited.

DDC FILE COPY

Preface

This report was prepared under NUSC Project No. 710V11 (L1) for W. A. Von Winkle (Code 10), Principal Investigator, F. R. DiNapoli (Code 312) and T. J. Deavenport (Code 312).

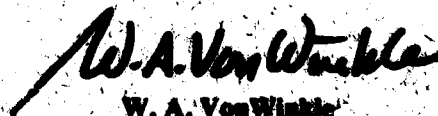
The Technical Reviewer for this report was J. S. Papadakis (Code 312).

A condensation of this work appears as chapter III in the Springer-Verlag book, "Ocean Acoustics," for which J. DeSanto was a contributor and editor. The authors wish to thank DeSanto for the opportunity to collaborate with him on this study and also for the stimulating discussions on the technical aspects of the study.

The authors were fortunate to have the opportunity to discuss this study with many of the people whose work was summarized here. It is a pleasure to acknowledge the time and effort provided by D. Lee, D. Wood, J. Papadakis, H. Weinberg, G. Leibiger, R. Lauer, D. Stickler, and C. Bartberger. Special mention is due to J. Kalinowski, who contributed the information on finite elements and applied that technique to underwater acoustic propagation.

The authors also owe a special debt of gratitude to W. Von Winkle for the confidence he expressed by supporting this effort over a long period of time, and to W. R. Schumacher for providing an atmosphere conducive to the successful completion of this study.

REVIEWED AND APPROVED: 2 January 1980



**W. A. Von Winkle
Associate Technical Director
for Technology**

The authors of this report are located at the New London Laboratory,
Naval Underwater Systems Center, New London, Connecticut 06320

20. (Cont'd)

dependent categories. Range-independent models assume that the ocean is cylindrically symmetrical, that the speed of sound is an arbitrary function of only the depth (z) coordinate, and that all boundaries are parallel with the range (r) coordinate. These models, discussed in section 1, are in a fairly complete state of development, as evidenced by the concern with reducing computer execution time and memory without significantly sacrificing accuracy. The range-dependent models, discussed in section 2, allow the speed of sound to be an arbitrary function of either two or three spatial coordinates, and boundaries need not be parallel. Their state of development is not as complete.

Accession For	
NTIS Grant	<input checked="" type="checkbox"/>
DDC TAP	<input type="checkbox"/>
Unannounced	<input type="checkbox"/>
Justification	<input type="checkbox"/>
By _____	
Distribution /	
Availability Codes	
Dist	Avail and/or special
A	

COMPUTER MODELS OF UNDERWATER ACOUSTIC PROPAGATION

FOREWORD

This report summarizes those models of propagation loss in the field of underwater acoustics that have been converted into an automated computer code capable of being executed by someone other than the originator for a wide variety of problems. No single model currently exists that is adequate for all applications. This is not surprising considering the diversity of the ocean environment and its boundaries, and the concomitant fact that the acoustic frequencies of interest range from less than 10 Hz to greater than 100 kHz. As a result, a large number of models, each with its own domain of validity (in many cases difficult to define precisely), has been developed. This evolutionary process has been strongly influenced by a combination of three major factors:

1. Capabilities of sonar equipment
2. Available experimental/environmental data
3. Advances in computer technology.

The trend in sonar equipment has been from predominantly high frequency (kHz), short range (less than a convergence zone, CZ) sonars, which are largely *energy* detectors, to lower frequency, longer range, physically larger sonars with signal processing schemes other than energy detectors. The corresponding model development went from semi-empirical/semi-analytical, requiring an extensive propagation loss (*total energy*) data base, to classical ray theory, and then to ray theory with corrections and wave solutions. The theory underlying these latter models was, for the most part, available earlier. However, the transformation into specific results could not take place until sufficient advances in computer technology occurred. Given this perspective and the necessity for restricting the number of models to be discussed (the sheer number of which makes an exhaustive summary impossible within the scope of these pages), it was decided to limit consideration to those models which purport to be solutions of the wave equation. Fundamentally, these models consider the ocean to be a deterministic environment for which the speed of sound is only a function of the spatial coordinates. Nondeterministic effects, if accounted for at all, are included in an ad hoc fashion following the ascertainment of the deterministic propagation loss result. Development of a model for the more general problem is required, as evidenced by the trends in future sonar designs, and is in progress. However, this effort has not reached the point where *hands off* computer codes are available. In part this is because experimental/environmental data are unavailable and the need for larger and faster computers.

The models to be discussed can be further segregated into range-independent and range-dependent categories. Range-independent models assume that the ocean is cylindrically symmetrical, that the speed of sound is an arbitrary function of only the depth (z) coordinate, and that all boundaries are parallel with the range (r) coordinate. These models, discussed in section 1, are in a fairly complete state of development, as evidenced by the concern with reducing computer execution time and memory without significantly sacrificing accuracy. The range-dependent models, discussed in section 2, allow the speed of sound to be an arbitrary function of either 2 or 3 spatial coordinates, and boundaries need not be parallel. Their state of development is not as complete.

In general, the models which fall within these two subdivisions consider the ocean surface to be a pressure release boundary. This is a result of the large mismatch in characteristic impedance between water and air. The water column itself is treated as an ideal fluid incapable of supporting sheer stresses and having a uniform or, at most, piecewise constant density variation. For some models, it is necessary to specify sound speed, attenuation, and density values within the bottom. In these instances, the bottom is treated in a manner analogous to that of the water column, i.e., as an ideal fluid. Otherwise, the effect of the ocean bottom is accounted for by ascribing to it a reflection loss versus grazing angle. The treatment given both boundaries is, of course, approximate. In the case of the ocean bottom, a clear point of departure is delineated between underwater acoustics and seismic propagation. Nonetheless, the approximations have been found to be generally adequate when comparing theoretical and experimental propagation loss results. This is perhaps related to the second point of departure, which is the concern with the infinite CW propagation loss (*total energy*) versus range in underwater acoustics, as opposed to a detailed analysis of waveform structure versus time in the seismic field.

TABLE OF CONTENTS

	Page
FOREWORD	i
LIST OF ILLUSTRATIONS	iv
LIST OF TABLES	iv
1. RANGE-INDEPENDENT MODELS	1
Introduction	1
Formal Solution	3
Direct Numerical Integration Fast Field Program (FFP)	16
Normal Modes (and Branch Line Integral) Models Stickler (EJP Cuts), Bartberger (Pekeris Cuts)	20
Depth Dependent Green's Function (Traveling Wave Formulation)	46
Multipath Expansion Models	57
Connection Between Modes and Rays	66
Quantitative Model Assessment	70
Waveform Prediction Models	78
2. RANGE-DEPENDENT MODELS	87
Introduction	87
Split Step Algorithm for Parabolic Equation	87
Parabolic Decomposition Method	90
Finite Differences	91
Range-Dependent Normal Mode Theory	94
Range-Dependent Ray Theory Models	95
Finite Element Approach	95
Transparent Boundary Simulation Techniques	100
Solid Domain Boundaries	101
Fluid Domain Boundaries	103
Combined Solid-Fluid Domain Boundaries	104
Fluid-Finite Elements	107
APPENDIX A -- SPECIAL CASES FOR $G(z, z_0)$ NOT CONSIDERED BY EQUATION (36)	A-1
APPENDIX B -- AN ALTERNATIVE NUMERICAL EVALUATION SCHEME FOR BESSEL TRANSFORMS	B-1
REFERENCES	R-1

LIST OF ILLUSTRATIONS

Figure		Page
1	Range-Independent Flow Diagram of Theoretical Solutions.....	2
2	Range-Independent Environmental Description.....	3
3	Definition of α and β for EJP and Pekeris Branch Cuts.....	21
4	Definition of β_N for EJP Branch Cut.....	34
5	Definition of β for Pekeris Branch Cut.....	34
6	Typical Deep Water Profile.....	61
7	Vector Mode Plot at 12.6 kyd.....	66
8	Mode Contribution to Propagation Loss.....	67
9	Factors Influencing Model Selection.....	71
10	Summary of Model Assessment Methodology.....	72
11	Scenario for Accuracy Assessment.....	74
12	Listing of Models Assessed.....	74
13	Standard Before and After Smoothing.....	75
14	Raymode X Before and After Smoothing.....	76
15	Difference Curves.....	77
16	Typical Arctic Profile.....	84
17	Impulse Response.....	85
18	Dispersion of First Mode.....	86
19	Definition of Interior Domain and Boundary.....	98
20	Ocean-Bottom Interaction Finite Element Method.....	102
21	Finite Element Amplitude-Phase Contours.....	106

LIST OF TABLES

Table		Page
1	Means and Standard Deviations of Differences Between the FFP (CW) and Model Results: Case II.....	79
2	Averages of Means and Standard Deviations Over All Cases and Range Intervals (Standard of Comparison: FFP Model Results).....	80
3	Model Running Times.....	81
4	Words of Computer Storage Required.....	82

COMPUTER MODELS OF UNDERWATER ACOUSTIC PROPAGATION

1. Range-Independent Models

INTRODUCTION

Studies of wave motion in a plane stratified medium are undertaken in many diverse fields. The techniques developed in one field, however, are often applicable to others. This is not surprising since the waves, whether electromagnetic, acoustic, seismic, etc., have common mathematical denominators. Of particular interest are the phenomena associated with wave propagation in a medium whose characteristic properties are not uniform. Although such phenomena are, in general, functions of all spatial coordinates and times, the case of arbitrary variation in only one spatial direction is a sufficiently accurate assumption for many applications.

It is rather easy to express the formal solution for the field produced by a point monochromatic source embedded in such a medium as a Fourier-Bessel transform¹ or, equivalently, a Green's function convolution.² However, the explicit general form for the kernel, which results when the variation within each layer is arbitrary and, in addition, when the source and field point depths are also arbitrary, has not appeared in the literature to date. Previous treatments^{3,4} are concerned with either a specific index of refraction variation or do not permit the source and field points to be in different layers. Wait,⁵ for example, uses the Fourier-Bessel method to generalize the Sommerfeld problem to the case of m -homogeneous layers. Harkrider⁶ and Kutschale⁷ have also given integral solutions for this case. Felsen and Marcuvitz² give an excellent account of the Green's function method for arbitrary depth variation within each layer. However, their explicit results hold only when the source and field points are within the same layer.

The formal Green's function integral to the reduced wave equation in cylindrical coordinates for an arbitrary index of refraction and source and receiver depths is given below. The formalism given pertains to the acoustic case but can be used to describe other types of wave propagation with the appropriate change of variables describing the characteristic properties of the medium. The integrand is defined as a product of a range r -dependent Bessel function and a depth, z -dependent Green's function. Since the index of refraction is independent of range, the derivation of the range-dependent Bessel function is straightforward. The result for the depth dependent Green's function is rather complicated owing to the piecewise nature of the depth dependence of the index of refraction.

The available models for computing the propagation loss versus range in such an environment can be grouped into five major categories dependent upon the method used for solving the integral:

1. Direct Numerical Integration
2. Residue (Normal Mode) Theory
3. Multipath Expansion
4. Ray Theory with Corrections
5. Classical Ray Theory

This is shown schematically in figure 1. Within each group, one or two particular models have been identified as being representative. These models are discussed in some detail to provide a familiarity with the overall features and shortcomings of all models falling within one category as opposed to those in another. It is also possible to quantitatively assess the accuracy of the models of this section. In addition, a description of the methodology used to obtain the results is provided. The same convention and notation for mathematical functions have been used throughout, rather than adopting those utilized by the originators. Thus, depth (z) is always taken to be measured positively downwards from the ocean surface, and the harmonic function, $e^{-i\omega t}$, has been uniformly suppressed.

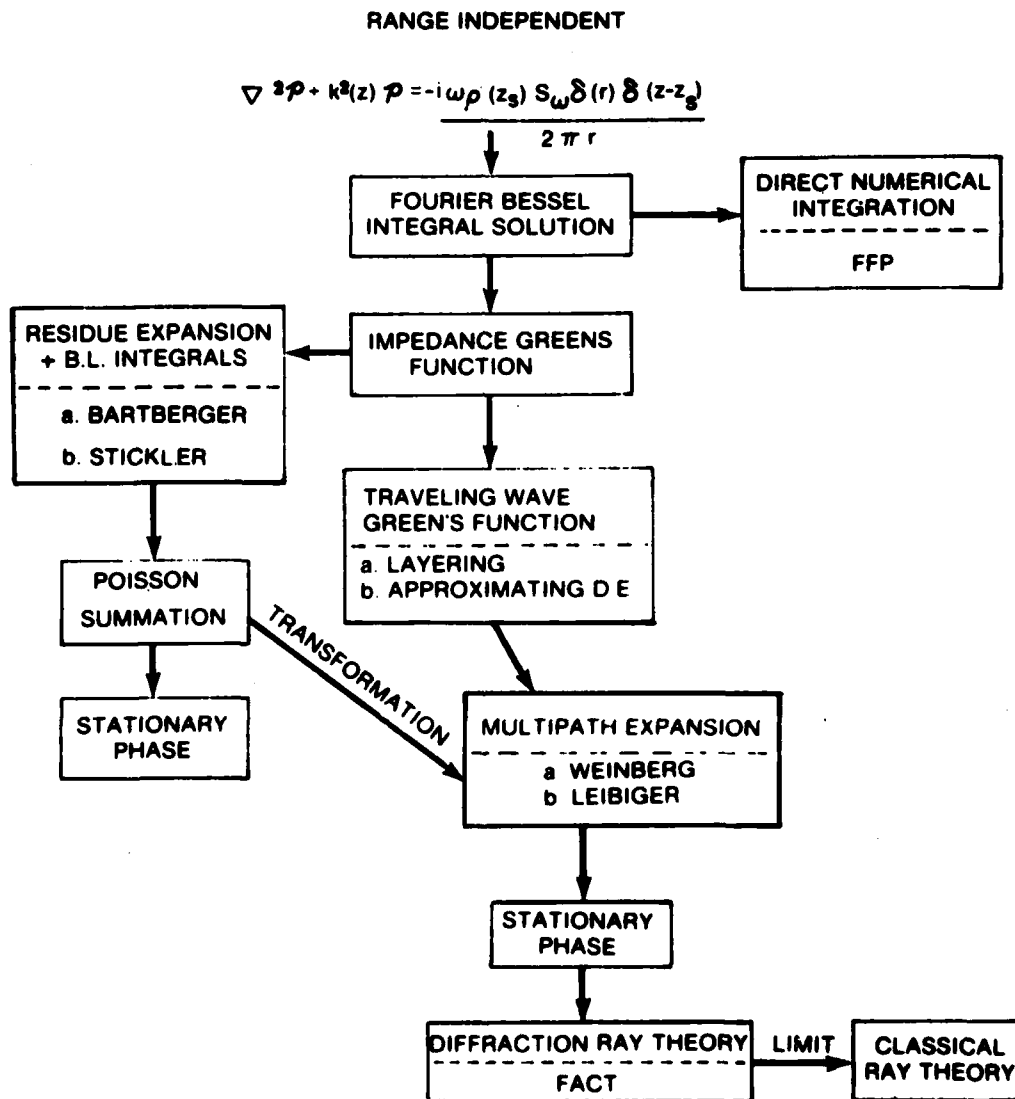


Figure 1. Range-Independent Flow Diagram of Theoretical Solutions

FORMAL SOLUTION

A given stratified medium is approximated by $N - 1$ inhomogeneous layers sandwiched between two homogeneous half spaces, as shown in figure 2. A point source of harmonic waves (time factor of $\exp(-i\omega t)$) has been suppressed is located at $(0, z_s)$ in the LS^{th} layer, where $0 \leq LS \leq N$. The field point is located at (r, z) in the LR^{th} layer, where $0 \leq LR \leq N$. It is assumed that $z = z \geq z_s$ when $z < z_s$, reciprocity is used.

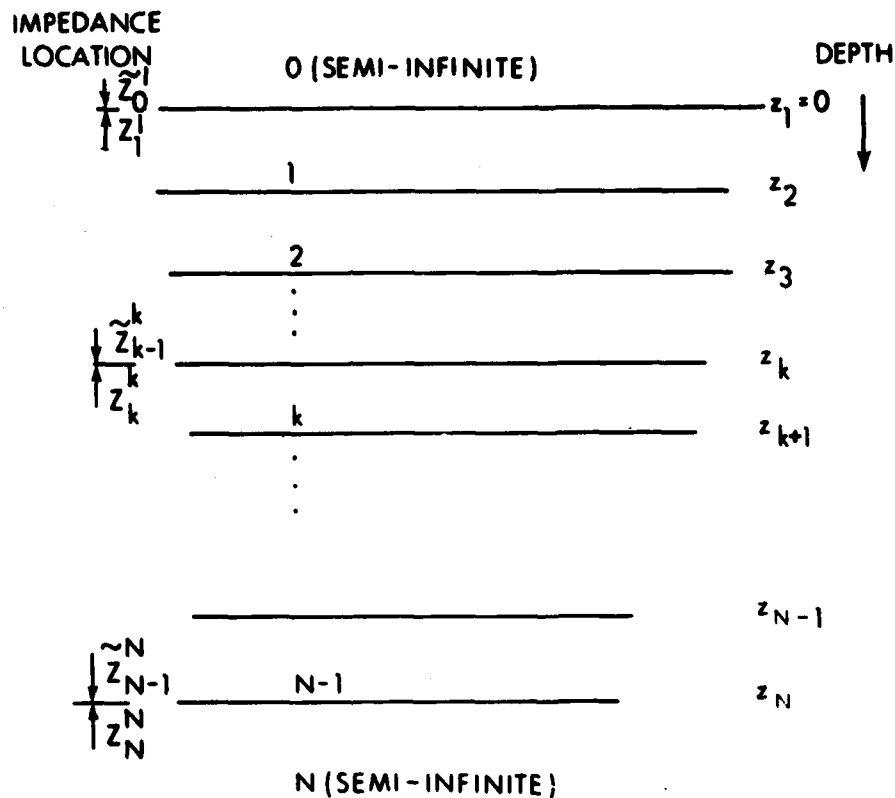


Figure 2. Range-Independent Environmental Description

The Helmholtz reduced wave equation for a point source located at \bar{r}_s in an inhomogeneous medium is given by

$$\nabla^2 \hat{G} + k_{\text{eff}}^2(z) \hat{G} = -1_{\omega p}^{1/2}(z_s) S_{\omega} \delta(\bar{r} - \bar{r}_s). \quad (1)$$

The effective wavenumber $k_{\text{eff}}(z)$ is assumed to vary piecewise with z . It is defined in terms of the usual wavenumber $k(z) [= \omega/\text{sound speed variation } c(z)]$ according to

$$k_{\text{eff}}^2(z) = k^2(z) - \sqrt{\rho(z)} \frac{d^2}{dz^2} \left(\frac{1}{\sqrt{\rho(z)}} \right), \quad (2)$$

where, for acoustics, $\rho(z)$ is the density. In electromagnetics, $\rho(z)$ may be either the dielectric parameter $\epsilon(z)$ or the permeability $\mu(z)$. In seismology $\rho(z)$ is the Lamé' parameter $\mu^{-1}(z)$ for SH waves.

By the simple transformation $\mathcal{P} = \sqrt{\rho} G$, equation (1) may be rewritten as

$$\nabla^2 \mathcal{P} + k^2(z) \mathcal{P} - \frac{\nabla \rho \cdot \nabla \mathcal{P}}{\rho} = -i\omega \rho(z_s) S_\omega \delta(\bar{r} - \bar{r}_s), \quad (3)$$

where \mathcal{P} represents the pressure (Green's function) at some point \bar{r} owing to the point source, and S_ω is the source strength.⁸ If cylindrical coordinates (r, θ, z) are assumed with azimuthal symmetry, the following equation is obtained:

$$\frac{1}{r} \frac{\partial}{\partial r} \left(r \frac{\partial \mathcal{P}}{\partial r} \right) + \rho(z) \frac{\partial}{\partial z} \left(\frac{1}{\rho(z)} \frac{\partial \mathcal{P}}{\partial z} \right) + k^2(z) \mathcal{P} = \frac{-i\omega \rho(z_s)}{2\pi r} S_\omega \delta(r) \delta(z - z_s). \quad (4)$$

The vertical depth coordinate z varies from $-\infty \leq z \leq +\infty$ and the range coordinate r varies from $0 < r < \infty$. The boundary conditions imposed on equation (4) are that

(1) \mathcal{P} must satisfy radiation conditions for

$$r \rightarrow \infty \text{ and } z \rightarrow \pm \infty \quad (5)$$

(2) $i\omega \rho \mathcal{P} / \partial z$ and \mathcal{P} must be continuous across all interfaces which are assumed to be parallel in the r direction.

Equation (4) can be separated as follows:

$$\left[\frac{d}{dr} \left(r \frac{d}{dr} \right) + \xi^2 r \right] G_r(r, \xi) = - \frac{\delta(r) S_\omega}{2\pi r} \quad (6)$$

$$\left[\rho(z) \frac{d}{dz} \left(\frac{1}{\rho(z)} \frac{d}{dz} \right) + k^2(z) - \xi^2 \right] G(z, z_s, \xi) = -i\omega \rho(z_s) \delta(z - z_s), \quad (7)$$

where ξ^2 is the separation constant. $G_r(r, \xi)$ represents a range-dependent Bessel function and $G(z, z_s; \xi)$ represents the depth dependent Green's function.

The integral solution to the above boundary value problem can be given either by the Fourier-Bessel transform first used by Lamb⁹ and Sommerfeld,¹⁰ or by the Green's function convolution first used by Marcuvitz,¹¹

$$\varphi(r, z, z_s) = \frac{S\omega}{2\pi} \int_0^{\infty} G(z, z_s; \xi) J_0(\xi r) \xi d\xi \quad (8)$$

$$\varphi(r, z, z_s) = \frac{S\omega}{4\pi} \int_{-\infty}^{\infty} G(z, z_s; \xi) H_0^{(1)}(\xi r) \xi d\xi \quad (9)$$

Many of the features/shortcomings of proceeding down one path versus another in figure 1 are intimately related to the particular manner in which the depth dependent Green's function $G(z, z_s; \xi, \omega)$, appearing in the integral solution, is obtained and numerically evaluated. For these reasons, this function will be discussed first.

Depth Dependent Green's Function (Impedance Formulation)

In cylindrical coordinates with azimuthal symmetry, the depth dependent Green's function G must satisfy

$$\mathcal{L}(G) = \frac{d}{dz} \left(\frac{1}{i\omega\rho(z)} \frac{dG}{dz} \right) + q(z) G = -\delta(z - z_s) \quad (10)$$

where $q(z) = (k^2(z) - \xi^2)/(i\omega\rho(z))$, $k(z)$ the wavenumber and $\rho(z)$ the density. All the models of this section assume that the density varies in a piecewise constant fashion within any layer. The differential operator \mathcal{L} is defined as

$$\mathcal{L} = \frac{d}{dz} \left(\frac{1}{i\omega\rho(z)} \frac{d}{dz} \right) + q(z)$$

The solution of equation (10) is found by using the matrizant method¹²⁻¹⁵ to obtain two linearly independent functions, F and F , which satisfy equation (10) for $z < z_s$ and $z > z_s$ and the respective continuity conditions of G and $(dG/dz)/i\omega\rho(z)$, [$= G(z)/(i\omega\rho(z))$] in those regions. These functions represent the depth dependent pressure and are unique up to an arbitrary constant. This constant may be chosen in such a way that equation (10) is also satisfied at the source depth z_s .

The notation used in this section was instituted to conserve space. Although compact, it is unorthodox, and will be explained at points where it is felt that confusion might arise. The symbol U without a subscript or superscript is an abbreviation for the depth dependent particle velocity, $U = (dF/dz)/(i\omega\rho(z))$, for $z > z_s$. When U appears with a subscript and superscript, e.g., U_k^{k+1} , the subscript (k) refers to the layer in which F is defined. The superscript ($k+1$) refers to the depth (z_{k+1} , see figure 2) at which the operation is evaluated.

Thus

$$U_k^{k+1} = \frac{1}{i\omega\rho_k(z)} \frac{dF_k}{dz} \Big|_{z=z_{k+1}} \quad (11)$$

As such, U_k^{k+1} is the depth dependent particle velocity in the k^{th} layer evaluated at the depth z_{k+1} . If the subscript is absent and the superscript is z , then U^z is the depth dependent particle velocity in any layer ($LS \leq k \leq N-1$) evaluated at any depth ($z_s \leq z \leq z_N$). The layer in which the source is located will be designated by LS and the receiver layer by LR . The depth dependent particle velocity $\dot{U} = (dF/dz)/(i\omega\rho(z))$ for $z < z_s$ is abbreviated similarly. Functions other than the depth dependent particle velocity will appear with a subscript and superscript (e.g., γ_k^{k+1}). Unless otherwise stated, the meaning of the subscript and superscript, when they occur with these functions, will be the same as that explained above for U .

Terms of the form $(df/dz)/(i\omega\rho(z))$ and $(dg/dz)/(i\omega\rho(z))$, appearing frequently throughout the analysis, have been abbreviated as (Df) and (Dg) , respectively. Thus

$$(Df)_k^{k+1} = \frac{1}{i\omega\rho_k(z)} \frac{df_k}{dz} \Big|_{z=z_{k+1}} \quad (12)$$

Although closely related to the depth dependent particle velocity U_k^{k+1} , Df and Dg differ from it in that the function being operated on is not the total depth dependent pressure. Rather, it is one of the linearly independent (fundamental) solutions used to form F .

Matrizant Method

The equation for the depth dependent pressure F , $z > z_s$, may be written as

$$\mathcal{L}(F) = \frac{d}{dz} \left(\frac{1}{i\omega\rho(z)} \frac{dF}{dz} \right) + q(z) F = 0, \quad (13)$$

where F is subject to the continuity conditions on G and $G'/i\omega\rho$ for $z > z_s$. In the matrizant method, equation (13) is written as the following two equations,

$$U(z) = \frac{1}{i\omega\rho(z)} \frac{dF}{dz}, \quad (14)$$

$$\frac{dU}{dz} + q(z) F = 0$$

or, equivalently, as the matrix equation,

$$\frac{d\psi(z)}{dz} = A(z) \psi(z), \quad (15)$$

where

$$\psi(z) = \begin{pmatrix} F(z) \\ U(z) \end{pmatrix}; \quad A(z) = \begin{pmatrix} 0 & i\omega\rho(z) \\ -q(z) & 0 \end{pmatrix}.$$

The solution of equation (15) satisfying initial conditions at z_i is given by

$$\psi(z) = \bar{M}(z, z_i) \psi(z_i),$$

where $\bar{M}(z, z_i)$ is the fundamental matrix (matrizant, propagator, etc.) which satisfies the matrix equation,

$$\frac{d\bar{M}(z, z_i)}{dz} = A(z) \bar{M}(z, z_i), \quad (16)$$

such that $\bar{M}(z_i, z_i) = I$, where I is the identity matrix.

It is not possible to find a closed form solution, other than the Peano-Baker expansion, when the entire interval ($z_1 \leq z \leq z_N$) is considered as a single layer with $k(z)$ arbitrary. An alternative is to subdivide the total interval into $N - 1$ subintervals, as in figure 2. In this case, known closed form solutions to a second order differential equation in $\gamma^z (= \gamma(z))$ can usually be found associated with some $k_l(z)$, which constitutes a good approximation to the given $k(z)$ over the subinterval ($z_l \leq z \leq z_{l+1}$). If two fundamental solutions, $f(\gamma^z)$ and $g(\gamma^z)$ of $\mathcal{L}(\cdot) = 0$, can be expressed in terms of the known solutions, then the matrizant

$$\bar{M}(z, z_i) = M(\gamma^z, \gamma^{z_i}) = \begin{pmatrix} Q(\gamma^z, \gamma^{z_i}) & P(\gamma^z, \gamma^{z_i}) \\ S(\gamma^z, \gamma^{z_i}) & R(\gamma^z, \gamma^{z_i}) \end{pmatrix}, \quad (17)$$

over some arbitrary subinterval $[z, z_i]$ can be expressed as

$$M(\gamma^z, \gamma^{z_i}) = \begin{pmatrix} f(\gamma^z) & g(\gamma^z) \\ (Df)^z & (Dg)^z \end{pmatrix} \begin{pmatrix} A_1 & A_2 \\ B_1 & B_2 \end{pmatrix}. \quad (18)$$

From equations (15) - (17) Q and P are also solutions of $\mathcal{L}(\cdot) = 0$ with $i\omega q(z)S$ and $i\omega q(z)R$ as their respective derivatives. Explicitly from equation (16)

$$\frac{dQ}{dz} = i\omega q(z)S, \quad \frac{dP}{dz} = i\omega q(z)R$$

$$\frac{dS}{dz} = -q(z)Q, \quad \frac{dR}{dz} = -q(z)P.$$

The constants in equation (18) are determined uniquely from the condition $\bar{M}(z_i, z_i) = I$. Thus,

$$\begin{pmatrix} A_1 & A_2 \\ B_1 & B_2 \end{pmatrix} = \begin{pmatrix} f(\gamma^{z_1}) & g(\gamma^{z_1}) \\ (Df)^{z_1} & (Dg)^{z_1} \end{pmatrix}^{-1},$$

and, since f and g are linearly independent solutions of $\mathcal{L}(\cdot) = 0$, the quantity $(A_1 \cdot B_2 - B_1 \cdot A_2)$ cannot be zero; hence, Q and P are linearly independent solutions of $\mathcal{L}(\cdot) = 0$. The argument γ^z is used as a visual reminder that f and g are to be expressed in terms of known solutions to a differential equation in γ^z . Then the matrizant for the entire interval can be obtained by making use of its group property,

$$M(\gamma^z, \gamma^{z_1}) = M(\gamma^z, \gamma^{z_k}) M(\gamma^{z_k}, \gamma^{z_1}), \quad z, z_1, z_k \in [z_1, z_N], \quad (19)$$

and $M^{-1}(\gamma^z, \gamma^{z_1}) = M(\gamma^{z_1}, \gamma^z)$. From equation (18), the elements of equation (17) are found to be

$$\begin{aligned} Q(\gamma^z, \gamma^{z_1}) &= \frac{[f(\gamma^z)(Dg)^{z_1} - (Df)^{z_1}g(\gamma^z)]}{[f(\gamma^{z_1})(Dg)^{z_1} - (Df)^{z_1}g(\gamma^{z_1})]}, & Q(\gamma^{z_1}, \gamma^{z_1}) &= 1 \\ R(\gamma^z, \gamma^{z_1}) &= \frac{[-(Df)^z g(\gamma^{z_1}) + (Dg)^z f(\gamma^{z_1})]}{[f(\gamma^{z_1})(Dg)^{z_1} - (Df)^{z_1}g(\gamma^{z_1})]}, & R(\gamma^{z_1}, \gamma^{z_1}) &= 1 \\ S(\gamma^z, \gamma^{z_1}) &= \frac{[(Df)^z (Dg)^{z_1} - (Df)^{z_1} (Dg)^z]}{[f(\gamma^{z_1})(Dg)^{z_1} - (Df)^{z_1}g(\gamma^{z_1})]}, & S(\gamma^{z_1}, \gamma^{z_1}) &= 0 \\ P(\gamma^z, \gamma^{z_1}) &= \frac{[-f(\gamma^z)g(\gamma^{z_1}) + g(\gamma^z)f(\gamma^{z_1})]}{[f(\gamma^{z_1})(Dg)^{z_1} - (Df)^{z_1}g(\gamma^{z_1})]}, & P(\gamma^{z_1}, \gamma^{z_1}) &= 0 \end{aligned} \quad (20)$$

and additionally

$$\begin{aligned} R(\gamma^{z_1}, \gamma^z) &= Q(\gamma^z, \gamma^{z_1}) \\ P(\gamma^{z_1}, \gamma^z) &= -P(\gamma^z, \gamma^{z_1}) \\ S(\gamma^{z_1}, \gamma^z) &= -S(\gamma^z, \gamma^{z_1}) \end{aligned}$$

$$Q(\gamma^z, \gamma^{z_1}) R(\gamma^z, \gamma^{z_1}) - P(\gamma^z, \gamma^{z_1}) S(\gamma^z, \gamma^{z_1}) = 1.$$

The Green's function solution to equation (10) can now be constructed from the following two matrix equations:

$$\begin{pmatrix} G(z) \\ G'(z)/(\omega\rho(z)) \end{pmatrix} = \tilde{\psi}(z) = \begin{pmatrix} \tilde{F}(z) \\ \tilde{U}(z) \end{pmatrix} = M(\gamma^z, \gamma^{z_1}) \tilde{\psi}(z_1), \quad (z < z_1) \quad (21)$$

$$\begin{pmatrix} G(z) \\ G'(z)/(\omega\rho(z)) \end{pmatrix} = \psi(z) = \begin{pmatrix} F(z) \\ U(z) \end{pmatrix} = M(\gamma^z, \gamma^{z_N}) \psi(z_N), \quad (z > z_N),$$

where z_1 and z_N , respectively, represent the lower and upper boundaries (see figure 2) of two homogeneous half spaces between which the index of refraction is allowed to vary arbitrarily. Thus the initial values are known up to some multiplicative constants a_0 and a_N , respectively:

$$\tilde{F}(z) = a_0 e^{-i\beta_0(z-z_1)}, \quad \tilde{U}(z) = \frac{-\beta_0}{\omega\rho_0(z)} \tilde{F}(z) \quad z < z_1$$

$$F(z) = a_N e^{i\beta_N(z-z_N)}, \quad U(z) = \frac{\beta_N}{\omega\rho_N(z)} F(z) \quad z > z_N,$$

where β_0 and β_N are the z components of the wavenumbers k_0 and k_N , respectively, and $\text{Im}\{\beta_0\}$ and $\text{Im}\{\beta_N\} > 0$ satisfy the radiation condition.

In what follows, it is useful to rewrite $\tilde{\psi}(z)$ and $\psi(z)$ in terms of the impedance defined as

$$\tilde{Z}(z) = \frac{\tilde{F}(z)}{\tilde{U}(z)} \quad \text{and} \quad Z(z) = \frac{F(z)}{U(z)} \quad (22)$$

since the terminal impedances,

$$Z_N^N = \frac{\omega\rho_N}{\beta_N} \quad \text{and} \quad Z_0^1 = \frac{-\omega\rho_0}{\beta_0}, \quad (23)$$

are known uniquely. The convention adopted is that the superscript always refers to the depth at which z is evaluated. The subscript always refers to the layer where the evaluation takes place. The impedance anywhere above the source can then be written uniquely in terms of its terminal impedance Z_0^1 as

$$\begin{pmatrix} \tilde{Z}(z) \\ 1 \end{pmatrix} = \frac{M(\gamma^z, \gamma^1) \begin{pmatrix} \tilde{Z}_0^1 \\ 1 \end{pmatrix}}{\left\{ \tilde{Z}_0^1 S(\gamma^z, \gamma^1) + R(\gamma^z, \gamma^1) \right\}}$$

Similarly, impedance below the source may be expressed as

$$\begin{pmatrix} Z(z) \\ 1 \end{pmatrix} = \frac{M(\gamma^z, \gamma^N) \begin{pmatrix} Z_N^N \\ 1 \end{pmatrix}}{\left\{ Z_N^N S(\gamma^z, \gamma^N) + R(\gamma^z, \gamma^N) \right\}}$$

where the denominators (terms in braces) of the above equations are constants. The continuity of impedance at the boundaries z_1 and z_N is satisfied automatically from the imposed condition that $M(\gamma^{z_i}, \gamma^{z_i})$ be the identity matrix.

The solutions $\tilde{\psi}(z)$ and $\psi(z)$, written in terms of their respective terminal impedance and multiplicative constant, are

$$\tilde{\psi}(z) = \begin{pmatrix} \tilde{F}(z) \\ \tilde{U}(z) \end{pmatrix} = M(\gamma^z, \gamma^1) \begin{pmatrix} \tilde{Z}_0^1 \\ 1 \end{pmatrix} \tilde{U}_0^1 \quad z_1 \leq z < z_s ;$$

and below the source

$$\psi(z) = \begin{pmatrix} F(z) \\ U(z) \end{pmatrix} = M(\gamma^z, \gamma^N) \begin{pmatrix} Z_N^N \\ 1 \end{pmatrix} U_N^N \quad z_s < z \leq z_N .$$

The impedance within any layer, written in terms of the terminal impedance of that layer, is

$$\begin{aligned} \begin{pmatrix} \tilde{Z}_k^z \\ 1 \end{pmatrix} &= M_k(\gamma_k^z, \gamma_k^k) \begin{pmatrix} \tilde{Z}_{k-1}^k \\ 1 \end{pmatrix} / \left[\tilde{Z}_{k-1}^k S_k(\gamma_k^z, \gamma_k^k) + R_k(\gamma_k^z, \gamma_k^k) \right] \\ \begin{pmatrix} Z_k^z \\ 1 \end{pmatrix} &= M_k(\gamma_k^z, \gamma_k^{k+1}) \begin{pmatrix} Z_{k+1}^{k+1} \\ 1 \end{pmatrix} / \left[Z_{k+1}^{k+1} S_k(\gamma_k^z, \gamma_k^{k+1}) + R_k(\gamma_k^z, \gamma_k^{k+1}) \right] \end{aligned} \quad (24)$$

$$1 \leq k \leq N,$$

$$z_k \leq z \leq z_{k+1} .$$

Since continuity of impedance is assured, they may also be expressed explicitly in terms of the impedances of the half spaces according to

$$\begin{pmatrix} \bar{z}_k^z \\ \bar{z}_k \\ 1 \end{pmatrix} = \frac{M_k(\gamma_k^z, \gamma_k^k) \left[\prod_{p=k-1}^1 M_p(b, a) \right] \begin{pmatrix} \bar{z}_1 \\ 0 \\ 1 \end{pmatrix}}{\left[\bar{z}_{k-1}^k S_k(\gamma_k^z, \gamma_k^k) + R_k(\gamma_k^z, \gamma_k^k) \right] \prod_{p=k-1}^1 \left[\bar{z}_{p-1}^p S_p(b, a) + R_p(b, a) \right]} \quad (25)$$

and

$$\begin{pmatrix} \bar{z}_k^z \\ \bar{z}_k \\ 1 \end{pmatrix} = \frac{M_k(\gamma_k^z, \gamma_k^{k+1}) \left[\prod_{p=k+1}^{N-1} M_p(a, b) \right] \begin{pmatrix} \bar{z}_N^N \\ 1 \end{pmatrix}}{\left[\bar{z}_{k+1}^{k+1} S_k(\gamma_k^z, \gamma_k^{k+1}) + R_k(\gamma_k^z, \gamma_k^{k+1}) \right] \prod_{p=k+1}^{N-1} \left[\bar{z}_{p+1}^p S_p(a, b) + R_p(a, b) \right]}, \quad (26)$$

where $a = \gamma_p^p$, $b = \gamma_p^{p+1}$.

If the total interval ($z_1 \leq z \leq z_N$) is partitioned into $N - 1$ subintervals, then the matrix $\tilde{\psi}_k(z)$ in the k^{th} layer may be expressed as

$$\tilde{\psi}_k(z) = M_k(\gamma_k^z, \gamma_k^{k+1}) \begin{pmatrix} \bar{z}_k^{k+1} \\ \bar{z}_k \\ 1 \end{pmatrix} \bar{u}_k^{k+1},$$

where $z_k \leq z \leq z_{k+1}$ for $1 \leq k \leq LS - 1$ and $z_{LS} \leq z \leq z_S$ for $k = LS$, the source layer. Applying equation (19) over $[z_{k-1}, z_{k+1}]$ yields

$$\bar{u}_k^{k+1} = \bar{u}_{k-1}^k \left(\bar{z}_{k-1}^k S_k(b, a) + R_k(b, a) \right), \quad a = \gamma_k^k \text{ and } b = \gamma_k^{k+1};$$

thus

$$\tilde{\psi}_k(z) = M_k(\gamma_k^z, \gamma_k^{k+1}) \begin{pmatrix} \bar{z}_k^{k+1} \\ \bar{z}_k \\ 1 \end{pmatrix} \left[\bar{u}_{k-1}^k \left(\bar{z}_{k-1}^k S_k(b, a) + R_k(b, a) \right) \right]. \quad (27)$$

Likewise, the matrix $\psi_k(z)$ may be expressed as

$$\psi_k(z) = M_k(\gamma_k^z, \gamma_k^{k+1}) \begin{pmatrix} z^{k+1} \\ z_{k+1} \\ 1 \end{pmatrix} U_{k+1}^{k+1}, \quad (28)$$

where $z_k \leq z \leq z_{k+1}$ for $LS + 1 \leq k \leq N - 1$ and $z_{LS+1} \geq z > z_s$ for $k = LS$. The impedances Z_k^{k+1} and Z_{k+1}^k are the terminal impedances Z_0^N and Z_N^0 referenced to the bottom of the k^{th} layer. They may be easily found from equations (25) and (26). The Green's function in the k^{th} layer for $z < z_s$ may now be written as

$$G_k(z) = \left[\bar{z}_k^{k+1} Q_k(\gamma_k^z, \gamma_k^{k+1}) + P_k(\gamma_k^z, \gamma_k^{k+1}) \right] \left[\bar{U}_{k-1}^k \left(\bar{z}_{k-1}^k S_k(b,a) + R_k(b,a) \right) \right] \quad (29)$$

Similarly the Green's function in the k^{th} layer for $z > z_s$ may be written as

$$G_k(z) = \left[Z_{k+1}^{k+1} Q_k(\gamma_k^z, \gamma_k^{k+1}) + P_k(\gamma_k^z, \gamma_k^{k+1}) \right] U_{k+1}^{k+1}. \quad (30)$$

The subscript on $G_k(z)$ generally will be omitted since the receiver is always located at (r,z) in the LR^{th} layer.

Thus the Green's function $G(z)$, $z < z_s$, may be written in terms of Z_k^{k+1} and the multiplicative constant $\bar{U}_{k-1}^k [Z_{k-1}^k S_k(b,a) + R_k(b,a)]$. Similarly $G(z)$, $z > z_s$ is given in terms of Z_{k+1}^{k+1} and the constant U_{k+1}^{k+1} . Since the local terminal impedances Z_k^{k+1} and Z_{k+1}^k are uniquely determined from equations (25) and (26) in terms of the known half space impedances Z_0^1 and Z_N^N , respectively, the Green's function $G(z)$ is completely specified upon determination of the multiplicative constants.

If continuity of $\bar{\psi}_k$ and \bar{U}_k is to hold everywhere above the source, we must insist that

$$\bar{\psi}_k(z_k) = \bar{\psi}_{k-1}(z_k)$$

or, equivalently, that

$$\bar{U}_{k-1}^k \left[\bar{z}_{k-1}^k S_k(b,a) + R_k(b,a) \right] = \bar{U}_k^{k+1} \quad 1 \leq k \leq LS-1,$$

where $a = \gamma_k^k$, $b = \gamma_k^{k+1}$. The relation to the constant in the source layer is

$$\bar{U}_{k-1}^k \left[\bar{z}_{k-1}^k S_k(b,a) + R_k(b,a) \right] = \frac{\bar{U}_{LS-1}^{LS} \left[\bar{z}_{LS-1}^{LS} S_{LS}(\gamma_{LS}^{LS+1}, \gamma_{LS}^{LS}) + R_{LS}(\gamma_{LS}^{LS+1}, \gamma_{LS}^{LS}) \right]}{\prod_{p=k+1}^{LS} \left[\bar{z}_{p-1}^p S_p(b,a) + R_p(b,a) \right]}$$

$$1 \leq k \leq LS-1.$$

Similarly, if the continuity of F_k and U_k is to hold everywhere below the source, then

$$\psi_k(z_{k+1}) = \psi_{k+1}(z_{k+1})$$

or

$$U_{k+1}^{k+1} = U_k^k / \left[z_{k+1}^{k+1} S_k(a,b) + R_k(a,b) \right], \quad (31)$$

which may be written in terms of the source constant as

$$U_{k+1}^{k+1} = \frac{U_{LS+1}^{LS+1}}{\prod_{p=LS+1}^k \left[z_{p+1}^{p+1} S_p(a,b) + R_p(a,b) \right]} \quad \begin{matrix} LS+1 \leq k \leq N-1 \\ a = \gamma_p^p, b = \gamma_p^{p+1} \end{matrix} \quad (32)$$

The two constants U_{LS}^S and \tilde{U}_{LS}^S are determined by integrating equation (10) between the limits $z_s - \epsilon$ and $z_s + \epsilon$ and taking the limit as ϵ goes to zero,

$$\lim_{\epsilon \rightarrow 0} \int_{z_s - \epsilon}^{z_s + \epsilon} \mathcal{L}(G) dz = -1,$$

or, equivalently, satisfying the source conditions,

$$F_{LS}^S - \tilde{F}_{LS}^S = 0$$

$$U_{LS}^S - \tilde{U}_{LS}^S = -1.$$

Upon substitution of equations (27) and (28) into the above three equations, one finds that the above conditions will be satisfied if the constants are defined according to

$$U_{LS+1}^{LS+1} = a_{12}/W$$

$$\tilde{U}_{LS-1}^{LS} \left[\tilde{z}_{LS-1}^{LS} S_{LS}(b,a) + R_{LS}(b,a) \right] = a_{11}/W,$$

where the Wronskian is

$$W = a_{11}a_{22} - a_{21}a_{12} ,$$

and it is convenient to express the components of W with $e = \gamma_{LS}^S$ as

$$a_{11} = \left(z_{LS+1}^{LS+1} - 1 \right) \begin{pmatrix} Q_{LS}(e,b) \\ -P_{LS}(e,b) \end{pmatrix} \quad a_{21} = \left(z_{LS+1}^{LS+1} - 1 \right) \begin{pmatrix} S_{LS}(e,b) \\ -R_{LS}(e,b) \end{pmatrix}$$

$$a_{12} = \begin{pmatrix} Q_{LS}(e,b) & P_{LS}(e,b) \end{pmatrix} \begin{pmatrix} \bar{z}_{LS}^{LS+1} \\ 1 \end{pmatrix} \quad a_{22} = \begin{pmatrix} S_{LS}(e,b) & R_{LS}(e,b) \end{pmatrix} \begin{pmatrix} \bar{z}_{LS}^{LS+1} \\ 1 \end{pmatrix} .$$

The explicit expression for W is then found to be

$$W = \begin{pmatrix} z_{LS+1}^{LS+1} - 1 \\ 1 \end{pmatrix} \begin{pmatrix} 0 & 1 \\ 1 & 0 \end{pmatrix} M_{LS}(b,c) M_{LS}(c,b) \begin{pmatrix} \bar{z}_{LS}^{LS+1} \\ 1 \end{pmatrix} ,$$

which reduces to

$$W = z_{LS+1}^{LS+1} - \bar{z}_{LS}^{LS+1} ,$$

the difference between the terminal impedance Z_N^N referenced up to the level $z = z_{LS+1}$ and the terminal impedance \bar{Z}_0^0 referenced down to that same level. The constants for $1 < k < LS - 1$ in each layer are then found to be

$$\left[\bar{z}_{k-1}^k S_k(b,a) + R_k(b,a) \right] \bar{u}_k^{k-1} = \left(\frac{a_{11}}{W} \right) \prod_{p=k+1}^{LS} \left[\bar{z}_{p-1}^p S_p(b,a) + R_p(b,a) \right]$$

and for $LS+1 < k < N - 1$,

$$u_{k+1}^{k+1} = \left(\frac{a_{12}}{W} \right) \prod_{p=LS+1}^k \left[z_{p+1}^{p+1} S_p(a,b) + R_p(a,b) \right] . \quad (33)$$

Thus $G(z, z_0)$ in any layer can be found by using these constants in equations (29) and (30). If both the source and receiver are the same layer (i.e., $LS = LR$), the Green's function for $z_{LS} < z < z_0$ and $1 < LS < N - 1$ is

$$G(z, z_s) = \frac{[z_{LR+1}^{LR+1} Q_{LR}^{LR+1}(z_{LR+1}^{LR+1}) + P_{LR}^{LR+1}(z_{LR+1}^{LR+1})]}{z_{LS+1}^{LS+1} - z_{LS}^{LS+1}} \frac{[z_{LS+1}^{LS+1} Q_{LS}^{LS+1}(z_{LS+1}^{LS+1}) + P_{LS}^{LS+1}(z_{LS+1}^{LS+1})]}{z_{LS+1}^{LS+1} - z_{LS}^{LS+1}} \quad (34)$$

$$z_{LS} \leq z \leq z_s$$

$$G(z, z_s) = \frac{[z_{LR+1}^{LR+1} Q_{LR}^{LR+1}(z_{LR+1}^{LR+1}) + P_{LR}^{LR+1}(z_{LR+1}^{LR+1})]}{z_{LS+1}^{LS+1} - z_{LS}^{LS+1}} \frac{[z_{LS}^{LS+1} Q_{LS}^{LS+1}(z_{LS}^{LS+1}) + P_{LS}^{LS+1}(z_{LS}^{LS+1})]}{z_{LS+1}^{LS+1} - z_{LS}^{LS+1}} \quad (35)$$

$$z_s \leq z \leq z_{LS+1}$$

If the receiver is below the source and in a different layer (i.e., $LR > LS$), the Green's function is

$$G(z, z_s) = \frac{[z_{LR+1}^{LR+1} Q_{LR}^{LR+1}(z_{LR+1}^{LR+1}) + P_{LR}^{LR+1}(z_{LR+1}^{LR+1})]}{z_{LS+1}^{LS+1} - z_{LS}^{LS+1}} \frac{[z_{LS}^{LS+1} Q_{LS}^{LS+1}(z_{LS}^{LS+1}) + P_{LS}^{LS+1}(z_{LS}^{LS+1})]}{z_{LS+1}^{LS+1} - z_{LS}^{LS+1}} \Delta_{LS+1}^{LR}$$

where

$$\Delta_{LS+1}^{LR} = \prod_{k=LS+1}^{LR} [z_{k+1}^{k+1} S_k(a, b) + R_k(a, b)]^{-1} \quad (36)$$

$$z_{LR} \leq z \leq z_{LR+1}, \quad LS+1 \leq LR \leq N-1.$$

From a notational standpoint, the results for G , when either the source or receiver are in the zero or N^{th} layer, are special cases. They are given in appendix A. The form of the solution for G provided above is the familiar way of expressing the Green's function solution. Felsen and Marcuritz² (p. 280,

equation (22)) and also Coddington and Levinson¹⁶ (p. 248) provide solutions which are identical in form to equation (36) except for the absence of the factor Δ_{LS+1}^{LR} . As can be seen by examining equation (35), this factor is absent if both the source and receiver are in the same layer ($LS = LR$). Thus our result represents an extension of this earlier work in that the source and receiver may be put at any depth in an arbitrary layered media.

The Green's function may be expressed in various alternative forms using the relations provided in this section. One such form which explicitly displays the dependence on the known terminal impedances Z_N^N and Z_0^1 is found to be

$$G(z, z_s) = \frac{(1 - \tilde{Z}_0^1) K_1^{LS} \phi_{LS} \phi_{LR}^{K_{LR+1}^{N-1}} \begin{pmatrix} z_N^N \\ 1 \end{pmatrix}}{(1 - \tilde{Z}_0^1) K_1^{N-1} \begin{pmatrix} z_N^N \\ 1 \end{pmatrix}}, \quad (37)$$

where $z_{LR} \leq z \leq z_{LR+1}$ for $LS + 1 \leq LR \leq N - 1$ and $z_s \leq z \leq z_{LS+1}$.

All of the terms in the above expression are matrices. In particular, the following abbreviations have been made:

$$\phi_{LS} = \begin{pmatrix} P_{LS}(\gamma_{LS}^S, \gamma_{LS}^{LS+1}) \\ -Q_{LS}(\gamma_{LS}^S, \gamma_{LS}^{LS+1}) \end{pmatrix} \quad \phi_{LR} = \begin{pmatrix} Q_{LR}(\gamma_{LR}^Z, \gamma_{LR}^{LR+1}) & P_{LR}(\gamma_{LR}^Z, \gamma_{LR}^{LR+1}) \end{pmatrix}$$

$$K_\ell^P = \prod_{k=\ell}^P M_k(\gamma_k^k, \gamma_k^{k+1}) .$$

The denominator of equation (37) is an expression for the characteristic or dispersion equation. It is the difference in impedance of the entire region between the half spaces evaluated at $z = z_1$; $(Z_1^1 - \tilde{Z}_0^1)$ or, equivalently, evaluated at $z = z_n$; $(Z_N^N - \tilde{Z}_{N-1}^N)$. The expression for $\tilde{F}_{LR}^N(z)$, valid above the source, is obtained from equation (37) by interchanging LS and LR and also z_s and z .

DIRECT NUMERICAL INTEGRATION FAST FIELD PROGRAM (FFP)

The observation that the Fast Fourier Transform (FFT) algorithm could be used to evaluate Bessel transform was first made by H. W. Marsh¹⁷ in 1967. It was subsequently developed into a general purpose model by DiNapoli.¹⁸

The first step in this method consists of replacing the Bessel function in the integral solution with the Hankel function associated with outward propagation. If the first term in the asymptotic expansion is substituted,

$$H_0^{(1)}(\epsilon r) = \left(\frac{2}{\pi}\right)^{1/2} e^{i\epsilon r} / \sqrt{\epsilon r} ,$$

the integral may be written as

$$\varphi(r, z, z_s) = \left(\frac{2}{\pi}\right)^{1/2} \frac{s_\omega}{4\pi} \int_0^\infty \sqrt{\epsilon/r} G(z, z_s; \epsilon, \omega) e^{i\epsilon r} d\epsilon \quad (38)$$

Next, let the horizontal wavenumber and the horizontal range be evaluated at the discrete values,

$$\epsilon_m = \epsilon_0 + m\Delta\epsilon, \quad r_n = r_0 + n\Delta r, \quad (m, n) = 0, 1, 2, \dots, L-1,$$

with the added restriction that

$$\Delta r \Delta \epsilon = 2\pi/L,$$

where L is equal to 2 raised to some integer power. Equation (38) is then given by the discrete Fourier Transform

$$\varphi(r_n, z_r, z_s) = \Delta\epsilon \left(\frac{2}{\pi}\right)^{1/2} \frac{s_\omega}{4\pi} \frac{e^{i\epsilon_0 r_n}}{r_n^{1/2}} \sum_{m=0}^{L-1} E_m e^{i2\pi mn/L}, \quad (39)$$

where the input values are obtained from

$$E_m = G(z, z_s; \epsilon_m, \omega) \epsilon_m^{1/2} e^{imr_0 \Delta\epsilon} \quad (40)$$

The evaluation of equation (39) via the FFT yields, essentially simultaneously, the value of the field at each of the unaliased $L/2$ ranges. As a result, this format is ideally suited for the rapid calculation of the field as a function of range for a fixed source and receiver depth.

The only restriction imposed upon the matrizant solution for G was that the sound speed variation $c_k(z)$ associated with the known solutions be a good approximation of the given sound speed variation within the subinterval $z_k \leq z \leq z_{k+1}$. The solution for the pressure field via the FFT necessitates the evaluation of equation (40) for each of the L equispaced discrete values ϵ_m ($m = 0, 1, 2, \dots, L-1$) of the horizontal component of the wavenumber. This calculation represents the major portion of the required execution time. It is evident that the particular manner in which f_k, g_k depend upon ξ will have a strong bearing upon the ease with which G can be found as a function of ξ_m . Consideration of a few possible choices for the fundamental solutions will illustrate the point:

Trigonometric functions:

$$c_k(z) = a_k, \quad z_k \leq z \leq z_{k+1}$$

$$f_k(\gamma_k^z, \epsilon_m) = \sin(\gamma_k^z) \quad g_k(\gamma_k^z, \epsilon_m) = \cos(\gamma_k^z),$$

where

$$\gamma_k^z = (z_k - z) \sqrt{\frac{\omega}{a_k}^2 - \xi_m^2}.$$

The evaluation of a square root and a trigonometric function are required for each of the L values of ξ_m .

Airy Function:
$$c_k^{-2}(z) = a_k + b_k(z_k - z), \quad z_k \leq z \leq z_{k+1}$$

$$f_k(\gamma_k^z, \xi_m) = Ai(\gamma_k^z), \quad g_k(\gamma_k^z, \xi_m) = Bi(\gamma_k^z),$$

where

$$\gamma_k^z = -L_k^{+2} \left[\omega^2 c_k^{-2}(z) - \xi_m^2 \right], \quad L_k^2 = \omega^{-4/3} b_k^{-2/3}.$$

The Airy functions must be recalculated L times.

In contrast to that above, allow the sound speed to vary exponentially within each layer according to

$$c_k(z) = a_k e^{(z - z_k)/H_k}, \quad z_k \leq z \leq z_{k+1}, \quad 1 \leq k \leq N-1,$$

where a_k is the sound speed at the top of the k^{th} layer, which need not equal $c_{k-1}(z_k)$, and H_k is an arbitrary scale factor. The fundamental solutions are then found to be

$$f_k(\gamma_k^z, \xi_m) = J_{(\nu_k)_m}(\gamma_k^z), \quad g_k(\gamma_k^z, \xi_m) = Y_{(\nu_k)_m}(\gamma_k^z), \quad (41)$$

i.e., cylindrical functions of complex order,

$$(\nu_k)_m = (\xi_m H_k - i\alpha H_k), \quad \text{where } k(z) \sim \omega/c_k(z) - i\alpha,$$

with α a positive constant and real argument,

$$\gamma_k^z = \frac{\omega H_k}{c_k(z)}; \quad \frac{d\gamma_k^z}{dz} = \gamma_k^z / H_k. \quad (42)$$

The dependence upon ξ_m can then be efficiently found by evaluating equation (41) once for a pair of hypothetical starting values, $(\nu_k)_0$, $(\nu_k)_1$, and utilizing the recurrence relations:

$$Q_{v+1} = \left(\frac{b\rho_a}{a\rho_b} \right) R_v - \left(\frac{b}{a\rho_b} \right) vP_v + \left(\frac{b}{a\rho_b} \right) (v+1)P_{v+1}$$

$$R_{v+1} = \left(\frac{a\rho_b}{b\rho_a} \right) Q_v + \left(\frac{a}{b\rho_a} \right) vP_v - \frac{(v+1)}{\rho_a} P_{v+1}$$

$$P_{v+2} = P_v + \frac{2(v+1)}{ab} \left[\rho_b Q_{v+1} - \rho_a R_{v+1} \right]$$

(43)

$$S_{v+1} = - \left(\frac{ab}{\rho_a \rho_b} \right) P_{v+2} + (v+1) \left[\frac{Q_{v+1}}{\rho_a} - \frac{R_{v+1}}{\rho_b} \right] + \frac{(v+1)^2}{\rho_a \rho_b} P_{v+1}$$

where

$$\rho_a = i\omega H_k \rho_k(z_k) \quad \rho_b = i\omega H_k \rho_k(z_{k+1})$$

The arguments of the matrizant elements, which have been suppressed for notational convenience, are as given in the discussion of the depth dependent Green's function (impedance formulation), i.e., $a = \gamma_k^k$, $b = \gamma_k^{k+1}$. The recurrence relation, equation (43), is stable except when the v falls between the arguments a, b . A discussion of their use in this situation is provided in reference 19.

Upon noting that the recurrence relations require that the change in v be unity, the wavenumber domain sampling distance, $\Delta\xi$, is found to be

$$\Delta\xi = 1/H_k \quad (44)$$

The fact that the FFT requires equispaced values of ξ_m is in conflict with equation (44). This is so because H_k is different for each of the $(N-1)$ possible layers. Let $\Delta\xi$ equal the reciprocal of the largest scale factor, H_{\max} ,

$$\Delta\xi = 1/H_{\max} \quad (45)$$

and restrict the remaining scale factors to be some arbitrary integer multiple, p_k , of this value; i.e.,

$$H_{\max}/H_k = p_k \quad k = 1, 2, \dots, N-1$$

This restriction limits the ability to approximate the given sound speed variation arbitrarily close but allows enough flexibility to model most cases of interest in underwater acoustics. If the discrete values of ξ_m are given by

$$\xi_m = \xi_0 + m\Delta\xi \quad m = 0, 1, 2, \dots, L-1,$$

then they yield the discrete values of the order of the cylindrical functions in each layer

$$(v_k)_m = (\xi_0 H_k - i a H_k) + m/p_k \quad \begin{matrix} m = 0, 1, 2, \dots, L-1, \\ 1 \leq k \leq N-1. \end{matrix}$$

The condition that the change in v_k be unity can be satisfied if p_k pairs of starting values are calculated and used in the recurrence relations.

The required computer memory for each layer with exponential sound speed is $2p_k$ complex values of $P_{(v)_k}$ and p_k complex values for both $Q_{(v)_k}$ and $R_{(v)_k}$. The values for $S_{(v)_k}$ can be obtained from equation (20). For some m , the appropriate values of $P_{(v)_k}$, and $Q_{(v)_k}$, and $R_{(v)_k}$ ($1 \leq k \leq N-1$) are selected and used to calculate equation (40). The result of this calculation is stored in a complex array of size L . Equation (43) is used again for $m+1$.

Since the minimum value of ξ should be zero and it can be shown that $G(z, z_1; \xi)$ decays when $\xi > \omega/C_{\min}$, where C_{\min} is the minimum sound speed within the region $z_1 \leq z \leq z_N$, one finds that the number of sample points needed, L , is approximately

$$L \sim \frac{\omega}{C_{\min}} H_{\max} \quad (46)$$

Typically $H_{\max} \sim 10^5$; thus at high frequencies not only does the number of calculations increase but also available core storage may be exceeded. A technique has been implemented²⁰ for rigorously circumventing the core storage problem when it arises. It is noted that although the execution time and storage requirements grow with increasing frequency, the solution remains perfectly valid and accurate.

The only remaining point involves the accuracy of replacing the Hankel function $H_0^{(1)}(\xi r)$ with the first term in its asymptotic expansion which was introduced without justification. A discussion of this approximation is provided in appendix B.

NORMAL MODES (AND BRANCH LINE INTEGRAL) MODELS STICKLER (EJP CUTS), BARTBERGER (PEKERIS CUTS)

Normal mode models may be viewed as the result obtained when the integral solution to the wave equation is solved by the utilization of Cauchy's residue theory. In that case, the pressure field is given by a sum (possibly infinite) of residues associated with discrete eigenvalues and a branch cut integral representing the contribution from the continuous portion of the eigenvalue spectrum. It is common to assume the ocean surface to be a pressure release boundary. If this is assumed, the single branch cut integral arises from the lower half space which is the N^{th} layer in figure 2. The particular manner in which the branch cuts are chosen determines the extent of the discrete portion of the eigenvalue spectrum and the associated physical interpretation of the modes (eigenfunctions).

In the past, normal mode models in underwater acoustics have generally ignored the branch cut contributions, assuming that they would be of nugatory importance at the horizontal ranges of interest. Two notable exceptions can be cited. One is the pioneering work of Pekeris²² which treated a simple ocean and also dealt with waveform structure rather than propagation loss. The second exception is the work of Kutschale²³ on the arctic environment. Kutschale is interested in propagation loss but at "seismic" frequencies as well as the higher underwater acoustic frequency regime. Kutschale's model is also unique in that it allows for solid and liquid constant sound speed layers.

The primary mathematical difference between the two models to be discussed is the manner in which the branch cuts are chosen. Stickler²⁴ uses the EJP (Ewing, Jardensky, Press)²⁵ cuts, which in the limiting case of no absorption, would run from the branch points $\pm k_N$ along the $\text{Re}\{\xi\}$ axis to the origin and then along the $\text{Im}\{\xi\}$ axis. Bartberger²⁶ prefers the Pekeris cuts, which are lines parallel to the $\text{Im}\{\xi\}$ axis (see figure 3).

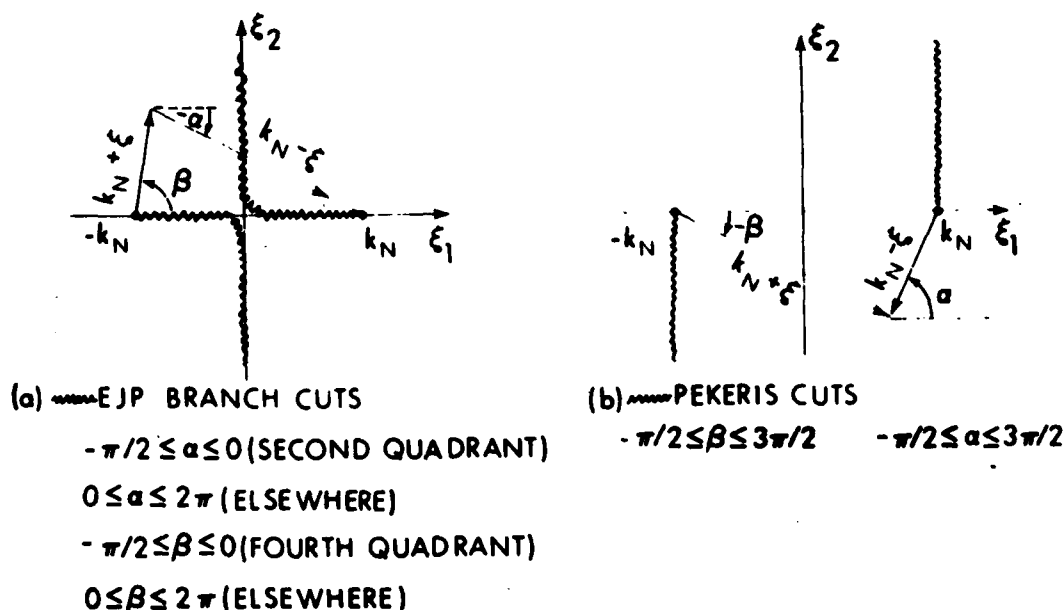


Figure 3. Definition of α and β for EJP and Pekeris Branch Cuts

For both models, the sound speed within each ocean layer is assumed to be well approximated by

$$c_k^{-2}(z) = a_k + b_k(z_k - z) \quad z_k \leq z \leq z_{k+1}$$

where a_k is the sound speed at the top of the k^{th} layer and need not equal $c_{k-1}^{-2}(z_k)$, and b_k is proportional to the sound speed gradient. In this case, the solutions f and g are given in terms of Airy functions according to

$$f_k(\gamma_k^2, \epsilon) = A i(\gamma_k^2), \quad g_k(\gamma_k^2, \epsilon) = B i(\gamma_k^2),$$

where the argument is found to be

$$\gamma_k^z = -L_k^{+2} \left[\omega^2 C_k^{-2}(z) - \epsilon^2 \right], \quad L_k^2 = \omega^{-4/3} b_k^{-2/3}.$$

The Green's function formulation previously given as equation (36) could be used to obtain a solution which would be equivalent to those obtained by Bartberger²⁶ and Stickler²⁴ but not of the same form. In order to obtain their results, equation (36) must first be rewritten by recalling that the impedance was defined at any level above the source as

$$\tilde{Z}(z) = \tilde{F}(z)/\tilde{U}(z)$$

and, similarly, below the source as

$$Z(z) = F(z)/U(z).$$

Upon substitution one then has

$$G(z, z_s) =$$

$$\frac{\left[F_{LR+1}^{LR+1} Q_{LR}^{LR+1}(d, b) + U_{LR+1}^{LR+1} P_{LR}^{LR+1}(d, b) \right] \left[\tilde{F}_{LS}^{LS+1} Q_{LS}^{LS+1}(e, b) + \tilde{U}_{LS}^{LS+1} P_{LS}^{LS+1}(e, b) \right] \Delta_{LS+1}^{LR}}{U_{LR+1}^{LR+1} U_{LS}^{LS+1} (Z_{LS+1}^{LS+1} - \tilde{Z}_{LS}^{LS+1})} \quad (47)$$

where

$$d = \gamma_{LR}^z \quad e = \gamma_{LS}^s$$

and b is the function γ evaluated at the lower boundary of the layer (in this case either LS or LR) in which it is defined.

Next, the difference in impedances evaluated at LS + 1 occurring in the denominator is transferred to the level z_N . In doing this, use is made of

$$\begin{pmatrix} \tilde{Z}_{LS}^{LS+1} \\ 1 \end{pmatrix} = \prod_{p=LS+1}^{N-1} M_p(a, b) \begin{pmatrix} \tilde{Z}_{N-1}^N \\ 1 \end{pmatrix} \prod_{p=LS+1}^{N-1} \left[\tilde{Z}_{p-1}^p S_p(b, a) + R_p(b, a) \right]$$

$$\begin{pmatrix} z_{LS+1}^{LS+1} \\ z_{LS+1}^{LS+1} \\ 1 \end{pmatrix} = \frac{\prod_{p=LS+1}^{N-1} M_p(a,b) \begin{pmatrix} z_N^N \\ z_N^N \\ 1 \end{pmatrix}}{\prod_{p=LS+1}^{LR} \left[z_{p+1}^{p+1} S_p(a,b) + R_p(a,b) \right] \prod_{p=LR+1}^{N-1} \left[z_{p+1}^{p+1} S_p(a,b) + R_p(a,b) \right]}$$

where as before $a = \gamma_p^p$, $b = \gamma_p^{p+1}$.

The constant in the denominator of the last equation has been written as a product of two constants in anticipation of cancellation of terms arising from the fact that

$$\Delta_{LS+1}^{LR} = \left\{ \prod_{p=LS+1}^{LR} \left[z_{k+1}^{k+1} S_k(a,b) + R_k(a,b) \right] \right\}^{-1}$$

Then

$$\begin{pmatrix} z_{LS+1}^{LS+1} - \bar{z}_{LS}^{LS+1} \\ z_{LS+1}^{LS+1} \\ 0 \end{pmatrix} = \begin{pmatrix} A & B \\ C & D \end{pmatrix} \begin{pmatrix} \alpha z_N^N - \beta z_{N-1}^N \\ \alpha - \beta \end{pmatrix}$$

where

$$\begin{pmatrix} A & B \\ C & D \end{pmatrix} = \prod_{p=LS+1}^{N-1} M_p(a,b)$$

$$\beta = \prod_{p=LS+1}^{N-1} \left[\bar{z}_{p-1}^p S_p(b,a) + R_p(b,a) \right]$$

$$\alpha = \left\{ \prod_{p=LS+1}^{N-1} \left[z_{p+1}^{p+1} S_p(a,b) + R_p(a,b) \right] \right\}^{-1}$$

Next

$$\alpha = \frac{[C \bar{z}_{N-1}^N + D] [z_{LS+1}^{LS+1} - \bar{z}_{LS}^{LS+1}]}{(z_N^N - \bar{z}_{N-1}^N) (AD - BC)}$$

$$\beta = \frac{[Cz_N^N + D] [z_{LS+1}^{LS+1} - \bar{z}_{LS}^{LS+1}]}{(z_N^N - \bar{z}_{N-1}^N) (AD - BC)} ;$$

but

$$AB - CD = \begin{vmatrix} A & B \\ C & D \end{vmatrix} = 1$$

or

$$\alpha = [Cz_N^N + D]^{-1} = \left\{ \prod_{p=LS+1}^{N-1} [z_{p+1}^{p+1} S_p(a,b) + R_p(a,b)] \right\}^{-1}$$

$$\beta = [Cz_N^N + D] = \prod_{p=LS+1}^{N-1} [\bar{z}_{p+1}^p S_p(b,a) + R_p(b,a)] .$$

Additionally one has that

$$\left(z_{LS+1}^{LS+1} - \bar{z}_{LS}^{LS+1} \right) = \alpha [Az_N^N + D] - \beta [A\bar{z}_{N-1}^N + B]$$

or

$$\left(z_{LS+1}^{LS+1} - \bar{z}_{LS}^{LS+1} \right) = \left(z_N^N - \bar{z}_{N-1}^N \right) \alpha \beta . \tag{48}$$

Substitution of the above into equation (47) gives a formulation

$$G(z, z_s) = \frac{\left[F_{LR+1}^{LR+1} Q_{LR}(d,b) + U_{LR+1}^{LR+1} P_{LR}(d,b) \right] \left[\bar{F}_{LS}^{LS+1} Q_{LS}(e,b) + \bar{U}_{LS}^{LS+1} P_{LS}(e,b) \right]}{U_{LR+1}^{LR+1} \bar{U}_{LS}^{LS+1} \left(z_N^N - \bar{z}_{N-1}^N \right) \prod_{p=LS+1}^{N-1} \left[\bar{z}_{p-1}^p S_p(b,a) + R_p(b,a) \right] \prod_{p=LR+1}^{N-1} \left[z_{p+1}^{p+1} S_p(a,b) + R_p(a,b) \right]}$$

which allows for the source and receiver to be in any layer. However, the evaluation of the Wronskian occurs at z_N . The denominator may be simplified considerably by noting first that if the identity

$$z_N^N - z_{N-1}^N = \frac{z_N^N}{\bar{u}_{N-1}^N} \left(\bar{u}_{N-1}^N - \frac{\bar{f}_{N-1}^N}{z_N^N} \right)$$

is substituted into the denominator, then one has

$$\frac{\prod_{p=LS+1}^{N-1} [\bar{z}_{p-1}^p S_p(b,a) + R_p(b,a)]}{\prod_{p=LR+1}^{N-1} [z_{p+1}^{p+1} S_p(a,b) + R_p(a,b)]} \frac{u_{LR+1}^{LR+1} \bar{u}_{LS}^{LS+1}}{u_N^N \bar{u}_{N-1}^N} F_N^N \left(\bar{u}_{N-1}^N - \frac{\bar{f}_{N-1}^N}{z_N^N} \right)$$

However, with the aid of equation (33), it is easy to show that

$$\frac{u_{LR+1}^{LR+1}}{u_N^N} = \frac{\prod_{p=LS+1}^{N-1} [z_{p+1}^{p+1} S_p(a,b) + R_p(a,b)]}{\prod_{p=LR+1}^{LR} [z_{p+1}^{p+1} S_p(a,b) + R_p(a,b)]} = \prod_{p=LR+1}^{N-1} [z_{p+1}^{p+1} S_p(a,b) + R_p(a,b)]$$

Thus

$$\frac{u_{LR+1}^{LR+1}}{u_N^N} \left\{ \prod_{p=LR+1}^{N-1} [z_{p+1}^{p+1} S_p(a,b) + R_p(a,b)] \right\}^{-1} = 1 \quad (49)$$

Similarly

$$\prod_{p=LS+1}^{N-1} [\bar{z}_{p-1}^p S_p(b,a) + R_p(b,a)] \frac{\bar{u}_{LS}^{LS+1}}{\bar{u}_{N-1}^N} = 1 \quad (50)$$

To show this successively substitute $k = N - 1, N - 2 \dots$ into equation (29) and it becomes evident that

$$\bar{U}_{N-1}^N = \bar{U}_{LS}^{LS+1} \prod_{p=LS+1}^{N-1} \left[\bar{Z}_{p-1}^p S_p(b,a) + R_p(b,a) \right],$$

which is the desired result.

The required result for Green's function is then

$$G(z, z_s) = \frac{\left[\bar{F}_{LR+1}^{LR+1} Q_{LR}(d,b) + \bar{U}_{LR+1}^{LR+1} P_{LR}(d,b) \right] \left[\bar{F}_{LS}^{LS+1} Q_{LS}(e,b) + \bar{U}_{LS}^{LS+1} P_{LS}(e,b) \right]}{F_N^N \left(\bar{U}_{N-1}^N - \frac{\bar{F}_{N-1}^N}{Z_N^N} \right)} \quad (51)$$

The residue contribution to the pressure field occurs for some value of ξ , labeled ξ_m , called the eigenvalue, for which

$$Z_N^N - \bar{Z}_{N-1}^N = 0;$$

i.e., the impedance of the last half space Z_N^N exactly equals the impedance of the entire medium above it, \bar{Z}_{N-1}^N evaluated at Z_N^N . Assuming that these eigenvalues give rise to simple poles, the residue contribution is found to be

$$\frac{-1S_\omega}{2} \sum_{m=0}^P \left[\frac{\left[\bar{F}_{LR+1}^{LR+1} Q_{LR}(d,b) + \bar{U}_{LR+1}^{LR+1} P_{LR}(d,b) \right] \left[\bar{F}_{LS}^{LS+1} Q_{LS}(e,b) + \bar{U}_{LS}^{LS+1} P_{LS}(e,b) \right]}{F_N^N \frac{\partial}{\partial \xi} \left(\bar{U}_{N-1}^N - \frac{\bar{F}_{N-1}^N}{Z_N^N} \right)} \right]_{\xi=\xi_m} \\ \times H_0^{(1)}(\xi_m r) \xi_m, \quad (52)$$

where the terminal impedance Z_N^N is known to be

$$Z_N^N = \omega \rho_N / \left(k_N^2 - \xi^2 \right)^{1/2}.$$

The residue contribution obtained by both Stickler²⁴ and Bartberger²⁶ can be obtained from equation (52). However, there are some important exceptions related to the choice of branch cuts.

Stickler's Residue Contribution

By choosing the EJP cuts and utilizing results from the spectral theory of ordinary differential equations,¹⁶ Stickler is able to conclude that all the eigenvalues which occur on the sheet of integration in the complex ξ plane are real. (It should be recalled that the entire medium is assumed to be a perfect fluid with no energy loss due to absorption.) Furthermore, only a finite number of such values exist. They give rise to simple pole type singularities. These modes are trapped within the medium. The only loss of energy with range, assumed to be sufficiently far from the source, may be interpreted as $r^{-1/2}$, i.e., cylindrical spreading. The equivalent mode-ray (a plot of $\xi_m = k(z)\sin\Theta(z)$ versus depth and range with Θ measured from the vertical) should either have a turning point between z_1 and z_n or be incident upon the boundary at z_n at an angle for which total reflection occurs.

To obtain Stickler's result, note from equation (48) that at the eigenvalues the functions F and U are equal to \bar{F} and \bar{U} at all levels. The Green's function portion of the residue may then be written as

$$\left. \frac{[\bar{F}_{LR+1}^{LR+1} Q_{LR}(d,b) + \bar{U}_{LR+1}^{LR+1} P_{LR}(d,b)] [\bar{F}_{LS+1}^{LS+1} Q_{LS}(e,b) + \bar{U}_{LS+1}^{LS+1} P_{LS}(e,b)]}{\bar{F}_{N-1}^N \frac{\partial}{\partial \xi} \left\{ \bar{U}_{N-1}^N - \frac{\bar{F}_{N-1}^N}{Z_N^N} \right\}} \right|_{\xi = \xi_m} \quad (53)$$

Performing the indicated differentiation yields

$$\frac{\partial}{\partial \xi} \left\{ \bar{U}_{N-1}^N - \frac{\bar{F}_{N-1}^N}{Z_N^N} \right\} = \frac{\partial \bar{U}_{N-1}^N}{\partial \xi} - \frac{1}{Z_N^N} \frac{\partial \bar{F}_{N-1}^N}{\partial \xi} + \frac{\bar{U}_{N-1}^N}{Z_N^N} \frac{\partial Z_N^N}{\partial \xi}, \quad (54)$$

where the identity

$$\frac{\bar{F}_{N-1}^N}{(Z_N^N)^2} = \frac{\bar{U}_{N-1}^N}{Z_N^N},$$

which holds when $(Z_N^N = Z_{N-1}^N)$ has been used.

Stickler²⁴ assumes the solution in each layer to be

$$P_k(z, \xi) = A_k A_1(\gamma_k^z) + B_k B_1(\gamma_k^z), \quad z_k \leq z \leq z_{k+1},$$

which corresponds to

$$\tilde{F}_k(z) = \tilde{F}_{k-1}^k Q_k(\gamma_k z^k) + \tilde{U}_{k-1}^k P_k(\gamma_k z^k), \quad z_k \leq z \leq z_{k+1}$$

in the notation used here. The relationship between the constants is

$$\begin{pmatrix} \tilde{F}_{k-1}^k \\ \tilde{U}_{k-1}^k \end{pmatrix} = \begin{pmatrix} A_1(b) & B_1(b) \\ \frac{A_1'(b)}{i\omega_{k-1} L_{k-1}} & \frac{B_1'(b)}{i\omega_{k-1} L_{k-1}} \end{pmatrix} \begin{pmatrix} A_{k-1} \\ B_{k-1} \end{pmatrix}, \quad (55)$$

where primes denote differentiation with respect to the argument b , which is

$$b = \gamma_{k-1}^k.$$

Then, in terms of Stickler's notation,²⁴ one finds that

$$\begin{aligned} \frac{\partial \tilde{F}_{N-1}^N}{\partial \xi} &= \left[\dot{A}_{N-1} A_1(\gamma_{N-1}^N) \right] + \dot{B}_{N-1} B_1(\gamma_{N-1}^N) + \left[A_{N-1} A_1'(\gamma_{N-1}^N) + B_{N-1} B_1'(\gamma_{N-1}^N) \right] 2L_{N-1}^2 \xi \\ &= \left[\dot{A}_{N-1} A_1(\gamma_{N-1}^N) \right] + \dot{B}_{N-1} B_1(\gamma_{N-1}^N) + 2L_{N-1}^3 \xi i\omega_{N-1} \tilde{U}_{N-1}^N \end{aligned}$$

upon recalling the definition of \tilde{U}_{N-1}^N .

Similarly,

$$\frac{\partial \tilde{U}_{N-1}^N}{\partial \xi} = \frac{\left[\dot{A}_{N-1} A_1'(\gamma_{N-1}^N) + \dot{B}_{N-1} B_1'(\gamma_{N-1}^N) \right]}{i\omega_{N-1} L_{N-1}} + \frac{2L_{N-1} \xi \gamma_{N-1}^N \tilde{F}_{N-1}^N}{i\omega_{N-1}}$$

where the dots denote differentiation with respect to ξ . It is also a straightforward matter to show that

$$\frac{\partial Z_N^N}{\partial \xi} = \frac{\xi (Z_N^N)^3}{(\omega_{N-1})^2}.$$

Upon substitution and noting that

$$\frac{U_{N-1}^N}{Z_N} \frac{\epsilon(Z_N^N)}{(\omega \rho_N)^2} = \frac{F_{N-1}^N Z_N^N \epsilon}{(\omega \rho_N)^2}$$

one finds that

$$\frac{\partial}{\partial \epsilon} \left\{ U_{N-1}^N - \frac{F_{N-1}^N}{Z_N} \right\} = \left\{ \frac{2L_{N-1} \epsilon \gamma_{N-1}^N}{1 \omega \rho_{N-1}} + \frac{\epsilon Z_N^N}{(\omega \rho_N)^2} - \frac{2L_{N-1}^3 \epsilon 1 \omega \rho_{N-1}}{(Z_N^N)^2} \right\} F_{N-1}^N$$

$$+ \frac{[\dot{A}_{N-1} A \dot{\gamma}_{N-1}^N + \dot{B}_{N-1} B \dot{\gamma}_{N-1}^N]}{1 \omega \rho_{N-1} L_{N-1}} - \frac{[\dot{A}_{N-1} A 1 (\gamma_{N-1}^N) + \dot{B}_{N-1} B 1 (\gamma_{N-1}^N)]}{Z_N^N}$$

The entire denominator of equation (53) may then be written as

$$F_{N-1}^N \frac{\partial}{\partial \epsilon} \left\{ U_{N-1}^N - \frac{F_{N-1}^N}{Z_N} \right\} = \frac{C_0^{-1}(\epsilon_m)}{1 \omega} \quad (56)$$

where

$$C_0^{-1}(\epsilon_m) = \left[\left\{ \frac{2L_{N-1} \epsilon \gamma_{N-1}^N}{\rho_{N-1}} + \frac{1 \omega \epsilon Z_N^N}{(\omega \rho_N)^2} - \frac{2(1 \omega)^2 \epsilon L_{N-1}^3 \rho_{N-1}}{(Z_N^N)^2} \right\} (F_{N-1}^N)^2 \right. \\ \left. + \frac{\dot{B}_{N-1} A_{N-1} - \dot{A}_{N-1} B_{N-1}}{\rho_{N-1} L_{N-1} \pi} \right] \Bigg|_{\epsilon = \epsilon_m}$$

which is identical to equation (12) of reference 24, with the exception of a multiplicative factor of k (ϵ_m in this notation) that arises from the original Bessel transform. A typographical error in Stickler's²⁴ equation 12 occurred by omitting the factor equivalent to γ_{N-1}^N in the first term inside the $\{ \}$ of equation (56). To facilitate the comparison between the results presented here and those found in reference 24, the following correspondence in notation is shown, in addition to that already given by equation (55):

Ours Stickler's

$$\frac{Z_N^N}{T\omega_N} = -\frac{1}{u(k)}$$

$$\xi = k$$

$$\gamma_N(z) = Z_N(z)$$

$$S_\omega = \frac{1}{i\omega\phi(z_s)}$$

The residue contribution may then be written as

$$\frac{\omega^S}{2} \sum_{m=0}^P C_0(\xi_m) \left[\tilde{F}_{LR+1}^{LR+1} Q_{LR}(d,b) + \tilde{U}_{LR+1}^{LR+1} P_{LR}(d,b) \right] \left[\tilde{F}_{LS}^{LS+1} Q_{LS}(e,b) + \tilde{U}_{LS}^{LS+1} P_{LS}(e,b) \right] \chi_{\xi_m H_0}^{(1)}(\xi_m r), \quad (57)$$

which is identical to Stickler's²⁴ corresponding residue contribution.

Bartberger's Residue Contribution (Pekeris Cuts)

Although Bartberger²⁶ assumes an $e^{i\omega t}$ time dependence, his work is summarized as if the harmonic factor $e^{i\omega t}$ had been used in keeping with the conventions adopted earlier.

The formulation used by Bartberger²⁶ is based upon Green's function given by equation (51). Thus the only difference in the form of his residue contribution versus Stickler's²⁴ is that the functions F_{LR+1}^{LR+1} , U_{LR+1}^{LR+1} defined below the source are not replaced with their counterparts, \tilde{F}_{LR+1}^{LR+1} , \tilde{U}_{LR+1}^{LR+1} , defined above the source.

In order to find the zeros of equation (48), the derivatives must be evaluated with respect to the wavenumber of the function F_{N-1}^N and U_{N-1}^N .

Utilizing equation (27) and recalling that

$$\tilde{U}_{k-1}^k \left[\tilde{Z}_{k-1}^k S_k(b,a) + R_k(b,a) \right] = \tilde{U}_k^{k+1},$$

one is able to write the functions in terms of their terminal values as

$$\begin{pmatrix} \bar{F}_k^k \\ \bar{U}_k^k \end{pmatrix} = M_k(a,b) \begin{pmatrix} \bar{z}_k^{k+1} \\ 1 \end{pmatrix} \bar{U}_k^{k+1} = M_k(a,b) \begin{pmatrix} \bar{F}_k^{k+1} \\ \bar{U}_k^{k+1} \end{pmatrix}.$$

However, from the continuity conditions, one has

$$\bar{\psi}_{k+1}(z_{k+1}) = \bar{\psi}_k(z_{k+1}),$$

and upon substitution it is found that

$$\begin{pmatrix} \bar{F}_k^k \\ \bar{U}_k^k \end{pmatrix} = M_k(a,b) \begin{pmatrix} \bar{F}_k^{k+1} \\ \bar{U}_k^{k+1} \end{pmatrix}.$$

Successive use of the above formula yields

$$\begin{pmatrix} \bar{F}_1^1 \\ \bar{U}_1^1 \end{pmatrix} = \prod_{p=1}^{N-1} M_p(a,b) \begin{pmatrix} \bar{F}_{N-1}^N \\ \bar{U}_{N-1}^N \end{pmatrix}, \quad (58)$$

where $a = \gamma_p^p$, $b = \gamma_p^{p+1}$.

An essential component in calculating the above mentioned derivatives is

$$\frac{\partial M_p}{\partial \xi}(a,b).$$

It is found by differentiating equation (19) that

$$\frac{\partial Q_p(a,b)}{\partial \xi} = 2L_p^3 \xi \omega_p(z_p) S_p(a,b) - \frac{2L_p \xi b P_p(a,b)}{\omega_p(z_{p+1})}$$

$$\frac{\partial P_p(a,b)}{\partial \xi} = -2L_p^3 \xi \omega_p(z_p) R_p(a,b) - \omega_p(z_{p+1}) 2L_p^3 \xi Q_p(a,b)$$

$$\frac{\partial S_p(a,b)}{\partial \xi} = \frac{-2L_p \xi b R_p(a,b)}{1\omega_p(z_{p+1})} + \frac{2L_p \xi a Q_p(a,b)}{1\omega_p(z_p)}$$

$$\frac{\partial R_p(a,b)}{\partial \xi} = \frac{2L_p a P_p(a,b)}{1\omega_p(z_p)} - 2L_p^3 \xi 1\omega_p(z_{p+1}) S_p(a,b)$$

(59)

$$a = \gamma_p^p, \quad b = \gamma_p^{p+1}.$$

The quantitative difference between the two residue contributions arises from the type and number of eigenvalues which satisfy the dispersion equation,

$$z_{LS+1}^{LS+1} = \bar{z}_{LS}^{LS+1},$$

or its equivalent form derived by setting equation (48) to zero. When the Pekeris branch cuts are chosen, the number of discrete eigenvalues will be infinite. Furthermore, the discrete eigenvalue spectrum can be thought of as containing two subsets spanning the regions on either side of the Pekeris branch cut. The first contains a finite number of eigenvalues with real parts larger than k_N , i.e., those lying to the right of the Pekeris branch cut. The imaginary part of these eigenvalues would be zero if the attenuation in each layer were set to zero. In this instance, Stickler's²⁴ total residue contribution would be identical to that portion of Bartberger's²⁶ residue series arising from this subset of his eigenvalues.

Bartberger's²⁶ second subset of eigenvalues lay to the left of the Pekeris cut. They are infinite in number and complex even with the attenuation set to zero. Then for these eigenvalues

$$\xi_m = A_m + iB_m,$$

where

$$0 < A_m < k_N, \quad A_{m+1} < A_m, \quad \lim_{m \rightarrow \infty} B_m = \infty, \quad B_{m+1} < B_m.$$

$$m \rightarrow \infty$$

Under the assumption that the Hankel function is well approximated by the first term in its asymptotic expansion, examination of the range dependence of the terms in equation (57) yields

$$e^{iA_m r - B_m r} / \sqrt{r}.$$

These modes, sometimes called *leaky modes*, suffer the same cylindrical spreading loss as the trapped modes from the first set. In addition, they are attenuated by an amount proportional to the imaginary part of the eigenvalue. It is common to physically interpret these modes in terms of bottom bounce energy since the mode-ray equivalent for a_m would be incident upon the boundary z_N at an angle between critical and normal incidence. The angle of incidence approaches 90° as m increases. The magnitude of the reflection coefficient for these angles would be less than unity, resulting in a loss of energy into the *bottom*. On this basis, it might be expected that, as the mode number m increased, the range at which these leaky modes would significantly contribute to the total field would diminish. Bartberger²⁶ has found this to be precisely the case.

On the other hand, an increasing number of higher order modes would have to be included in the sum as the range point approached the source. Five-hundred is the maximum number of modes calculated in Bartberger's AP2 program. Thus for some hypothetical combination of frequency, water depth, and source/receiver depths it is possible that some hypothetical range interval exists close to the source but not necessarily starting at $r = 0$. Bartberger's²⁶ results for the total field will be in error due to the truncation of the infinite series. The end point of this interval is associated with that range at which the mode-ray equivalent for the first omitted mode would have reached the receiver. The beginning of the interval is usually marked by a sudden drop in level of the propagation loss versus range curve.

Branch Cuts and Branch Cut Integrals

The two choices of branch cuts discussed in this section are shown schematically in figure 3. The behavior of the square root

$$\beta_N = \pm \sqrt{k_N^2 - \xi^2}$$

in the complex plane ($\xi = \xi_1 + i\xi_2$) is determined by first defining

$$k_N - \xi = \rho_+ e^{i\alpha}, \quad k_N + \xi = \rho_- e^{i\beta}$$

so that

$$\beta_N = (\rho_+ \rho_-)^{1/2} e^{i(\alpha+\beta)/2} = a_N + ib_N,$$

where the reference line and direction of measurement for α and β are shown in figures 4 and 5. The values of α and β at critical points are shown in figure 4 for the EJP cuts. With this information, it is possible to show that $b_N > 0$ everywhere on the top sheet and that $a_N > 0$ in quadrants 2 and 4 while $a_N < 0$ in quadrants 1 and 3.

The analogous information for the Pekeris cuts is given in figure 5. It can be seen that the imaginary part of β_N is positive everywhere in the upper half plane except for that sector of the first quadrant between the $\text{Im}\{\xi\}$ axis and the branch cut. It is in this sector that the complex eigenvalues associated with the leaky wave modes are located.

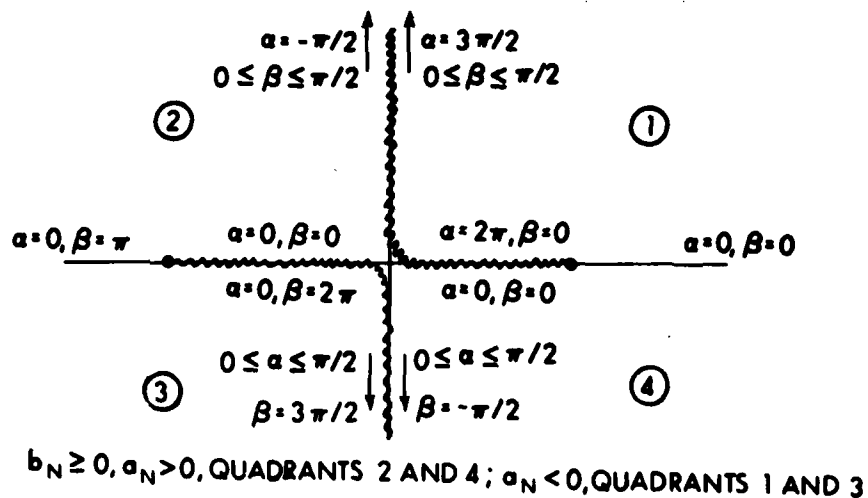


Figure 4. Definition of β_N for EJP Branch Cut

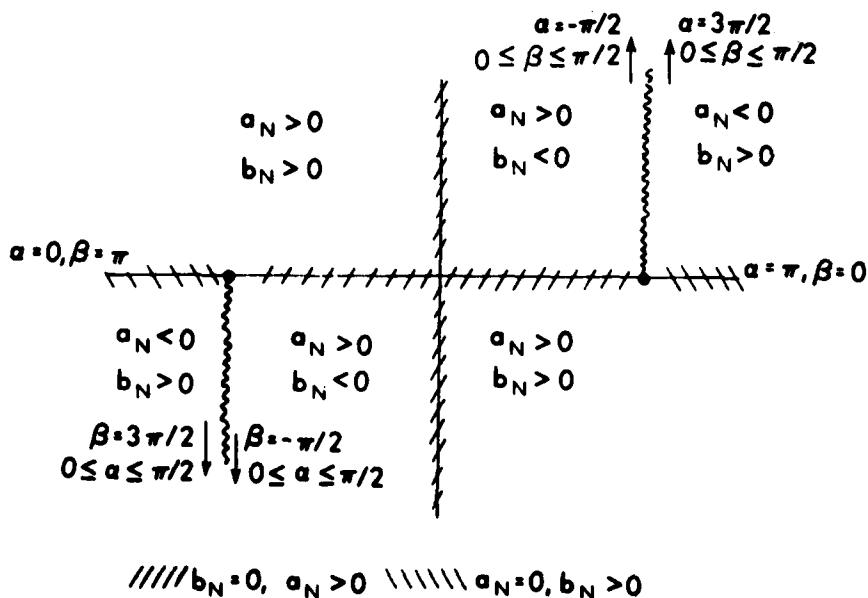


Figure 5. Definition of β for Pekeris Branch Cut

It can also be seen that the value of β_N approaches a purely real positive value on the left hand side of the branch cut in the first quadrant and a purely real negative value on the right hand side as $\xi_2 \rightarrow \infty$. Thus β_N assumes purely real values at the extremities of the branch cut and complex values elsewhere. In both cases, after indenting around the respective branch cuts, the contour is closed in the upper half plane.

Jordan's Lemma and the Pekeris Cuts

It is of some interest to examine β_N along some line connecting the branch cut and the positive imaginary axis as this line approaches infinity. For this purpose we introduce the equivalent definition of the square root,

$$\sqrt{R + iS} = T + i \operatorname{sign}(S) \frac{|S|}{2T}, \quad R > 0$$

$$\frac{|S|}{2T} + i \operatorname{sign}(S)T, \quad R < 0,$$

where

$$T = \left\{ \frac{R^2 + S^2 + R}{2} \right\}^{1/2}$$

and

$$\sqrt{R + iS} = +\sqrt{R} \quad \text{when } S=0.$$

Then, with $\xi = \xi_1 + i\xi_2$, in this sector

$$\sqrt{k_N - \epsilon} = \sqrt{R_1 - iS_1},$$

where $R_1 = k_N - \xi_1 > 0$, $S_1 = -\xi_2 < 0$ and

$$\sqrt{k_N - \epsilon} = T_1 - \frac{i|S_1|}{2T_1}.$$

Similarly

$$\sqrt{k_N + \epsilon} = \sqrt{R_2 + iS_2}, \quad R_2 = k_N + \epsilon_1 > 0, \quad S_2 = \epsilon_2 > 0.$$

Thus

$$\sqrt{k_N + \epsilon} = T_2 + \frac{i|S_2|}{2T_2},$$

and upon multiplication it is found that

$$\sqrt{k_N^2 - \epsilon^2} = \left(T_1 T_2 + \frac{\epsilon_2^2}{4T_1 T_2} \right) - \frac{\epsilon_2}{2} \left(\frac{T_2}{T_1} - \frac{T_1}{T_2} \right)$$

Since $T_2 > T_1$, it is seen that $a_N > 0$, $b_N < 0$, as it should be in this sector.

From

$$\frac{T_2}{T_1} = \left\{ \frac{\frac{R_2}{\epsilon_2} + 1 + \frac{R_2}{\epsilon_2}}{\frac{R_1}{\epsilon_2} + 1 + \frac{R_1}{\epsilon_2}} \right\}^{1/2}$$

it can be seen that

$$\lim_{\epsilon_2 \rightarrow \infty} \frac{T_2}{T_1} = 1$$

and $\epsilon_2 \rightarrow \infty$ $\lim b_N$ is indeterminate.

Application of L'Hospital's rule yields

$$\lim_{\epsilon_2 \rightarrow \infty} \left[-\frac{1}{2} \left(\frac{T_2}{T_1} - \frac{T_1}{T_2} \right)^2 \frac{d}{d\epsilon_2} \left(\frac{T_2}{T_1} - \frac{T_1}{T_2} \right) \right]$$

where

$$\frac{d}{d\epsilon_2} \left(\frac{T_2}{T_1} - \frac{T_1}{T_2} \right) = \left\{ x_1 - x_2 + \frac{x_1 \sqrt{x_1 + y_1} - x_2 \sqrt{x_2 + y_2}}{(x_1 + y_1)(x_2 + y_2)} \right\} / \left(2\epsilon_2^2 x_1 x_2 \sqrt{x_1 + y_1} \sqrt{x_2 + y_2} \right)$$

$$x_2 = \left\{ \left(\frac{R_2}{\epsilon_2} \right)^2 + 1 \right\}^{1/2}, \quad y_2 = R_2/\epsilon_2$$

$$x_1 = \frac{R_1}{\epsilon_2} + 1, \quad y_1 = R_1/\epsilon_2$$

and

$$\lim_{\epsilon_2 \rightarrow \infty} \frac{d}{d\epsilon_2} \left(\frac{T_2}{T_1} - \frac{T_1}{T_2} \right) = \frac{1}{\epsilon_2}$$

Thus

$$\lim_{\epsilon_2 \rightarrow \infty} b_N \rightarrow 0$$

The behavior of the integrand is now examined for the case $LS = LR = N, z > z_S$. In this case, both the source and receiver are in the lower semiinfinite half space. Here the depth dependent Green's function is found to be

$$G(z, z_S; \epsilon, \omega) = \frac{\tilde{F}_{LS}^S F_{LR}^Z}{W_{LS}},$$

where

$$\tilde{F}_{LS}^S = (iZ_N^N) \sin \beta_N (z_S - z_N) + \tilde{Z}_{N-1}^N \cos \beta_N (z_S - z_N)$$

$$F_{LR}^Z = -i e^{i\beta_N (z - z_N)} / \beta_N$$

$$W_{LS} = Z_N^N - \tilde{Z}_{N-1}^N$$

Recalling that in the sector under consideration $\beta_N = a_N - ib_N$, $\frac{\tilde{F}_{LS}^S}{W_{LS}}$ is rewritten as

$$\frac{F_{LS}^S}{W_{LS}} = \frac{e^{ia_N(z_S - z_N)} e^{b_N(z_S - z_N)} \left[\frac{z_N^N + \bar{z}_{N-1}^N}{z_N^N - \bar{z}_{N-1}^N} \right]}{e^{-ia_N(z_S - z_N)} e^{-b_N(z_S - z_N)}} \cdot \frac{1}{2}$$

and the total Green's function becomes

$$G(z_1, z_S; \epsilon_1, \omega) = \frac{\left[\frac{z_N^N + \bar{z}_{N-1}^N}{z_N^N - \bar{z}_{N-1}^N} \right]}{\left[\frac{z_N^N + \bar{z}_{N-1}^N}{z_N^N - \bar{z}_{N-1}^N} \right]} e^{ia_N(z + z_S - 2z_N)} e^{b_N(z + z_S - 2z_N)} - \frac{1}{2} e^{ia_N(z - z_S)} e^{b_N(z - z_S)},$$

where the first term represents the wave which initially started upwards struck the boundary at $z = z_N$. At this point, its amplitude is modified by the reflection coefficient referenced to that level and then propagates downward. The second term, of course, corresponds to the direct wave which propagates downward from the source.

When this information is coupled with the first term on the asymptotic expansion for $H_0^{(1)}$, the portion of the integrand corresponding to the direct path is

$$-\frac{1}{2} e^{i \left[a_N(z - z_S) + \epsilon_1 r \right]} e^{- \left[\epsilon_2 r - b_N(z - z_S) \right]}$$

In all other regions of the upper half complex plane, b_N has the opposite sign of that above and Jordan's Lemma would be satisfied for z finite. Without regard to the behavior of b_N as $\epsilon_2 \rightarrow \infty$, it would appear that, unless r is sufficiently large, Jordan's Lemma would not be satisfied in the sector which gives rise to the leaky modes. However, on recalling that

$$\lim_{\epsilon_2 \rightarrow \infty} b_N = 0,$$

it is seen that Jordan's Lemma is satisfied in this region for z finite as well. Beyond this, it is noted that, if $z = z_S$ the direct wave satisfies Jordan's Lemma irrespective of the sign of b_N .

The mathematically esoteric problem of the satisfaction of Jordan's Lemma in the case of z becoming infinite is not considered. In this case, the model itself is of questionable physical value.

Now that the behavior of the square root, β_N , on the top Riemann sheet has been specified, it is possible to obtain explicit results for the branch cut integrals. It becomes necessary to evaluate

$$\frac{S_\omega}{4\pi} \int G(z, z_S; \xi, \omega) H_0^{(1)}(\xi r) \xi d\xi$$

along paths on either side of the branch cut in the upper half plane. For this evaluation, the formulation of the Green's function equation (37) will be used. The equation explicitly displays the dependence upon the terminal impedance Z_N . Next we introduce the abbreviations

$$\begin{pmatrix} A & B \\ C & D \end{pmatrix} = K_1^{N-1} = \prod_{p=1}^{N-1} M_p(a, b)$$

$$\begin{pmatrix} E & F \\ G & H \end{pmatrix} = K_1^{LS} \phi_{LS} \phi_{LR} K_{LR+1}^{N-1}$$

Then Green's function may be expressed as

$$G(z, z_S; \xi, \omega) = \frac{(E - G\bar{z}_0^1) + (F - H\bar{z}_0^1) Z_N^N}{(A - C\bar{z}_0^1) + (B - D\bar{z}_0^1) Z_N^N}$$

It is noted that for a pressure release surface $\bar{z}_0^1 = 0$.

For the Pekeris cut

$$\xi = k_N + i\tau, \quad 0 < \tau < \infty,$$

and on the right hand side of the cut, where

$$\sqrt{k_N - \xi} = \tau^{1/2} e^{-i\pi/4},$$

one obtains

$$\frac{1S_\omega}{4\pi} \int_0^\infty \left(\frac{A_1 + A_2}{A_3 + A_4} \right) EH_0^{(1)}(\xi r) d\tau,$$

where

$$A_1 = E - GZ_0^{-1} \quad A_2 = (F - HZ_0^{-1}) \frac{\sqrt{k_N + \epsilon}}{\omega \rho_N} \tau^{1/2} e^{-i\pi/4}$$

$$A_3 = A - CZ_0^{-1} \quad A_4 = (B - DZ_0^{-1}) \frac{\sqrt{k_N + \epsilon}}{\omega \rho_N} \tau^{1/2} e^{-i\pi/4}$$

To the left of the cut

$$\sqrt{k_N - \epsilon} = -\tau^{1/2} e^{-i\pi/4}$$

which results in

$$\frac{iS_\omega}{4\pi} \int_0^\tau \left(\frac{A_1 - A_2}{A_3 - A_4} \right) \epsilon H_0^{(1)}(\epsilon r) d\tau$$

Reversing the limits of integration of the first integral and combining yields

$$\frac{iS_\omega}{2\pi} \int_0^\tau \frac{(EB - FA)}{Z_N^2 A^2 - (B/Z_N)^2} H_0^{(1)}(\epsilon r) \epsilon d\tau$$

With some straightforward but lengthy manipulation summarized below, this may be expressed in the same notation as that used for the residue series:

$$EB - FA = (1 \ 0) \begin{pmatrix} E & F \\ G & H \end{pmatrix} \begin{pmatrix} A & B \\ C & D \end{pmatrix}^{-1} \begin{pmatrix} 0 \\ -1 \end{pmatrix}$$

which, upon substitution for the 2×2 matrices, reduces to

$$EB - FA = (1 \ 0) K_1^{LS} \phi_{LS} \phi_{LR} \frac{1}{\pi} \prod_{p=LR} M_p^{(b,a)} \begin{pmatrix} 0 \\ -1 \end{pmatrix}$$

Now examine

$$F_{LR}^{LR+1} Q_{LR}(d,b) + \bar{U}_{LR}^{LR+1} P_{LR}(d,b) = (Q_{LR}(d,b) P_{LR}(d,b)) \begin{pmatrix} \bar{F}_{LR}^{LR+1} \\ \bar{U}_{LR}^{LR+1} \end{pmatrix}.$$

Substituting for the column matrix from equation (58) with $N - 1 = LR$ and setting $\bar{Z}_1 = 0$ yields

$$- \frac{F_{LR}^{LR+1} Q_{LR}(d,b) + \bar{U}_{LR}^{LR+1} P_{LR}(d,b)}{\bar{U}_1} = \phi_{LR} \prod_{p=LR}^1 M_p(b,a) \begin{pmatrix} 0 \\ -1 \end{pmatrix}.$$

Next rewrite the source term as

$$\left[\bar{F}_{LS}^{LS+1} Q_{LS}(e,b) + \bar{U}_{LS}^{LS+1} P_{LS}(e,b) \right] = \begin{pmatrix} \bar{F}_{LS}^{LS+1} & \bar{U}_{LS}^{LS+1} \\ 1 & 0 \end{pmatrix} \begin{pmatrix} 0 & -1 \\ 1 & 0 \end{pmatrix} \phi_{LS}.$$

With the use of equation (58) with $N - 1 = LS$ and the identity

$$M_k^T(b,a) \begin{pmatrix} 0 & -1 \\ 1 & 0 \end{pmatrix} = \begin{pmatrix} 0 & -1 \\ 1 & 0 \end{pmatrix} M_a(a,b)$$

this term may be expressed as

$$\left[\bar{F}_{LS}^{LS+1} Q_{LS}(e,b) + \bar{U}_{LS}^{LS+1} P_{LS}(e,b) \right] = (1 \ 0) K_1^{LS} \phi_{LS}.$$

The numerator of the Green's function is then given by

$$EB - FA = - \frac{\left[\bar{F}_{LS}^{LS+1} Q_{LS}(e,b) + \bar{U}_{LS}^{LS+1} P_{LS}(e,b) \right] \left[\bar{F}_{LR}^{LR+1} Q_{LR}(d,b) + \bar{U}_{LR}^{LR+1} P_{LR}(d,b) \right]}{(\bar{U}_1)^2}.$$

The denominator of that function may be written as

$$z_N^N \left[A^2 - (B/z_N^N)^2 \right] = -(z_N^N)^{-1} \left[B^2 - A(z_N^N)^2 \right],$$

or, equivalently, in matrix notation as

$$\begin{aligned} & (z_N^N)^{-1} \begin{pmatrix} -z_N^N & 1 \end{pmatrix} \begin{pmatrix} A \\ B \end{pmatrix} \begin{pmatrix} A & B \end{pmatrix} \begin{pmatrix} z_N^N \\ 1 \end{pmatrix} \\ &= (z_N^N)^{-1} \begin{pmatrix} -z_N^N & 1 \end{pmatrix} \begin{pmatrix} A & B \\ C & D \end{pmatrix}^T \begin{pmatrix} 1 & 0 \\ 0 & 0 \end{pmatrix} \begin{pmatrix} A & B \\ C & D \end{pmatrix} \begin{pmatrix} z_N^N \\ 1 \end{pmatrix}. \end{aligned}$$

Utilizing the fact that

$$\prod_{p=N-1}^1 M_p^T(a,b) = \begin{pmatrix} 0 & -1 \\ 1 & 0 \end{pmatrix} \prod_{p=N-1}^1 M_p(b,a) \begin{pmatrix} 0 & 1 \\ -1 & 0 \end{pmatrix}$$

yields

$$(z_N^N)^{-1} \prod_{p=N-1}^1 M_p(b,a) \begin{pmatrix} 0 \\ 1 \end{pmatrix} \begin{pmatrix} -1 & 0 \end{pmatrix} \prod_{p=1}^{N-1} M_p(a,b) \begin{pmatrix} z_N^N \\ 1 \end{pmatrix}$$

and upon substitution from equation (58)

$$(z_N^N)^{-1} \begin{pmatrix} 1 & z_N^N \end{pmatrix} \begin{pmatrix} \bar{F}_{N-1}^N \\ \bar{U}_{N-1}^N \end{pmatrix} \bar{F}_{N-1}^N \bar{U}_{N-1}^N \begin{pmatrix} 0 & -1 \\ 1 & 0 \end{pmatrix} \begin{pmatrix} -z_N^N \\ -1 \end{pmatrix}.$$

Finally, then, the denominator of the Green's function is

$$z_N^N \left[A^2 - (B/z_N^N)^2 \right] = \left[(\bar{U}_{N-1}^N)^2 - (\bar{F}_{N-1}^N/z_N^N)^2 \right] \frac{z_N^N}{(u_1^N)^2}.$$

The Pekeris branch cut integral is then

$$\lim_{\tau \rightarrow \infty} \frac{-iS}{2\pi} \int_0^{\tau} \omega$$

$$\frac{[\tilde{F}_{LS}^{LS+1} Q_{LS}(e,b) + \tilde{U}_{LS}^{LS+1} P_{LS}(e,b)] [\tilde{F}_{LR}^{LR+1} Q_{LR}(d,b) + \tilde{U}_{LR}^{LR+1} P_{LR}(d,b)] \epsilon H_0^{(1)}(\epsilon r) d\tau}{[(\tilde{U}_{N-1}^N)^2 - (\tilde{F}_{N-1}^N/Z_N^N)^2] Z_N^N}$$

where $\xi = k_N + i\tau$

$$Z_N^N = \frac{\omega \rho_N}{\sqrt{k_N + \xi} \tau^{1/2} e^{-i\pi/4}}, \quad (Z_N^N)^2 = \frac{(\omega \rho_N)^2}{k_N^2 - \xi^2}$$

The form of the Green's function given by equation (37) may also be used to arrive at the EJP branch cut integral obtained by Stickler.²⁴ In this case, explicit expressions are found for the integrals along the real and imaginary axis. Above the real axis let

$$\xi = \tau \quad 0 < \tau < k_N$$

$$\sqrt{k_N - \xi} = \rho_1$$

while below,

$$\sqrt{k_N - \xi} = -\rho_1.$$

Following the same procedure used with the Pekeris cut, one obtains for the branch cut integral along the real axis

$$\frac{S}{2\pi} \int_0^{k_N} \frac{[\tilde{F}_{LS}^{LS+1} Q_{LS}(e,b) + \tilde{U}_{LS}^{LS+1} P_{LS}(e,b)] [\tilde{F}_{LR}^{LR+1} Q_{LR}(d,b) + \tilde{U}_{LR}^{LR+1} P_{LR}(d,b)]}{[(\tilde{U}_{N-1}^N)^2 - (\tilde{F}_{N-1}^N)^2] \frac{k_N^2 - \tau^2}{(\omega \rho_N)^2}}$$

$$\times \frac{\sqrt{k_N^2 - \tau^2}}{\omega \rho_N} \tau H_0^{(1)}(\tau r) d\tau.$$

This is identical to Stickler's²⁴ integral containing $C_1(k)$ upon multiplying that answer by $i\omega_0 S_\omega$, substituting for the difference in the notation given earlier in this section, and noting that an extra multiplicative factor of k appears in Stickler's result.

For the integral on that portion of the branch cut along the positive imaginary axis, let

$$\xi = i\tau$$

$$\sqrt{k_N - \xi} = \sqrt{k_N - i\tau}$$

on the right hand edge, and let

$$\sqrt{k_N - \xi} = -\sqrt{k_N - i\tau}$$

on the left hand edge. The result is identical to the Pekeris branch cut integral except for the translation in ξ :

$$\lim_{\tau \rightarrow \infty} \frac{-(S_\omega)}{\pi^2} \int_0^\tau$$

$$\frac{[\bar{F}_{LS}^{LS+1} Q_{LS}(e,b) + \bar{U}_{LS}^{LS+1} P_{LS}(e,b)] [\bar{F}_{LR}^{LR+1} Q_{LR}(d,b) + \bar{U}_{LR}^{LR+1} P_{LR}(d,b)]}{[(\bar{U}_{N-1}^N)^2 - (\bar{F}_{N-1}^N)^2 \frac{(k_N^2 + \tau^2)}{(\omega \rho_N)^2}]}$$

$$\times \sqrt{\frac{k_N^2 + \tau^2}{\omega \rho_N}} K_0(\tau r) d\tau .$$

Numerical Considerations

As one might expect, the implementation problems are roughly similar for all normal mode programs. Thus a summary of one program, in this case Bartberger's²⁶ AP2 program, should provide the reader with an overall feeling for what might be expected in general. The reader interested in greater detail should consult reference 26.

In AP2, the effect of the ocean bottom is accounted for in one of two ways: (1) an empirical bottom represented by a bottom reflection loss curve as a function of grazing angle at a given CW frequency or (2) a physical ocean bottom consisting of up to 9 layers (excluding the semiinfinite half space; N^{th} layer in figure 1) with constant sound speed, density, and attenuation. The attenuation α is introduced by letting the wavenumber

$$k_p = \frac{\omega}{c_p} + i\alpha_p$$

be complex.

The AP2 program is broadly divided into a section for the computation of the eigenvalues and a section for the calculation of propagation loss. The execution time for each section is comparable. The maximum number of modes allowed is 500, a number sufficient for typical deep ocean problems at frequencies below approximately 100 Hz. Excluded are the higher order modes ($m > 500$ in the residue summation) which introduce an error at the short bottom bounce ranges but not beyond. The attenuation (α_ω dB/distance) within the water column, which is small at these frequencies, is initially set to zero. Later the attenuation is accounted for by adding the term $\alpha_\omega r$ to the propagation loss calculation. Almost all the limitations imposed upon the applicability of normal mode programs stem from the difficulty encountered in numerically locating the eigenvalues which are the zeros of the Wronskian $W_{N-1}(\xi)$,

$$W_{N-1}(\xi) = \tilde{U}_{N-1}^N - \tilde{F}_{N-1}^N / Z_N^N,$$

appearing in the denominator of equation (51). This is done iteratively. An initial estimate $(\tilde{\xi}_m)_i$ is made and the $\tilde{F}_{N-1}^N((\tilde{\xi}_m)_i)$ and $\tilde{U}_{N-1}^N((\tilde{\xi}_m)_i)$ are found from equation (58) where $\tilde{F} = 0$ pressure release and surface \tilde{U} is an arbitrary normalization constant which is properly accounted for in the Green's function formulation. In addition, the derivatives of these functions with respect to ξ are also calculated with the aid of equation (59). The initial conditions assumed by Bartberger²⁶ in this case are $\partial F / \partial \xi = \partial \tilde{U} / \partial \xi = 0$. Since $W_{N-1}((\tilde{\xi}_m)_i)$ will in general not be zero, a new estimate $(\tilde{\xi}_m)_{i+1}$ is obtained from

$$(\tilde{\xi}_m)_{i+1} = (\tilde{\xi}_m)_i - \frac{W_{N-1}}{\frac{\partial W_{N-1}}{\partial \xi}} \bigg|_{(\tilde{\xi}_m)_i},$$

where the derivative of the Wronskian with respect to ξ is given by equation (54). The iterations are terminated when the modulus of the last term in the above equation falls below a preset minimum value.

If the initial estimates are not sufficiently accurate, the above procedure may fail to converge and the mode will be missed. Alternatively, it may converge to the wrong mode resulting in a duplicate eigenvalue. If the eigenvalues are evenly spaced, it is usually sufficient to obtain initial estimates by extrapolating from previously found eigenvalues. This procedure is used for higher order modes (phase velocity exceeding the maximum sound speed, including that of the first bottom layer). The spacing of the eigenvalues for lower order modes may be sufficiently irregular to render this procedure unreliable. In response to this, Bartberger²⁶ has devised a scheme for obtaining initial estimates of these modes based upon Wentzel, Kramers, and Brillouin (WKB) approximations which explicitly display the mode number. The total phase of the mode depth function is calculated for a

two-way transit from ocean surface to bottom. Included are the phase changes in the oscillatory region both between and at mode turning points and discrete phase shifts at ocean boundaries. The value of ξ is varied iteratively until the round trip phase change equals $\alpha(m-1)\tau$. If multiple sound channels which give rise to different families of trapped modes exist, the AP2 scheme computes the phase changes in all channels. Except for a few isolated instances of complete failure, this process provides the initial estimates of the eigenvalues rapidly. The failures have been observed to occur in instances when ξ is very close to the wavenumber at one of the layer boundaries. This case must also be treated with care in the multipath expansion programs and has been examined by Tolstoy.²⁷ In this case, successive values for the initial estimate oscillate around this wavenumber. Bartberger²⁶ then switches to an extrapolated value based upon previously computed eigenvalues.

The WKB iterations for the first mode begin with the initial estimate $\tilde{\xi}_0 = \omega/(V_{\text{MIN}} + \epsilon)$, where V_{MIN} is normally equal to the minimum sound speed. However, deep water problems are frequently encountered for which a number of low order modes are weakly excited. This results from the fact that their phase velocities are appreciably less than the sound speed at the source and receiver depths. In such instances, an algorithm exists which excludes the calculation of the associated eigenvalues.

DEPTH DEPENDENT GREEN'S FUNCTION (TRAVELING WAVE FORMULATION)

Summarized in this section are results for the depth dependent Green's function analogous in form to equation (36), but expressed in terms of *generalized reflection coefficients* instead of impedances.

The matrix $\tilde{\psi}_k(z)$ above the source may be expressed directly in terms of the fundamental solutions by using equations (18), (19), and (21):

$$\tilde{\psi}_k(z) = \begin{pmatrix} f_k(\gamma_k^z) & g_k(\gamma_k^z) \\ (Df)_k^z & (Dg)_k^z \end{pmatrix} \begin{pmatrix} f_k(\gamma_k^{z_k}) & g_k(\gamma_k^{z_k}) \\ (Df)_k^{z_k} & (Dg)_k^{z_k} \end{pmatrix}^{-1} \begin{pmatrix} \tilde{F}_{k-1}^k \\ \tilde{U}_{k-1}^k \end{pmatrix}, \quad z_k < z < z_{k+1}. \quad (60)$$

The above expression may then be put into the form

$$\tilde{\psi}_k(z) = \begin{pmatrix} f_k(\gamma_k^z) & g_k(\gamma_k^z) \\ (Df)_k^z & (Dg)_k^z \end{pmatrix} \begin{pmatrix} \tilde{R}_k^k \\ 1 \end{pmatrix} \tilde{\Delta}_k, \quad \tilde{\Delta}_k = \frac{-(Df)_k^k \tilde{F}_{k-1}^k + f_k(a) \tilde{U}_{k-1}^k}{(Dg)_k^k f_k(a) - g_k(a) (Df)_k^k}. \quad (61)$$

The *generalized reflection coefficient* in the k^{th} layer evaluated at z_k is

$$\tilde{R}_k^k = - \frac{(Dg)_k^k}{(Df)_k^k} \frac{[z_{k-1}^k - g_k(a)/(Dg)_k^k]}{[z_{k-1}^k - f_k(a)/(Df)_k^k]}, \quad a = \gamma_k^k, \quad (62)$$

where f_k and g_k are chosen to be independent traveling wave solutions (reference 2) to $\mathcal{L}(\cdot) = 0$. The ratios $g_k(a)/(Dg)_k^k$ and $f_k(a)/(Df)_k^k$ are partial impedances whose importance will be discussed shortly. The physical interpretation of \tilde{R}_k^k (and its counterpart R_k^{k+1} soon to be introduced) continues to be the subject of considerable discussion (see references 28-33). For constant sound speed and density layers, the partial impedances are independent of depth and it is possible to uniquely separate upgoing and downgoing waves. Thus the angle between the normal to the surface of constant phase and the vertical remains the same throughout the layer. For example, a wave which initially moves in a downward direction never changes its direction of propagation within a layer. The reflection coefficient is thus independent of depth. It may be thought of as originating at the boundary where a mismatch occurs between the local partial impedances and the total impedance Z_{k-1}^k of the medium above. When the product of sound speed and density is a function of depth, the *generalized reflection coefficient* is also a function of depth through the partial impedances. Thus reflection occurs at all depths within the layer, as well as at the boundary. Functions f_k and g_k can then be written as having upgoing and downgoing components. It is apparent that the ratio f_k/g_k or vice versa cannot be interpreted in the same manner as that of constant sound speed and density layers.

In underwater acoustics, however, the *generalized reflection coefficients* have been and continue to be treated as if they were identical to the plane wave counterparts. The error of this approximation has recently become apparent, as evidenced by determination of negative experimental values for bottom loss (see reference 34).

With this short dialogue firmly established, the word *generalized* will be abandoned for the remainder of the section.

Proceeding in exactly the same manner used for $\tilde{\psi}_k$, the solution below the source may be reexpressed in the form

$$\psi_k(z) = \begin{pmatrix} f_k(\gamma_k^z) & g_k(\gamma_k^z) \\ (Df)_k^z & (Dg)_k^z \end{pmatrix} \begin{pmatrix} 1 \\ R_k^{k+1} \end{pmatrix} \Delta_k, \quad b = \gamma_k^{k+1}, \quad (63)$$

where

$$\Delta_k = \frac{(Dg)_k^{k+1} f_{k+1}^{k+1} - g_k(b) u_{k+1}^{k+1}}{(Dg)_k^{k+1} f_k(b) - g_k(b) (Df)_k^{k+1}},$$

and

$$R_k^{k+1} = \frac{-(Df)_k^{k+1}}{(Dg)_k^{k+1}} \frac{[z_{k+1}^{k+1} - f_k(b)/(Df)_k^{k+1}]}{[z_{k+1}^{k+1} - g_k(b)/(Dg)_k^{k+1}]}. \quad (64)$$

The reflection coefficients in any layer may be written in terms of the reflection coefficients in any other layer and, ultimately, in terms of the terminal values. To accomplish this, the matrix form of equation (62),

$$\begin{pmatrix} \tilde{R}_k^k \\ 1 \end{pmatrix} = \frac{\begin{pmatrix} -(Dg)_k^k & g_k(a) \\ (Df)_k^k - f_k(a) \end{pmatrix} \begin{pmatrix} \tilde{z}_{k-1}^k \\ 1 \end{pmatrix}}{[\tilde{z}_{k-1}^k (Df)_k^k - f_k(a)]} \quad (65)$$

is introduced. A similar equation involving \tilde{z}_{k+1}^k results for \tilde{R}_k^k . If equation (24) is used to express \tilde{R}_k^k in terms of \tilde{z}_{k+1}^k and if that expression is substituted into equation (65), one finds that

$$\begin{pmatrix} \tilde{R}_{k+1}^k \\ 1 \end{pmatrix} = \begin{pmatrix} -(Dg)_{k+1}^k & g_{k+1}(a) \\ (Df)_{k+1}^k - f_{k+1}(a) \end{pmatrix} M_k(b,a) \begin{pmatrix} f_k(a) & g_k(a) \\ (Df)_k^k & (Dg)_k^k \end{pmatrix} \begin{pmatrix} \tilde{R}_k^k \\ 1 \end{pmatrix} \tilde{\lambda}_k$$

where the constant $\tilde{\lambda}_k$ is found to be

$$\tilde{\lambda}_k = \frac{[\tilde{z}_{k-1}^k (Df)_k^k - f_k(a)]}{[\tilde{z}_k^{k+1} (Df)_{k+1}^k - f_{k+1}(a)] [\tilde{z}_{k-1}^k S_k(b,a) + R_k(b,a)] W[g_k, f_k; z_k]}$$

and the function $W[g_k, f_k, z_k]$ is the Wronskian of the fundamental solutions evaluated at z_k . With some additional algebraic manipulations, it can also be shown that

$$\begin{aligned} \tilde{\lambda}_k = & \left\{ \tilde{R}_k^k \left[(Df)_{k+1}^k f_k(b) - f_{k+1}(a) (Df)_k^{k+1} \right] \right. \\ & \left. + \left[(Df)_{k+1}^k g_k(b) - f_{k+1}(a) (Df)_k^{k+1} \right] \right\}^{-1} \end{aligned}$$

The desired relationship may then be abbreviated as

$$\begin{pmatrix} \tilde{R}_{k+1}^k \\ 1 \end{pmatrix} = \frac{\begin{pmatrix} \tilde{A}_k & \tilde{B}_k \\ \tilde{C}_k & \tilde{D}_k \end{pmatrix} \begin{pmatrix} \tilde{R}_k^k \\ 1 \end{pmatrix}}{[\tilde{R}_k^k \tilde{C}_k + \tilde{D}_k]} \quad (66)$$

where

$$\begin{pmatrix} \tilde{A}_k & \tilde{B}_k \\ \tilde{C}_k & \tilde{D}_k \end{pmatrix} = \begin{pmatrix} -(Dg)_{k+1}^{k+1} & g_{k+1}(a) \\ (Df)_{k+1}^{k+1} & -f_{k+1}(a) \end{pmatrix} \begin{pmatrix} f_k(b) & g_k(b) \\ (Df)_k^{k+1} & (Dg)_k^{k+1} \end{pmatrix}$$

Another common form of the above relationship is

$$\frac{(Df)_{k+1}^{k+1}}{(Dg)_{k+1}^{k+1}} \tilde{R}_{k+1}^{k+1} = \frac{\tilde{r}_{k+1}^{k+1} - \tilde{R}_k^k \frac{(Df)_k^{k+1}}{(Dg)_k^{k+1}} [1 + \tilde{r}_{k+1}^{k+1} + \tilde{r}_k^{k+1}]}{1 + \tilde{R}_k^k \frac{(Df)_k^{k+1}}{(Dg)_k^{k+1}} \tilde{r}_k^{k+1}}$$

where \tilde{r}_{k+1}^{k+1} is a local reflection coefficient in the $(k+1)^{st}$ layer evaluated at z_{k+1}

$$\tilde{r}_{k+1}^{k+1} = \frac{\left[\frac{g_k(b)}{(Dg)_k^{k+1}} - \frac{g_{k+1}(a)}{(Dg)_{k+1}^{k+1}} \right]}{\left[\frac{f_{k+1}(a)}{(Df)_{k+1}^{k+1}} - \frac{g_k(b)}{(Dg)_k^{k+1}} \right]}$$

and \tilde{r}_k^{k+1} the local reflection coefficient in the k^{th} layer evaluated at z_{k+1}

$$\tilde{r}_k^{k+1} = \frac{\left[\frac{f_k(b)}{(Df)_k^{k+1}} - \frac{f_{k+1}(a)}{(Df)_{k+1}^{k+1}} \right]}{\left[\frac{f_{k+1}(a)}{(Df)_{k+1}^{k+1}} - \frac{g_k(b)}{(Dg)_k^{k+1}} \right]}$$

The expression relating \tilde{R}_k^k to the terminal reflection coefficient \tilde{R}_1^1 follows directly from equation (66) and is found to be

$$\begin{pmatrix} \tilde{R}_{k+1}^{k+1} \\ 1 \end{pmatrix} = \begin{pmatrix} -(Dg)_{k+1}^{k+1} & g_{k+1}(a) \\ (Df)_{k+1}^{k+1} & -f_{k+1}(a) \end{pmatrix} \prod_{p=k}^1 M_p(b,a) \begin{pmatrix} f_1(a) & g_1(a) \\ (Df)_1^1 & (Dg)_1^1 \end{pmatrix} \begin{pmatrix} \tilde{R}_1^1 \\ 1 \end{pmatrix}$$

$$\frac{\prod_{p=k}^2 W[g_p, f_p; z_p]}{\prod_{p=k} [R_p^p \tilde{C}_p + \tilde{D}_p]} \quad (67)$$

Results for the coefficient below the source are obtained in the same manner and given by

$$\frac{(Dg)_{k-2}^{k-1}}{(Df)_{k-2}^{k-1}} R_{k-2}^{k-1} = \frac{r_{k-2}^{k-1} + \frac{(Dg)_{k-1}^{k-1}}{(Df)_{k-1}^{k-1}} R_{k-1}^k [1 + r_{k-2}^{k-1} + r_{k-1}^{k-1}]}{1 - \frac{(Dg)_{k-1}^{k-1}}{(Df)_{k-1}^{k-1}} R_{k-1}^k r_{k-1}^{k-1}}$$

$$r_{k-2}^{k-1} = \left[\frac{f_{k-1}(a)}{(Df)_{k-1}^{k-1}} - \frac{f_{k-2}(b)}{(Df)_{k-2}^{k-1}} \right] / \left[\frac{g_{k-2}(b)}{(Dg)_{k-2}^{k-1}} - \frac{f_{k-1}(a)}{(Df)_{k-1}^{k-1}} \right]$$

$$r_{k-1}^{k-1} = \left[\frac{g_{k-1}(a)}{(Dg)_{k-1}^{k-1}} - \frac{g_{k-2}(b)}{(Dg)_{k-2}^{k-1}} \right] / \left[\frac{g_{k-2}(b)}{(Dg)_{k-2}^{k-1}} - \frac{f_{k-1}(a)}{(Df)_{k-1}^{k-1}} \right]$$

The term $\frac{(Dg)_{k-2}^{k-1}}{(Df)_{k-2}^{k-1}} R_{k-2}^{k-1}$ is a reflection coefficient measured at the level z_{k-1} but referenced to the level z_{k-2} :

$$\begin{pmatrix} R_{k-2}^{k-1} \\ 1 \end{pmatrix} = \begin{pmatrix} -(Df)_{k-2}^{k-1} & f_{k-2}(b) \\ (Dg)_{k-2}^{k-1} & -g_{k-2}(b) \end{pmatrix} \prod_{p=k-1}^{N-1} M_p(a,b) \begin{pmatrix} g_{N-1}(b) & f_{N-1}(b) \\ (Dg)_{N-1}^N & (Df)_{N-1}^N \end{pmatrix} \begin{pmatrix} R_{N-1}^N \\ 1 \end{pmatrix} \quad (68)$$

$$\frac{\prod_{p=k-1}^{N-2} W[f_p, g_p; z_{p+1}]}{\prod_{p=k-1}^{N-1} [R_p^{p+1} C_p + D_p]}$$

where C_p and D_p are defined by the matrix equation,

$$\begin{pmatrix} A_p & B_p \\ C_p & D_p \end{pmatrix} = \begin{pmatrix} -(Df)_{p-1}^D & f_{p-1}(\gamma_{p-1}^D) \\ (Dg)_{p-1}^D & -g_{p-1}(\gamma_{p-1}^D) \end{pmatrix} \begin{pmatrix} g_p(\gamma_p^D) & f_p(\gamma_p^D) \\ (Dg)_p^D & (Df)_p^D \end{pmatrix}.$$

Satisfaction of the source conditions

$$F_{LS}^S - \bar{F}_{LS}^S = 0$$

$$U_{LS}^S - \bar{U}_{LS}^S = -1$$

yields

$$\begin{pmatrix} \Delta_{LS} \\ - \\ \Delta_{LS} \end{pmatrix} = \begin{pmatrix} a_{12} \\ a_{11} \end{pmatrix} (a_{11}a_{22} - a_{21}a_{12})^{-1}$$

$$a_{11} = [f_{LS}(e) + R_{LS}^{LS+1} g_{LS}(e)], \quad a_{12} = [f_{LS}(e) \bar{R}_{LS}^{LS} + g_{LS}(e)]$$

$$a_{21} = [(Df)_{LS}^S + R_{LS}^{LS+1} (Dg)_{LS}^S], \quad a_{22} = [(Df)_{LS}^S \bar{R}_{LS}^{LS} + (Dg)_{LS}^S]$$

from which the Wronskian of Green's function is found to be

$$a_{11}a_{22} - a_{21}a_{12} = W[f_{LS}, g_{LS}; z_S] [1 - \bar{R}_{LS}^{LS} R_{LS}^{LS+1}].$$

Green's function with both the source and receiver in the same layer ($LS = LR$) is

$$G(z, z_S) = \frac{[f_{LS}(\gamma_{LS}^z) \bar{R}_{LS}^{LS} + g_{LS}(\gamma_{LS}^z)] [f_{LS}(\gamma_{LS}^S) + R_{LS}^{LS+1} g_{LS}(\gamma_{LS}^S)]}{W[f_{LS}, g_{LS}; z_S] [1 - \bar{R}_{LS}^{LS} R_{LS}^{LS+1}]},$$

$$z_{LS} \leq z \leq z_S$$

$$G(z, z_s) = \frac{[f_{LS}(y_{LS}^z) + R_{LS}^{LS+1} g_{LS}(y_{LS}^z)] [f_{LS}(y_{LS}^s) \bar{R}_{LS}^{LS} + g_{LS}(y_{LS}^s)]}{W[f_{LS}, g_{LS}; z_s] [1 - \bar{R}_{LS}^{LS} R_{LS}^{LS+1}]}$$

(69)

$$z_s \leq z \leq z_{LS+1}$$

With $LR > LS$ the result is

$$G(z, z_s) = \frac{[f_{LR}(y_{LR}^z) + R_{LR}^{LR+1} g_{LR}(y_{LR}^z)] [f_{LS}(y_{LS}^s) \bar{R}_{LS}^{LS} + g_{LS}(y_{LS}^s)]}{W[f_{LS}, g_{LS}; z_s] [1 - \bar{R}_{LS}^{LS} R_{LS}^{LS+1}]} \Delta_{LS+1}^{LR}$$

(70)

where

$$\Delta_{LS+1}^{LR} = \prod_{p=LS+1}^{LR} \frac{[f_{p-1}(a) + R_{p-1}^p g_{p-1}(b)]}{[f_p(a) + R_p^{p+1} g_p(a)]}, \quad a = y_p^p, \quad b = y_{p-1}^p$$

The above results are identical to those obtained previously, equations (34), (35), and (36), with the impedance formulation.

In proving this equivalence, it is helpful to note that, whereas equation (62) expresses \bar{R}_k^k in terms of the impedance $Z_k^k - 1$, above, it can also be expressed in terms of Z_k^{k+1} as

$$\begin{pmatrix} \bar{R}_k^k \\ 1 \end{pmatrix} = \frac{\begin{pmatrix} -(Dg)_k^{k+1} & g_k(b) \\ (Df)_k^{k+1} & -f_k(b) \end{pmatrix} \begin{pmatrix} Z_k^{k+1} \\ 1 \end{pmatrix}}{[Z_k^{k+1} (Df)_k^{k+1} - f_k(b)]}$$

It will also be required to have a form of the Green's function, similar to equation (47), which explicitly displays the dependence upon the terminal reflection coefficients \bar{R}_1^1 and R_{N-1}^N . Substitution from equation (47) and the matrix form of equation (48) gives

$$\frac{\begin{pmatrix} \bar{R}_1^1 & 1 \end{pmatrix} \begin{pmatrix} f_1(a) & (Df)_1^1 \\ g_1(a) & (Dg)_1^1 \end{pmatrix} \begin{pmatrix} 0 & -1 \\ 1 & 0 \end{pmatrix} K_1^{LS} \Phi_{LS} \Phi_{LR} K_{LR+1}^{N-1} \begin{pmatrix} g_{N-1}(b) & f_{N-1}(b) \\ (Dg)_{N-1}^N & (Df)_{N-1}^N \end{pmatrix} \begin{pmatrix} R_{N-1}^N \\ 1 \end{pmatrix}}{\begin{pmatrix} \bar{R}_1^1 & 1 \end{pmatrix} \begin{pmatrix} f_1(a) & (Df)_1^1 \\ g_1(a) & (Dg)_1^1 \end{pmatrix} \begin{pmatrix} 0 & -1 \\ 1 & 0 \end{pmatrix} K_1^{N-1} \begin{pmatrix} g_{N-1}(b) & f_{N-1}(b) \\ (Dg)_{N-1}^N & (Df)_{N-1}^N \end{pmatrix} \begin{pmatrix} R_{N-1}^N \\ 1 \end{pmatrix}}$$

which is more useful when written in the form

$$\frac{\begin{pmatrix} 1-R_1^{-1} \\ \end{pmatrix} \begin{pmatrix} (Dg)_1^2 - g_1(b) \\ -(Df)_1^2 & f_1(b) \end{pmatrix} K_2^{LS} \phi_{LS} \phi_{LR} K_{LR+1}^{N-1} \begin{pmatrix} g_{N-1}(b) & f_{N-1}(b) \\ (Dg)_{N-1}^N & (Df)_{N-1}^N \end{pmatrix} \begin{pmatrix} R_{N-1}^N \\ 1 \end{pmatrix}}{\begin{pmatrix} 1-R_1^{-1} \\ \end{pmatrix} \begin{pmatrix} (Dg)_1^2 - g_1(b) \\ -(Df)_1^2 & f_1(b) \end{pmatrix} K_2^{N-1} \begin{pmatrix} g_{N-1}(b) & f_{N-1}(b) \\ (Dg)_{N-1}^N & (Df)_{N-1}^N \end{pmatrix} \begin{pmatrix} R_{N-1}^N \\ 1 \end{pmatrix}} \quad (71)$$

In order to provide some insight into the role played by the partial impedances, examine the inner product of matrices within $M_k(a,b) M_{k+1}(a,b)$. Then

$$\begin{pmatrix} (Dg)_k^{k+1} & -g_k(b) \\ -(Df)_k^{k+1} & f_k(b) \end{pmatrix} \begin{pmatrix} f_{k+1}(a) & g_{k+1}(a) \\ (Df)_{k+1}^{k+1} & (Dg)_{k+1}^{k+1} \end{pmatrix} =$$

$$\begin{pmatrix} f_{k+1}(a) g_k(b) \left[\frac{(Dg)_k^{k+1}}{g_k(b)} - \frac{(Df)_{k+1}^{k+1}}{f_{k+1}(a)} \right] & g_{k+1}(a) g_k(b) \left[\frac{(Dg)_k^{k+1}}{g_k(b)} - \frac{(Dg)_{k+1}^{k+1}}{g_{k+1}(a)} \right] \\ -f_{k+1}(a) f_k(b) \left[\frac{(Df)_k^{k+1}}{f_k(b)} - \frac{(Df)_{k+1}^{k+1}}{f_{k+1}(a)} \right] & g_{k+1}(a) f_k(b) \left[-\frac{(Df)_k^{k+1}}{f_k(b)} + \frac{(Dg)_{k+1}^{k+1}}{g_{k+1}(a)} \right] \end{pmatrix}$$

If the assumption is now made that the partial impedances are equal, i.e.,

$$\frac{(Df)_k^{k+1}}{f_k(b)} = \frac{(Df)_{k+1}^{k+1}}{f_{k+1}(a)} = \frac{(Dg)_k^{k+1}}{g_k(b)} = \frac{(Dg)_{k+1}^{k+1}}{g_{k+1}(a)}$$

then the diagonal terms reduce to

$$f_{k+1}(a) g_k(b) \left[\frac{(Dg)_k^{k+1}}{g_k(b)} - \frac{(Df)_{k+1}^{k+1}}{f_{k+1}(a)} \right] = \frac{g_k(b)}{g_{k+1}(a)} W[f_{k+1}, g_{k+1}; z_{k+1}]$$

$$g_{k+1}(a) f_k(b) \left[\begin{array}{c} (Df)_k^{k+1} \\ f_k(b) \end{array} + \frac{(Dg)_{k+1}^{k+1}}{g_{k+1}(a)} \right] = \frac{f_k(b)}{g_k(a)} W[f_{k+1}, g_{k+1}; z_{k+1}] ,$$

and the off diagonal terms are zero so that

$$\frac{\begin{pmatrix} (Dg)_k^{k+1} - g_k(b) \\ -(Df)_k^{k+1} & f_k(b) \end{pmatrix} \begin{pmatrix} f_{k+1}(a) g_{k+1}(a) \\ (Df)_{k+1}^{k+1} & (Dg)_{k+1}^{k+1} \end{pmatrix}}{W[f_k, g_k; z_{k+1}]} = \begin{pmatrix} \frac{g_k(b)}{g_{k+1}(a)} & 0 \\ 0 & \frac{f_k(b)}{f_{k+1}(a)} \end{pmatrix} W[f_{k+1}, g_{k+1}; z_{k+1}] ,$$

and in general

$$\begin{pmatrix} (Dg)_k^{k+1} - g_k(b) \\ -(Df)_k^{k+1} & f_k(b) \end{pmatrix} \prod_{p=k+1}^L M_p(a, b) = \begin{pmatrix} B_k^L & 0 \\ 0 & A_k^L \end{pmatrix} \begin{pmatrix} (Dg)_L^{L+1} - g_L(b) \\ -(Df)_L^{L+1} & f_L(b) \end{pmatrix} , \quad (72)$$

where

$$B_k^L = \frac{g_k(b)}{g_L(a)} \prod_{p=k+1}^{L-1} \left[\frac{g_p(b)}{g_p(a)} \right]$$

$$A_k^L = \frac{f_k(b)}{f_L(a)} \prod_{p=k+1}^{L-1} \left[\frac{f_p(b)}{f_p(a)} \right] .$$

If the above result is used in conjunction with

$$\begin{pmatrix} (Dg)_{LS}^{LS+1} - g_{LS}(b) \\ -(Df)_{LS}^{LS+1} & f_{LS}(b) \end{pmatrix} \phi_{LS} = \begin{pmatrix} g_{LS} & (\gamma_{LS}^S) \\ -f_{LS} & (\gamma_{LS}^S) \end{pmatrix}$$

and

$$\phi_{LR} \begin{pmatrix} f_{LR}^{(b)} & g_{LR}^{(b)} \\ (Df)_{LR}^{LR+1} & (Dg)_{LR}^{LR+1} \end{pmatrix} = \frac{(f_{LR}^{(y^z)} g_{LR}^{(y^z)})}{W[f_{LR}^{(y^z)} g_{LR}^{(y^z)}]} = \frac{(f_{LR}^{(y^z)} g_{LR}^{(y^z)})}{W[f_{LR}^{(y^z)} g_{LR}^{(y^z)}]}$$

in equation (71), one finds that the Green's function may be written in non-matrix form explicitly in terms of the terminal reflection coefficients:

$$G(z, z_s) = \frac{[A_1^{LS} f_{LS}^S(\gamma_{LS}) \tilde{R}_1^1 + B_1^{LS} g_{LS}^S(\gamma_{LS})] [B_{LR}^{N-1} f_{LR}^Z(\gamma_{LR}) + A_{LR}^{N-1} R_{N-1}^N g_{LR}^Z(\gamma_{LR})]}{W[f_{LR}^{(y^z)} g_{LR}^{(y^z)}] B_1^{N-1} [1 - \frac{A_1^{N-1}}{B_1^{N-1}} \tilde{R}_1^1 R_{N-1}^N]} \quad (73)$$

In making the assumption of continuity of partial impedances in equations (67) and (68), one also finds that

$$\tilde{R}_{k+1}^{k+1} = \frac{A_1^{k+1}}{B_1^{k+1}} \tilde{R}_1^1, \quad R_{k-2}^{k-1} = \frac{A_{k-2}^{N-1}}{B_{k-2}^{N-1}} R_{N-1}^N$$

In order to carry the analysis further, specific forms for the fundamental solutions are required. For the moment let these solutions be represented by the WKB approximations. In order to avoid the problem of their validity at turning points, attention can be limited to values of ξ associated with bottom bounce energy for which no turning point exists between z_1 and z_N . Then it can be seen that

$$f_k(z) = \rho^{1/2}(z) q_k^{-1/4}(z) \exp[i(\phi_k^z + \pi/4)], \quad g_k(z) = \rho^{1/2}(z) q_k^{-1/4}(z) \exp[-i(\phi_k^z + \pi/4)]$$

$$q_k(z) = (\omega^2/c_k^2(z) - \nu\rho(z) \frac{d^2}{dz^2} \left(\frac{1}{\nu\rho(z)} \right) - \epsilon^2), \quad \phi_k^z = \int_k^z q_k^{1/2}(t) dt \quad (74)$$

and the partial impedances are found to be

$$(Df)_k^z / f_k(z) = i q_k^{1/2}(z) - \frac{1}{4} (q_k^{-1/2}(z) dq_k/dz)$$

$$(Dg)_k^z / g_k(z) = -iq_k^{1/2}(z) - \frac{1}{4} (q_k^{-1/2}(z) dq_k/dz).$$

Continuity of the partial impedances is obtained if

$$q_k^{1/2}(z_{k+1}) = q_{k+1}^{1/2}(z_{k+1})$$

and

$$dq_k/dz = dq_{k+1}/dz \quad \text{at } z = z_{k+1},$$

i.e., the sound speed and its first derivative with respect to depth must be continuous in addition to the density. Assuming this to be the case, it is a straightforward matter to verify that Green's function reduces to

$$G(z, z_s) = \frac{q_{LS}^{-1/4}(z_s) \left[e^{i[\phi_1^s + \pi/4]} \bar{R}_1^{-1} + e^{-i[\phi_1^s + \pi/4]} \right] q_{LR}^{-1/4}(z) \left[e^{i[\phi_{N-1}^z + \pi/4]} \bar{R}_{N-1}^N + e^{-i[\phi_{N-1}^z + \pi/4]} \right]}{W[f_{LR}, g_{LR}; z_{LR+1}] e^{-i\phi_1^{N-1}} [1 - \bar{R}_1^N \bar{R}_{N-1}^N] e^{2i\phi_1^{N-1}}}$$

(75)

where

$$W[f_{LR}, g_{LR}; z_{LR+1}] = -2i, \quad \bar{R}_{k-2}^{k-1} = e^{2i\phi_{k-2}^{N-1}} \bar{R}_{N-1}^N, \quad \bar{R}_{k+1}^{k+1} = e^{2i\phi_1^{k+1}} \bar{R}_1^{-1}.$$

Thus the absolute magnitude of the reflection coefficient at any level (with no turning points) below the source equals that of the reflection coefficient at the bottom and, similarly, above the source. Furthermore, the resulting equation (75) is identical to that which would be obtained if, instead of layering, the fundamental solutions over the entire interval ($z_1 \leq z \leq z_N$) were approximated by WKB solutions. For this approach to be useful, the sound speed and its first derivative plus the density must be continuous throughout the interval. Alternatively, if a discontinuity in the local partial impedances exists at any level, it gives rise to a reflection at that level whose magnitude is frequency dependent.

The sound speed in the deep water column has generally been thought to exhibit a smooth behavior with the possible exception occurring at the bottom of a surface duct. However, recent developments in the study of sound speed microstructure (see reference 35) show that the sound speed can exhibit a step like behavior in both the lower and upper portions of the water column. Two alternatives suggest themselves to properly account for the effects caused by such a sound speed structure utilizing the approach which approximates the fundamental solutions over the entire interval: (1) more terms would have to be introduced into the approximate solution or (2) the sound speed profile would have to be layered over the appropriate depth intervals.

MULTIPATH EXPANSION MODELS

The models to be discussed in this section use a combination of wave and ray theory. The mathematics involved is concerned with expanding the kernel of the field integral in terms of an infinite series of integrals (sometimes referred to as the Rainbow or Debye expansion (see references 36-44)) which correspond to various types of multiple reflections. Weinberg⁴⁵ does not consider the sound speed profile to be layered except under some special instances which are to be taken up separately. Instead, approximate solutions for f and g are found for the entire depth interval $z_1 < z < z_N$. These are then used to construct the depth dependent Green's function. Weinberg's model of the ocean with respect to figure 2 would consist of the 3 layers air, water, and bottom, with the water layer contained between z_1 and z_2 . In this case LS is always equal to LR. From equation (69), the depth dependent Green's function above the source is

$$G(z, z_s) = \frac{[f_1(z)R_1^1 + g_1(z)] [f_1(z_s) + R_1^2 g_1(z_s)]}{W[f_1, g_1; z_s] [1 - R_1^1 R_1^2]}, \quad z_1 < z < z_s. \quad (76)$$

The solution for one of the functions used in the program,

$$f_1(z) = CV_0(z) \{B1(\gamma^2) + jA1(\gamma^2)\}, \quad (77)$$

arises from taking the first term of an asymptotic expansion. The constant C is defined as

$$C = \pi^{1/2} \omega^{1/6} e^{j\omega Q(z_0, z_t; \lambda)} e^{-j\pi/4} \quad \text{and} \quad Q(a, b; \lambda) = \int_a^b [c^{-2}(z) - \lambda^2]^{1/2} dz. \quad (78)$$

The argument of the Airy functions is $\gamma^2 = \omega^{2/3} Q(z, \lambda)$ and the functions Q , and V_0 must satisfy the Eikonal and transport equations (see reference 45), respectively. The constant j is either ± 1 , depending upon the juxtaposition of z_t (the turning point depth), and z_0 , some arbitrary depth usually taken as that depth where the sound speed is a minimum. In particular $j = 1$ when $z_0 < z_t$ (lower turning point) and $j = -1$ when $z_0 > z_t$ (upper turning point). Finally, the parameter λ is related to the separation constant ξ according to $\lambda = \omega\xi$.

The solution for g_1 is obtained from equation (77) by systematically replacing i with $-i$. Whereas the full solution (if it converges) accommodates an arbitrary sound speed variation, it can be shown that equation (77) exactly satisfies $\mathcal{L}(f_1) = 0$ when $c^{-2}(z)$ is linear in depth. This is the same sound speed variation assumed by Bartberger²⁶ and Stickler²⁴ (discussed earlier) within each of their layers. An indication then of the approximation made by using the truncated solution, equation (77), can be obtained by comparing the given sound speed profile with

$$c^{-2}(z) = \alpha_1 + \gamma_1(z_1 - z) \quad z_1 < z < z_2 \quad (79)$$

which can have at most one turning point. For this variation

$$\rho(z, \lambda) = -\gamma_1^{1/3} (z - z_t) \quad , \quad V_0(z, \lambda) = |\partial \rho / \partial z|^{-1/2} \quad . \quad (80)$$

Thus the argument of the Airy functions is zero at the turning point. Then, if for large γ^2 the Airy functions are replaced by their asymptotic expansions with $\zeta = \omega^{2/3} \rho(z; \lambda)$,

$$A_1(-\zeta) = \pi^{-1/2} \zeta^{-1/4} \text{SIN} \left(\frac{2}{3} \zeta^{2/3} + \pi/4 \right) \quad , \quad B_1(-\zeta) = \pi^{-1/2} \zeta^{-1/4} \text{COS} \left(\frac{2}{3} \zeta^{2/3} + \pi/4 \right) . \quad (81)$$

The functions next reduce to the WKB solutions given by equation (74) (multiplied by $\omega^{1/2}$) with $z_k = z_0$.

Another indication of the approximation introduced by using the truncated solution, equation (77), was provided at the end of the previous section. Discussed in that section were the approaches of modeling the ocean with layers and that of approximating the solutions over the entire interval (in this case $z_1 < z < z_2 = N$). It was noted that the latter approach fails whenever the exact partial impedances become discontinuous, which is related to the continuity of sound speed and its first derivative. In such instances, the approximate solution approach must be modified either by the insertion of layers or the inclusion of higher order terms from the full solution. For the time being, consideration should be limited to cases where at most one turning point exists and equation (77) is exact.

Before proceeding to the multipath expansion, it is convenient to redefine the reflection coefficients (\tilde{R}_1^1, R_1^2) previously given as equations (62) and (64) as

$$\tilde{R}_1^1 = \frac{g_1(z_1)}{f_1(z_1)} \tilde{R}_1^1 \quad , \quad \tilde{R}_1^1 = \frac{\tilde{Y}_0^1 - (Dg)_1^1 / g_1(z)}{(Df)_1^1 / f_1(z_1) - \tilde{Y}_0^1} \quad (82)$$

$$R_1^2 = \frac{f_1(z_2)}{g_1(z_2)} R_1^2 \quad , \quad R_1^2 = \frac{Y_2^2 - (Df)_1^2 / f_1(z_2)}{(Dg)_1^2 / g_1(z_2) - Y_2^2} \quad (83)$$

with \tilde{Y}_0^1, Y_2^2 representing the admittance at the surface and bottom, respectively. The behavior of the reflection coefficients when z is close to a turning point is, from equation (77),

$$\begin{aligned} \tilde{R}_1^1 &= e^{-2i\omega Q(z_0, z; \lambda)} e^{j\pi/2} e^{-2i \text{Jtan}^{-1} [A_1(\gamma_1^1) / B_1(\gamma_1^1)]} \\ R_1^2 &= -e^{2i\omega Q(z_0, z; \lambda)} e^{-j\pi/2} e^{2i \text{Jtan}^{-1} [A_1'(\gamma_1^2) / B_1'(\gamma_1^2)]} \quad . \quad (84) \end{aligned}$$

When z is not close to a turning point, the WKB solutions yield

$$\tilde{R}_1^{-1} = e^{-i [2\omega Q(z_0, z_1 \cdot \lambda) + \pi]} \quad , \quad R_1^2 = e^{2i\omega Q(z_0, z_2 \cdot \lambda)}$$

The Green's function may be expanded in two ways. Multiplication of the components of the numerator gives four terms. Each term represents a ray path type which includes all cycles of the ray.

The individual cycles of the rays may be obtained by expanding the term $(1 - \tilde{R}_1^{-1} R_1^2)$ appearing in the denominators of the four terms in a binomial series. This expansion and simultaneous substitution from equations (82) and (83) yield the multipath expansion for $z < z_s$,

$$\sum_{n=0}^{\infty} \left\{ \tilde{R}_1^{-1} R_1^2 \frac{A_1^1/B_1^1}{-2i\omega} \right\}^n \left\{ \frac{g_1(z) f_1(z_s)}{-2i\omega} + \frac{f_1(z) f_1(z_s) g_1(z_1) \tilde{R}_1^{-1}}{-2i\omega f_1(z_1)} \right. \\ \left. + \frac{f_1(z) g_1(z_s) g_1(z_1) f_1(z_2)}{-2i\omega f_1(z_1) g_1(z_2)} \tilde{R}_1^{-1} R_1^2 + \frac{g_1(z) g_1(z_s) f_1(z_2)}{-2i\omega g_1(z_2)} R_1^2 \right\} \quad (85)$$

where

$$B_1^1 = g_1(z_2)/g_1(z_1) \quad , \quad A_1^1 = f_1(z_2)/f_1(z_1).$$

For the cases of either no turning points (e.g., bottom bounce paths) or a solution at a sufficiently large distance from a turning point, the WKB solutions are appropriate. Then $A_1^1/B_1^1 = e^{2iQ(z_1, z_1; \lambda)}$. On replacing the Hankel function in the field integral with the first term in its asymptotic expansion,* one obtains the multipath integral representation for the pressure, $\mathcal{P}(z, z_s, r)$, as

$$\mathcal{P}(z, z_s, r) = \sum_{n=0}^{\infty} \int_0^{\infty} G(z, z_s; \lambda, f) e^{i\omega[Q(z, z_s; \lambda) + 2nQ(z_1, z_2 \cdot \lambda) - \pi/4]} e^{i\omega\lambda r} d\lambda + () + () + () \quad (86)$$

where the terms in () would be of a form similar to that shown explicitly and G is an expression involving Airy functions which reduces to

$$G(z, z_s; \lambda, f) = \frac{q^{-1/4}(z) q^{-1/4}(z_s) \omega \lambda}{-2i \sqrt{2+2\pi\omega\lambda r}} \left(\tilde{R}_1^{-1} R_1^2 \right)^n$$

*Weinberg modifies the usual argument asymptotic expansion so that

$$H_0^{(1)}(\omega\lambda r) = (2+2\pi\omega\lambda r)^{-1/2} e^{i(\omega\lambda r - \pi/4)}$$

provides a closer approximation for small values of the argument.

far away from turning points. The integrals above are of the form

$$I = \int_{\lambda_1}^{\lambda_2} G(\lambda) e^{i\psi(\lambda)} d\lambda \quad (87)$$

and can be evaluated by the method of stationary phase.

The stationary phase points can be related to the eigenrays of classical ray theory. (This is discussed here under the heading entitled *Connection Between Modes and Rays*.) In the event that the stationary phase evaluation fails, Weinberg's⁴⁵ response is to evaluate the phase integrals in equation (86) numerically. The breakdown occurs in the vicinity of caustics which can be located from classical ray theory. After locating these regions, the difference in phase between a ray on the caustic and a ray near the caustic is calculated. If this difference is small, the integrals are evaluated numerically. Otherwise, the stationary phase technique is used. Weinberg has found that for the deep ocean and for acoustic frequencies greater than 100 Hz most integrals are evaluated by the method of stationary phase.

Before discussing the numerical integration procedure, it is appropriate here to note a significant difference in emphasis between the models previously discussed and those of this section and also the classical ray theory models with corrections (*Connection Between Modes and Rays*) such as FACT.⁴⁶ In the latter case, the primary emphasis was upon accuracy. A minimum number of approximations were introduced after the initial statement of the problem. The resulting execution speed was fundamentally that which were needed to evaluate the mathematics. Stickler's²⁴ branch cut integral, for example, might be routinely evaluated even though in many instances it would not significantly contribute to the total field. Similarly, the limits of integration for the FFP are generally larger than required from a practical standpoint.

In the former case, the models were developed with the goal of minimizing execution speed without significantly effecting accuracy. To meet this end approximations are introduced based, in many instances, upon the long experience of the developer. It is impossible to summarize all such approximations. Indeed, when examined in isolation, a false perception of their validity with respect to the overall answer may result. However, in order to provide an indication of what is involved, the major steps in the program are outlined below for a typical deep water profile shown schematically in figure 6.

In order to perform the numerical integration, formulas for the amplitude of G must be obtained. To illustrate the process, let it be assumed that both source and receiver are in the surface duct. In this case, the lower limit of equation (87) is set to zero (corresponding to infinite sound speed) and λ_2 is taken to be the sound speed at the surface (z_1), which is the local minimum sound speed. The λ domain is then divided into the subintervals,

$$0 \text{ to } \lambda_B, \lambda_B \text{ to } \lambda_{\text{DUCT}}, \lambda_{\text{DUCT}} \text{ to } \lambda_z, \lambda_z \text{ to } \lambda_{z_s} \text{ and } \lambda_{z_s} \text{ to } \lambda_{z_1},$$

which are identified in figure 6. Each of these subintervals is further divided by tracing 16 non-vertexing rays (0 to λ_B), 32 vertexing rays (λ_B to λ_{z_s}), and 16 rays vertexing above the source (λ_{z_s} to

λ_{z_1}). In addition, 30 rays are traced through (0 to λ_{z_1}). In each instance the spacing between the rays is nonuniform in angle so as to improve the numerical evaluation of integrals to be discussed below.

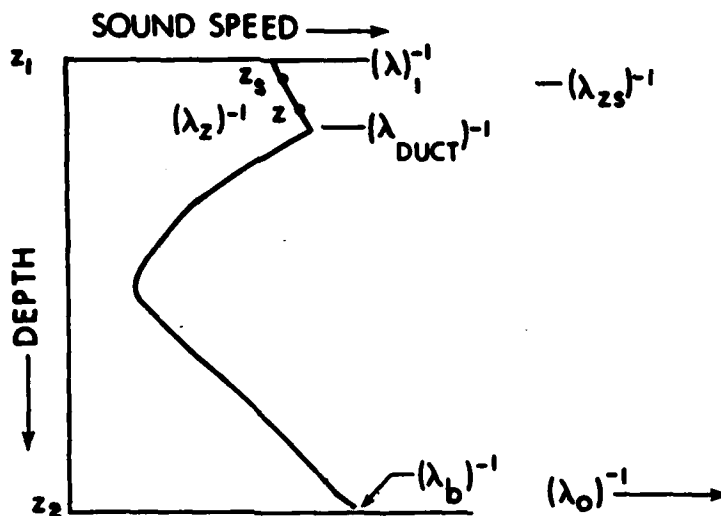


Figure 6. Typical Deep Water Profile

The particular formulas used for the amplitudes of f and g within each subinterval are chosen based upon the size of $\zeta = \omega^{2/3} \rho(z; \lambda)$. If $\zeta < -0.8477$, no turning points are encountered and the amplitudes are calculated from the WKB solutions. For example, this might occur in the interval 0 to λ_b where steep bottom bounce rays exist. However, if $\zeta > 20$, a turning point exists but it is far removed from either z or z_s so that the amplitude would be exponentially decaying. Such a case would exist for $(\lambda_{z_s}, \lambda_{z_1})$ with rays vertexing far above either the source or receiver depth. In such cases, Weinberg⁴⁵ sets the amplitude to zero on the basis that contributions from other subintervals would dominate the total answer. Finally, if ζ falls between these two limits, turning points exist near either the source or receiver depths. In this instance, the amplitudes are obtained from the Airy functions.

As mentioned earlier, the truncated solution approach used by Weinberg⁴⁵ must be modified when either the partial impedances are not continuous or when two or more turning points are in close proximity. Such a situation exists for the profile considered within the interval $(\lambda_{DUCT}, \lambda_z)$. Green's function for the multipath integral, equation (86), corresponding to the direct path connecting source and receiver in the surface duct, is modified by replacing R_f^2 with a reflection coefficient referenced to the bottom of the surface duct. This new reflection coefficient is obtained by replacing the profile below the duct with a semiinfinite layer. Within this layer the sound speed is given by equation (79), with γ_1 obtained from that portion of the original profile immediately below the surface duct. The reflection coefficient for this bilinear profile, obtained by satisfying the continuity conditions, is then approximated so that the final result is a ratio of the difference and sum of Airy functions.

The reflection coefficient R_f^2 is also modified for the interval $(\lambda_0, \lambda_{DUCT})$, which, in this case, corresponds to refracted-surface reflected (RSR) ray paths. When the turning point is sufficiently above the bottom, the magnitude of R_f^2 is set to unity and its phase to $-\pi/2$. In those cases where the turning point is close to the bottom, R_f^2 is replaced with equation (84).

The interval of integration (λ_1, λ_2) in equation (87) is initially approximated by $(0, \lambda_{z_1})$. This is further divided into subintervals,

$$(0 < \lambda_1 < \lambda_2 \cdots \lambda_i < \lambda_j < \cdots \lambda_{z_1}),$$

where λ_i and λ_j correspond to caustic regions defined by either λ_B , $\min(\lambda_{z_s}, \lambda_2)$, or λ 's for minimum and maximum range values. Thus a typical integral to be evaluated numerically is of the form

$$I = \int_{\lambda_i}^{\lambda_j} G(\lambda) e^{i\psi(\lambda)} d\lambda. \quad (88)$$

For this subinterval, the phase $\psi(\lambda)$ is fit with a cubic function. The amplitude $G(\lambda)$ is fit with a linear function. If λ is sufficiently far from a point of stationary phase, $\psi(\lambda)$ is monotonic so that equation (88) can be transformed to

$$I = \int_{\lambda_i}^{\lambda_j} \left[G(\psi) \frac{d\lambda}{d\psi} \right] e^{i\psi} d\psi. \quad (89)$$

Then the quantity in brackets can be approximated by a polynomial in ψ and the expression can be evaluated in closed form. However, if λ is near a point of stationary phase (but still close to a caustic), equation (88) is evaluated by the trapezoidal rule.

The philosophy adopted in Leibiger's Raymode X program^{47,48} is to utilize, whenever possible, the simpler tools of ray theory while retaining the more exact formulation of mode theory. Two important benefits are thus realized: (1) It is possible to interpret mode theory expressions in a manner similar to ray theory* and, (2) the use of ray theory simplifies some of the computational aspects of the normal mode theory, allowing for considerable savings in computer execution time.

Leibiger initially assumes the medium to be layered with the sound speed given by equation (79) within each layer. A fundamental solution of $\mathcal{L}(\cdot) = 0$ may then be written as $f(z; \xi) = V(z; \xi) e^{i\phi_0 z}$, where

$$V(z; \xi) = K \{ \phi_0^2 / q \}^{1/2} (z; \xi)^{1/2} H_{1/3}^{(1)}(\phi_0 z) e^{-i\phi_0 z}, \quad K = (\pi/2)^{1/2} e^{+15\pi/12}$$

In the definition of q and ϕ in equation (74), $q(z)$ is assumed to be unity. The solution for $g(z; \xi)$ is taken to be the complex conjugate of f . When sufficiently far from a turning point, $V(z; \xi) \sim q^{-1/4}$ and the exact solutions reduce to the usual WKB approximations. It is also noted that Leibiger's fundamental solutions, f and g , are formally equivalent to Weinberg's truncated solutions.

*The discussion of this aspect of Raymode X seemed more appropriately suited to the discussion under the heading *Connection Between Modes and Rays*.

Leibiger makes the approximation that the wave is totally transmitted across all interfaces until either a layer is reached where a turning point exists or the wave interacts with either the ocean surface or bottom. At a turning point, the *reflection coefficient*, R , is assigned unit magnitude and a $\pi/2$ phase shift. The magnitude of R is obtained from a scattering model and the phase shift is assumed to be $-\pi$ at the ocean surface. At the ocean bottom the phase of R is zero. The magnitude of R is obtained from an input table of values.

With these provisos, the approximate expression for the exact depth dependent Green's function, equation (70), for $z > z_s$ is

$$G(z, z_s; \xi; \omega) = \frac{[f(z_s; \xi) \tilde{R}_1^{-1} + g(z_s; \xi)] [f(z; \xi) + R_{N-1}^N g(z; \xi)]}{2i e^{-i\phi_1^N} [1 - \tilde{R}_1^{-1} R_{N-1}^N e^{2i\phi_1^N}]}$$

The subscript of ϕ_1^N is a phase reference depth for the numerator term containing \tilde{R}_1 , which is either the ocean surface or an upper turning point associated with a downward refracted wave. The superscript N is the phase reference depth for the remaining numerator term, and it is either the bottom depth or the depth of a lower turning point corresponding to an upward refracted wave.

The conditions for which the above expression is a reasonable approximation for G are the same as those discussed here under the heading *Depth Dependent Green's Function (Traveling Wave Formulation)*, namely that the partial impedances be continuous. In the presence of a surface duct, the formula is modified by replacing R_{N-1}^N with the reflection coefficient at the bottom of the duct obtained from the continuity conditions for a bilinear profile.

Although Leibiger^{47,48} and Weinberg⁴⁵ initially approach the problem from different viewpoints (layering versus asymptotic solutions) both make fundamentally the same approximation (continuity of partial impedances) and arrive at basically the same Green's function. For the profile shown in figure 6, Leibiger would replace the $(0, \infty)$ limits of integration with the subintervals (ξ_N, ξ_{BOT}) , (ξ_{BOT}, ξ_{DUCT}) , (ξ_{DUCT}, ξ_{SURF}) , where ξ_N is an input parameter related to the largest source angle to be considered. Next, the integral expression for the pressure field is rewritten in terms of the four integrals obtained when the numerator of the Green's function is expanded. These integrals over the previously defined limits of integration are evaluated by either normal mode theory when the number of trapped modes (the default criterion is 10) within the ξ partition is small, or via the multipath expansion.

In both instances, the integrals to be evaluated are of the form

$$\mathcal{P}(r, z, z_s) = \int_{\xi_A}^{\xi_B} \frac{G(z, z_s, \xi) e^{i[\phi_1^z - \phi_1^{z_s} + \epsilon r]}}{[1 - \tilde{R}_1^{-1} R_{N-1}^N e^{2i\phi_1^N}]} d\xi \quad (90)$$

$$G(z, z_s; \xi) = i \left[e^{-i\pi/2} \epsilon / (2\pi r) \right]^{1/2} \tilde{V}(z_s; \xi) V(z; \xi),$$

where, for illustrative purposes only, the integral resulting from the product of gf and substitution of the first term of the asymptotic expansion for $H_0^{(1)}$ is considered here.

When normal mode theory is utilized, the branch out contribution is not included. However, when equation (90) is evaluated by the multipath expansion for different limits of integration, the branch cut contribution to the total field is at least partially accounted for. The singularities ξ_p associated with the modes are assumed to be simple poles obtained by solving

$$W(\xi_p) = 1 - \tilde{R}_1^{-1} R_{N-1}^N e^{+2i\phi_1^N} = 0.$$

If the reflection coefficients are defined in terms of a magnitude and phase (θ_1 and θ_N), one sees that

$$|\tilde{R}_1^{-1}| |R_{N-1}^N| = e^{+2\text{Im}\{\phi_1^N\}}; \quad \text{and} \quad \theta_1 + \theta_N + 2\text{Re}\{\phi_1^N\} = -2p\pi, \quad p = 0, 1, 2, \dots \quad (91)$$

The real part of the eigenvalue $\hat{\xi}_p = \text{Re}\{\xi_p\}$ is found by solving equation (91) without recourse to iterative methods which results in a considerable savings in execution time. To accomplish this, the extreme mode numbers (N_A, N_B) are determined by substituting ξ_A and ξ_B into the second part of equation (91) and solving for p . In addition, differentiation yields

$$\frac{dp}{d\xi} = \frac{1}{2\pi} \left(R_c - \frac{\partial\theta_1}{\partial\xi} + \frac{\partial\theta_N}{\partial\xi} \right), \quad \text{where} \quad R_c = \left. \frac{-\partial}{\partial\xi} 2\text{Re}\{\phi_1^N\} \right|_{\xi_p}$$

is the cycle range, R_c , associated with the mode eigenvalue.

In the next section, it is shown that R_c is also twice the horizontal distance traversed by an eigenray which connects the phase reference point 1 to the phase reference point N . The value for R_c is available in closed form due to the assumed sound speed variation within each layer. If one assumes that the phase of the reflection coefficients is a slowly varying function of ξ , the above equation may then also be solved for the extreme values ξ_A, ξ_B . Thus a curve of $\hat{\xi}_p$ versus p passing through the end points $(\xi_A, N_A), (\xi_B, N_B)$ and having the slopes prescribed above can be obtained. This curve is approximated by a cubic polynomial. The unknown coefficients are determined by interpolation. This expression is then evaluated for each integer p such that $N_A \leq p \leq N_B$ for a direct (noniterative) evaluation of the real part of the eigenvalues.

The imaginary part of ξ_p can be shown to be given approximately, with the use of WKB approximations, by

$$I_m(\xi_p) = \frac{-\ln[|\tilde{R}_1^{-1}| |R_{N-1}^N|]}{R_c} \Big|_{\xi_p}$$

Then the residue expansion associated with equation (90) becomes

$$\varphi(r, z, z_s) \sim 2\pi i \sum_{p=N_A}^{N_B} \frac{G(z, z_s; \xi_p)}{\left. \frac{\partial W}{\partial \xi} \right|_{\xi_p}} e^{i[\phi_1^z - \phi_1^{z_s} + \xi_p r]} \quad (92)$$

The normalization term in the denominator can be written approximately as

$$\left. \frac{\partial W}{\partial \xi} \right|_{\xi_p} \approx - \frac{\partial \bar{R}_1^{-1}}{\partial \xi} (\bar{R}_1^{-1})^{-1} + \frac{\partial (R_{N-1}^N)}{\partial \xi} (R_{N-1}^N)^{-1} - i R_C \Big|_{\hat{\xi}_p}$$

and further approximated by retaining only the term involving R_C . The final form of the residue series is obtained by expanding the phase terms (e.g. ϕ_1^z) in a Taylor's series about $\hat{\xi}_p$ and retaining only the first two terms since $\text{Im}\{\xi_p\}$ is small for trapped modes. Then

$$\varphi(r, z, z_s) \sim 2\pi \sum_{p=N_A}^{N_B} \frac{G(z, z_s; \hat{\xi}_p)}{(R_C)_p} e^{i[\phi_1^z - \phi_1^{z_s} + \hat{\xi}_p r]} e^{-\text{Im}\{\xi_p\}[r(z_1, z) - r(z_1, z_s) - r]}$$

where $r(z_1, z)$, $r(z_1, z_s)$ are the horizontal ranges obtained from ray theory from z_1 to z and z_s , respectively.

For the multipath approach, the denominator of equation (90), for example, is expanded so that

$$\varphi(r, z, z_s) \sim \sum_{q=0}^{\infty} \int_{\xi_A}^{\xi_B} G(z, z_s; \xi) (\bar{R}_1^{-1} R_{N-1}^N)^q e^{i[\phi_1^z - \phi_1^{z_s} + 2q\phi_1^N + \xi r]} d\xi$$

The interval of integration is divided into a number of unequal sections based on the number of rays traced. This number is an input parameter. For some of these subsections the value of ξ is sufficiently far from a stationary phase point so that their contribution is excluded.

Although stationary phase techniques are not used, the stationary phase point is available from ray calculations. (See discussion at the end of *Connection Between Modes and Rays*.) The justification for neglecting such subsections is based on the spiral-like nature of the cumulative result for the field discussed in the beginning of *Connection Between Modes and Rays*. When the subsection does not meet these criteria, the phase term is approximated by a quadratic expression in ξ . The amplitude of the kernel is assumed to be slowly varying over the subinterval, evaluated at an interior point and removed outside of the integral. By a suitable transformation, the resulting integral can be expressed in terms of Fresnel integrals. Leibiger^{47,48} evaluates the multipath integrals by quadrature. Weinberg⁴⁵

utilizes a combination of quadrature and stationary phase. An indication of the relative accuracy of the two methods, for a single example, can be obtained by examining the accuracy assessment results provided in *Quantitative Model Assessment*.

CONNECTION BETWEEN MODES AND RAYS

Pedersen and Gordon⁴⁹ have compared normal mode theory with ray theory and obtained many useful results regarding diffraction corrections to classical ray theory. Bartberger⁵⁰ has investigated the behavior of the mode (residue) summation at a fixed range in order to gain a better insight into normal mode theory. Leibiger^{47,48} has conducted a similar study as part of the development of Raymode X. He utilized the results to considerably reduce the required execution time (see table 3) of that program.

Before examining the underlying mathematics (the notation will be that pertaining to Raymode X (see text under the paragraph heading *Multipath Expansion Models*)) it is instructive to consider the example of a cumulative mode sum Bartberger⁵⁰ shown in figure 7. A straight line is drawn from the origin in the complex plane to the point representing the first mode. From there, another straight line is drawn to the point representing the sum of the first two modes and so on. The vector distance from the origin to the final point represents the resultant acoustic pressure at the fixed horizontal range (12.6 kyd in this case) examined. At this range, which ray theory states is dominated by bottom bounce paths, a broad peak caused by multipath interference results in the plot of propagation loss versus range. The composite plot, figure 8, is a useful tool for interpreting the behavior of the spiral-like curve of figure 7. A smoothed version of the propagation loss is shown in the upper right hand corner. Observe the dashed line, intersecting the peak at 12.6 kyd, to the lower right hand portion of the figure. The curve shown there is a plot of $\text{Re}\{\xi_n - \xi_{n-1}\}$ $r = 2\pi$ where the difference between the real parts of the eigenvalues is labeled Δk in figure 8. Next observe the dashed line to the lower left hand portion where the locus of Δk 's for successive modes is plotted versus mode number. Finally the dashed line intersects the plot (upper left hand corner of figure 8) of relative mode amplitude (depth functions only) versus mode number at a peak value occurring between mode numbers 355 and 360.

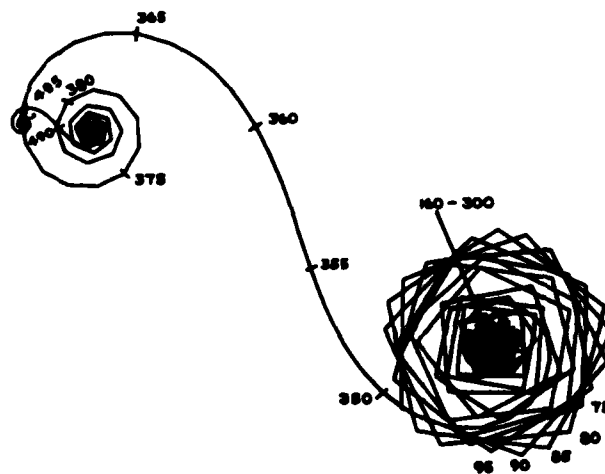


Figure 7. Vector Mode Plot at 12.6 kyd

Returning to figure 7, it can be seen that the low order modes, which have a large amplitude, wrap around themselves to form large polygons and then return to the origin. These modes would be important at the convergence zone range, about 65.6 kyd. However, they contribute essentially nothing to the resultant intensity at the bottom bounce range considered here. As the mode number increases (160-300, which surrounds the second peak of the upper left hand portion of figure 8), the phase difference between successive modes gradually passes through 180 degrees, leading to the spiky appearance of the plot in figure 7. This group of modes also contributes little to the final mode sum. As the mode number approaches the third peak (upper left portion of figure 8), the phase difference passes through 360 degrees in the vicinity of mode 355 and the flat portion of the spiral is formed. Later, at about mode 480, the phase difference between successive modes approaches 720 degrees and the curve has another smaller flat portion. Finally, a third flat portion is barely visible at the end of the plot which corresponds to a phase difference of 1080 degrees.

Thus the dominant contribution to the mode sum at this range is made by a relatively small group of modes (350-360) whose phase difference is approximately 2π . These modes are associated with rays which reach the receiver after interacting once with the bottom. Their contribution to the propagation loss curve would be similar to the smooth result shown in figure 8. Additional smaller contributions come from the second flat portion of the spiral associated with a group of higher order modes, whose successive phase difference is approximately 4π . These modes are associated with rays reaching the receiver after interacting twice with the bottom. Their contribution to the propagation loss result would produce a higher frequency oscillation on top of the previously mentioned smooth curve. A still smaller contribution is made by the group of modes (successive phase difference of approximately 6π) associated with rays which have interacted three times with the bottom.

The explanation for the dominance of a small group of modes within the total mode sum can be obtained with the aid of the Poisson summation formula (see references 51-57),

$$\sum_{p=N_A}^{N_B} I_p = \sum_{q=0}^{\infty} \int_{N_A}^{N_B} I_p e^{-12\pi pq} dp ,$$

where on the right hand side I_p is taken to be a continuous function of p . If this formula is applied to Leibiger's residue series, equation (92), one of the four terms in the field expression is given by

$$\varphi(r, z, z_s) = \sum_{q=0}^{\infty} 2\pi i \int_{N_A}^{N_B} \frac{G(z, z_s; \bar{\xi})}{\partial w / \partial \bar{\xi}} \Big|_{\bar{\xi}} e^{i[\phi_1^z - \phi_1^z s + \bar{\xi} r - 2\pi pq]} dp , \quad (93)$$

where $\bar{\xi} = \xi_p$.

Although the stationary phase technique will not be used to evaluate this expression, it is informative to examine the points of stationary phase given by

$$\frac{\partial}{\partial p} [\phi_1^z - \phi_1^z s + \bar{\xi} r] = 2\pi q .$$

This implies that for a fixed range only the successive modes whose phase changes are integer multiples of 2π will make a significant contribution to the total field. The phase difference of the remaining modes leads to cancellation and gives nonflat regions of spirals similar to those discussed previously.

The equation for locating points of stationary phase can also be written as

$$\frac{\partial}{\partial \bar{\xi}} (\phi_1^z - \phi_1^s) + r = 2\pi q \frac{\partial p}{\partial \bar{\xi}}.$$

However, from the mode equation it is understood that

$$\frac{\partial \bar{\xi}}{\partial p} = 2\pi \left[\left(-2 \frac{\partial}{\partial \bar{\xi}} \phi_1^N \right) + i \frac{\partial}{\partial \bar{\xi}} \ln(R_1^{-1} R_{N-1}^N) \right]^{-1}$$

and to a good approximation $\frac{\partial \bar{\xi}}{\partial p} = 2\pi/R_c$, where R_c is the cycle range for the p^{th} mode, i.e. the horizontal range needed for the angle associated with the eigenvalue to return to its initial value when plotted as a function of depth and range. Specifically

$$R_c = -2 \frac{\partial}{\partial \bar{\xi}} \text{Re}\{\phi_1^N\}.$$

From classical ray theory the horizontal range between two points, say z_1 and z , on a ray path is given by

$$r(z_1, z) = - \frac{\partial}{\partial \bar{\xi}} \text{Re}\{\phi_1^z\}.$$

Thus the stationary phase equation may also be written as

$$r = r(z_1, z) - r(z_1, z_s) + qR_c(z_1, z_N),$$

which is also the equation satisfied by an eigenray from classical ray theory.

Although the number of modes in the residue summation is identical for all ranges, at a given range only a finite subset satisfying the equation

$$\frac{\partial \bar{\xi}}{\partial p} - 2\pi q [-r(z_1, z) + r(z_1, z_s) + r]^{-1}$$

will constitute the major portion of the field. Furthermore, this subset of modes can be associated with the eigenrays from classical ray theory. At that range they connect the source and receiver. Viewed in another way, since $[-r(z_1, z) + r(z_1, z_s)]$ is generally small, the acoustic pressure for a stated

range, as given by mode theory, is produced almost entirely by those modes whose skip distance, R_c , times an integer multiple corresponds to that range.

Although equation (93) can be approximately evaluated by stationary phase, in demonstrating the connection between modes and the multipath expansion it is more informative to transform that result to

$$\mathcal{P}(r, z, z_s) = \sum_{q=0}^{\infty} \int_{\bar{\xi}_A}^{\bar{\xi}_B} G(z, z_s; \bar{\xi}) [\bar{R}_1^{-1}(\bar{\xi}) R_{N-1}^N(\bar{\xi})]^q e^{i[\phi_1^z - \phi_1^z s + 2q\phi_1^N + \bar{\xi}r]} d\bar{\xi},$$

where use has been made of

$$\frac{\partial}{\partial \bar{\xi}} [-\bar{R}_1^{-1} R_{N-1}^N \exp(2i\phi_1^N)] = 2\pi i \frac{\partial p}{\partial \bar{\xi}} \text{ and } 2q\phi_1^N - i q \ln(\bar{R}_1^{-1} R_{N-1}^N) = -2pq\pi.$$

This integral over $\bar{\xi}$ is one of the four terms previously derived for the multipath expansion.

If this integral is evaluated by stationary phase, the following is obtained:

$$\mathcal{P}(r, z, z_s) = \sum_{q=0}^{\infty} [\pi/\psi''(\xi^*)]^{1/2} G(\xi^*) [\bar{R}_1^{-1}(\xi^*) R_{N-1}^N(\xi^*)]^q e^{i\psi(\xi^*)} \int_a^{v_b} e^{iV^2\pi/2} dV; \quad V(\bar{\xi}) = (\psi''(\xi^*)/\pi)^{1/2}(\bar{\xi} - \xi^*),$$

where the phase $\psi(\xi) = \phi_1^z - \phi_1^z s + 2q\phi_1^N + \xi r$ has been expanded in a Taylor's series about the stationary phase point ξ^* with only terms up to the second order retained. This result represents a diffraction correction to classical ray theory since, in the limit of increasing frequency, it yields classical ray theory except for a factor of $c(z_s)/c(z)$. For the details, one should consult the illuminating paper by Haskell.⁵⁸ Haskell has also obtained corrections at caustics ($\psi''(\xi^*) = 0$) by retaining higher order terms in the Taylor expansion for $\psi(\xi)$. Similar corrections, sometimes called nonuniform, have also been derived by Brekhovskikh.⁵⁹ Thus it is possible to show (1) the connection between the multipath expansion and classical ray theory as well as (2) the nonuniform caustic corrections used to modify classical ray theory models such as the FACT (Fast Asymptotic Coherent Transmission) Model.⁴⁶

QUANTITATIVE MODEL ASSESSMENT

The discussion to this point has been tacitly concerned with the accuracy of those models of propagation loss in underwater acoustics which have been converted into an automated computer code capable of being executed by someone other than the originator for a wide variety of problems. An indication of accuracy can be obtained in general terms by understanding the approximations

involved in going from the exact integral solution to the equations calculated in the computer code. However, a user must be able to translate this general understanding into a decision regarding suitability for a particular application. One recourse is to ask the opinion of experts. However, their subjective opinion is often found to be in conflict with that of other experts. This results in a fair amount of confusion.

Additionally, as can be seen from examining figure 9, although accuracy is a concern, it is not the only factor involved in the selection of a model. The amount of required execution time is of obvious concern because of the cost involved. Similarly, if the model is accurate but requires more core storage than is available, it is of limited viability. If the model is not operational at a facility, time delays will be encountered with its implementation. Some models can only be properly run by the originator because of subjective choices for input parameters controlling the accuracy of approximations. If the originator is not available, the user may choose another, less accurate model. Very often it may be possible to decrease the execution time of a model for an application at hand without seriously affecting accuracy. This would be difficult without extensive documentation. Finally, the model may provide only propagation loss between omnidirectional sources and receivers when a beamformer output may be required.

- A. ASSESSMENT OF ACCURACY
- B. RUNNING TIME
- C. AMOUNT OF COMPUTER MEMORY REQUIRED
- D. EASE OF IMPLEMENTATION
- E. COMPLEXITY OF PROGRAM EXECUTION
- F. EASE OF EFFECTING SLIGHT ALTERATIONS TO THE PROGRAM
- G. AVAILABLE ANCILLARY INFORMATION

Figure 9. Factors Influencing Model Selection

Given a multitude of candidates, the analyst must arrive at a decision based upon tradeoffs between accuracy and the above mentioned factors in the context of the application at hand. The problem of merging the user's requirements with the proper model has recently received considerable attention. The effort of the Panel On Sonar System Models (POSSM)^{60,61} is fairly typical of the activity in this area and will be summarized. That group decided that quantitative information should be provided about candidate models for the factors contained in figure 9. With such information available, the analyst could then arrive at objective decisions regarding the required tradeoffs within the context of his application.

The assessment of accuracy is the most difficult portion of the matrix to complete. One reason for this is the desire that the methodology used be more objective than the older subjective technique of overplotting predictions and arriving at a value judgement. The methodology adopted is summarized in figure 10.

The process begins by selecting a standard against which a model is to be evaluated for accuracy. The standard may be either an experimental data set or the output of a model. Since accuracy is assessed in terms of the mean level (which, of course, varies with the independent variable, be it range, azimuth, time, etc.), fluctuations about this mean must be eliminated before meaningful comparison can be made.

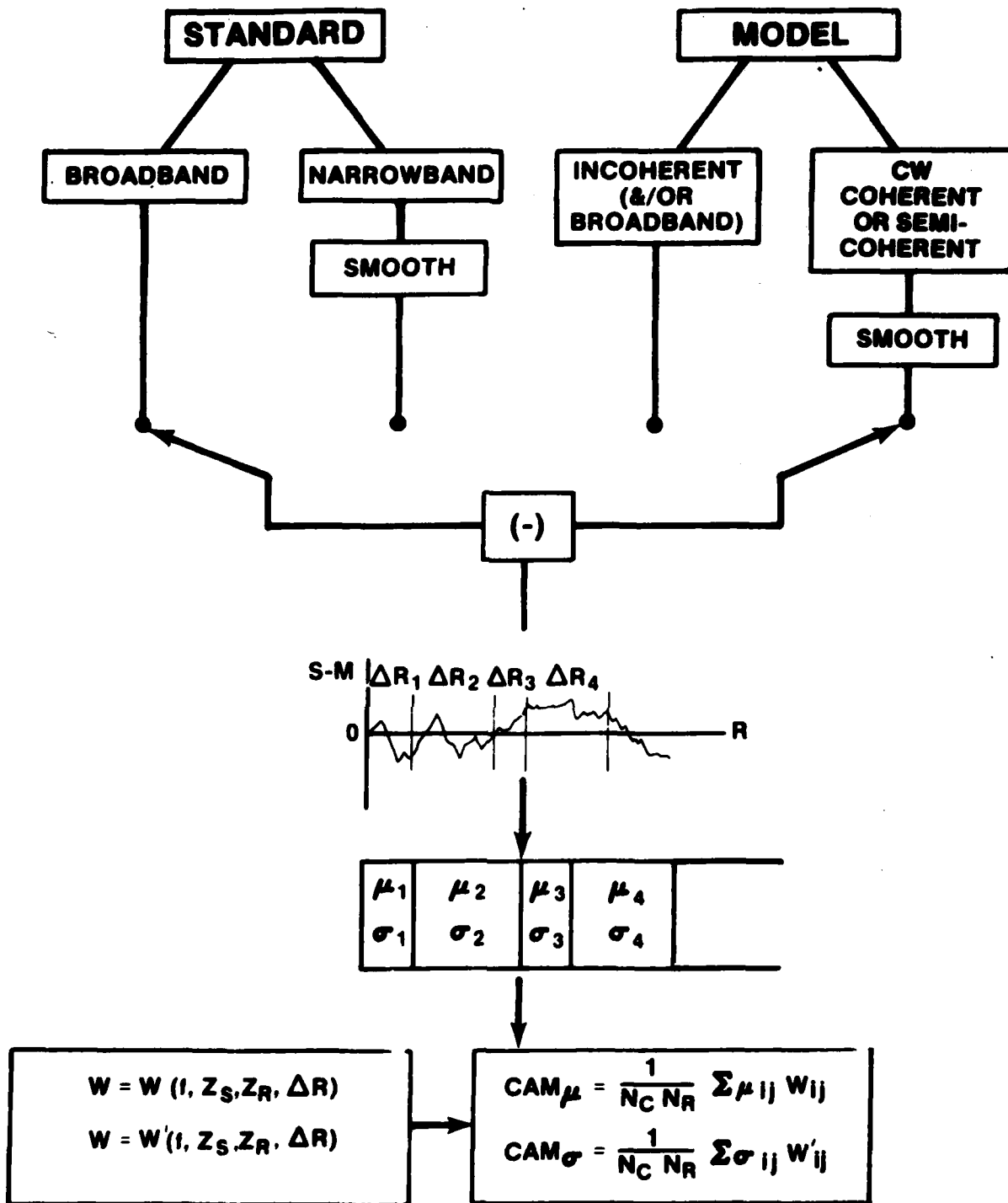


Figure 10. Summary of Model Assessment Methodology

In the discussion and examples to follow, the data considered will be transmission loss versus range. The applicability of the comparison method, however, is not restricted to such data. Typically, data which are broadband or derived using incoherent phase addition show little or no fluctuations and are suitable for comparison without modification. Conversely, narrowband data and/or CW coherent or semicoherent model outputs typically show significant rapid fluctuations about the mean. In such cases, the range dependent mean is obtained by smoothing the data by applying a moving average. The width of the moving window is determined from considerations of sonar system integration times and own-ship's and target's speed of advance. Given the range dependent means of standard and model, the difference between the two curves is obtained and divided into range intervals. These intervals correspond to ray path regimes such as direct path, first and second bottom bounce regions, and first, second, and third CZ's. The next step is calculation of the mean and standard deviation of the differences within each interval. Finally, these means and standard deviations are appropriately weighted and averaged, resulting in Cumulative Accuracy Measures. In the example to follow, only a single scenario is examined, a fairly simple one environmentally. Therefore, the accuracy results should not be considered to be indicative of a model's expected performance in other environments.

The scenario used by the various models is described in figure 11. The water depth is 2743.2 m, the source at 24.384 m, receiver at 106.68 m, and sound speed profile approximately bilinear. The bottom reflection loss, extracted in part from measured data, had a critical angle of 22° . At normal incidence the bottom loss is 6 dB. Four cases were examined, corresponding to the four frequencies shown. The standard chosen was the results of the Fast Field Program (FFP). All models compared against the standard used a single sound speed profile and a flat bottom and were provided with identical input information.

The models used in this example were supplied by various Navy laboratories* as shown in figure 12. Note that two versions of the FACT model were used. The version at Fleet Numerical Weather Central (FNWC) is, of course, an operational model and, therefore, cannot be altered to generate results with the requested data density. Perhaps more important, as will be seen shortly, the running time of the FNWC version is of an order of magnitude greater than what might be termed a *bare bones* version of FACT generally available at Navy laboratories. The bare bones version is free of the input/output requirements necessitated by a variety of Fleet support needs. Similarly, it should be pointed out that the version of Raymode X used in this study is not the Fleet operational version. In that version certain parameters which would be assigned fixed values for such usage were varied in this example. These parameters basically determine the tradeoff between accuracy and running time. If the choice of phase addition is considered, a total of 21 models were put through the accuracy assessment procedure.

In figure 13 the results of the standard (FFP) before and after smoothing for 67.5 Hz are shown. The window used for the running average was 2 km, which is nearly equivalent to a 5 minute average on a 12 knot target. A similar plot is shown in figure 14 for the Raymode X model.

The difference between the smoothed versions of FFP and Raymode X is shown in figure 15. Sets of curves such as these were generated for each model and type of phase addition. Although no CZ was obvious in the FFP and Raymode X results, the range intervals chosen for dividing the difference

*Information regarding documentation of these models is given in references 18, 26, 45-48, and 62-68.

curves were direct path region, first bottom bounce region, CZ, second bottom bounce regions, and 50 km intervals thereafter. It is the large critical angle of the actual bottom loss that accounts for the *filling in* of the inter-CZ regions.

NAVYWIDE PROPAGATION LOSS MODEL COMPARISONS

- **MEDITERRANEAN SCENARIO**
- **FREQUENCIES**
35, 67.5, 100, 200 Hz
- **STANDARDS**
HAYS-MURPHY DATA
FAST FIELD PROGRAM
- **MODELS**
SINGLE PROFILE
FLAT BOTTOM
INPUTS PROVIDED

Figure 11. Scenario for Accuracy Assessment

CONTRIBUTORS

LABORATORY	MODEL	PHASE ADDITION
FNWC	FACT	S
NADC	AP2 PLRAY	C S,I
NOSC	GORDON N. M. LORA RAYWAVE II	C C,S,I I
NRL	RTRACE	C,I
NSWC	NSWC N. M.	C
NUSC	CONGRATS V FACT FFP FFP (1/3-OCT) RAYMODE X	C,I C,S,I C C C,I

C = COHERENT
I = INCOHERENT
S = SEMICOHERENT

Figure 12. Listing of Models Assessed

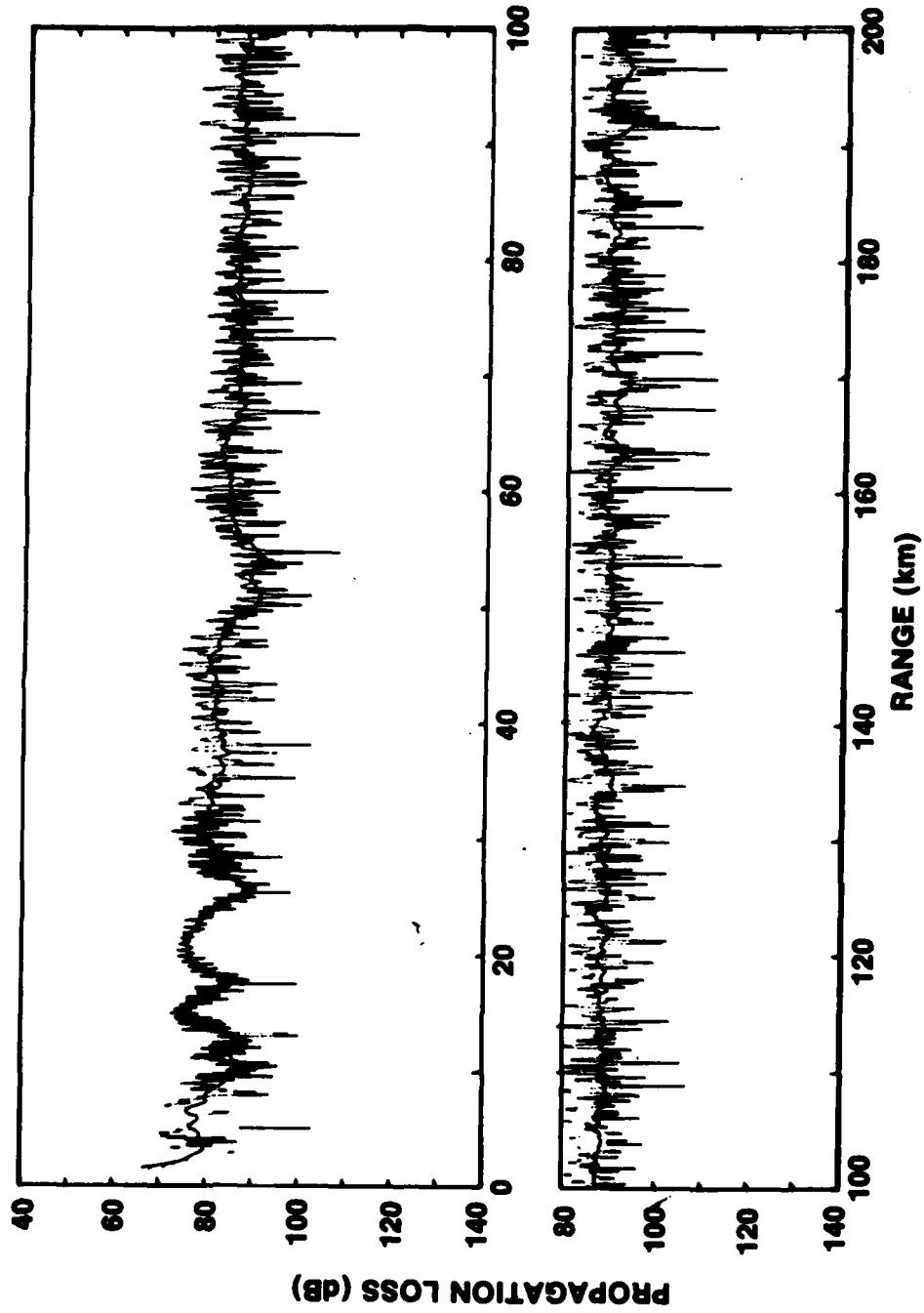


Figure 13. Standard Before and After Smoothing (FFP (CW), Case II Sliding Averages of 25 Points (2.01 km))

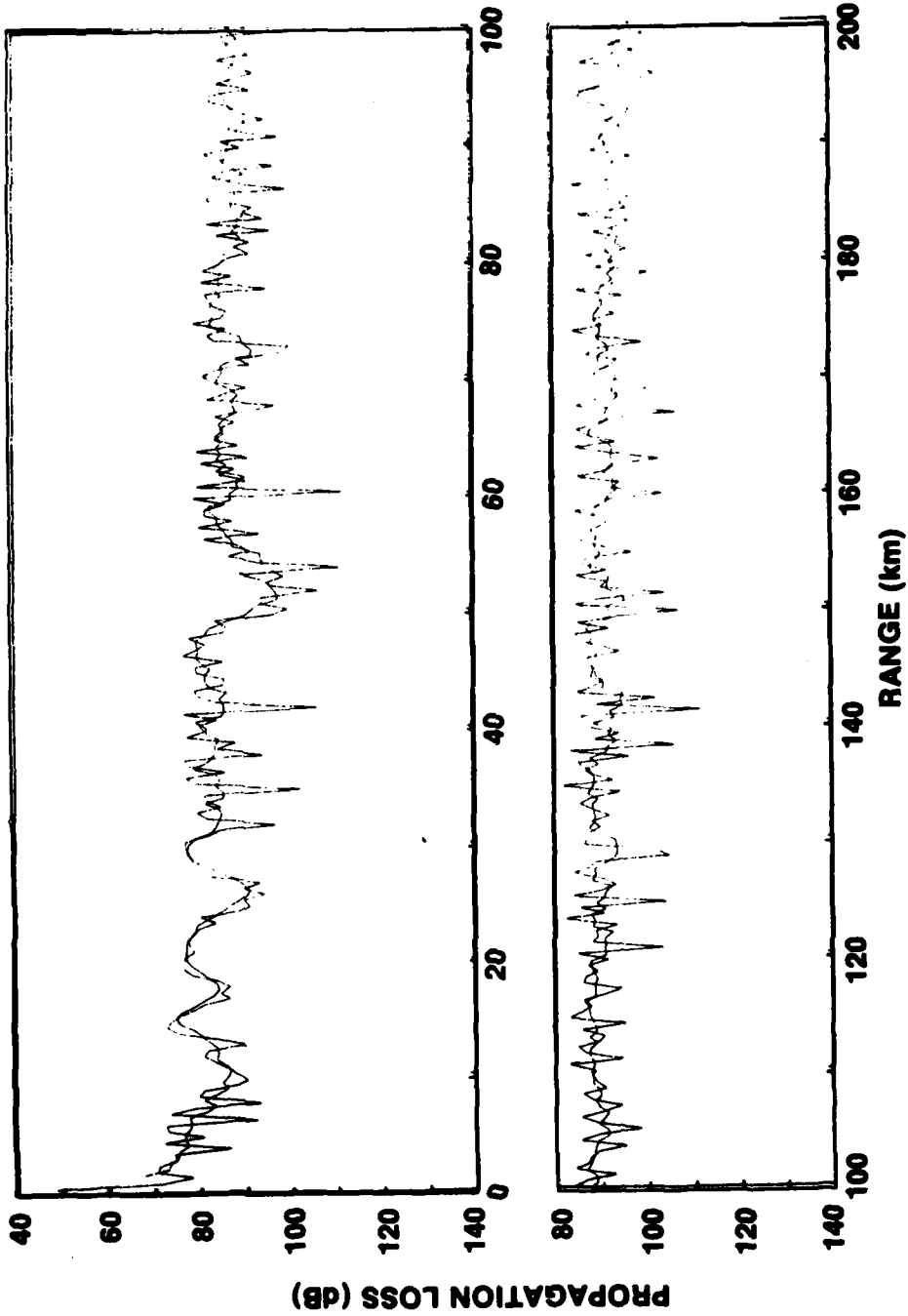


Figure 14. Raymode X Before and After Smoothing (Raymode X (Coherent), Case II Sliding Averages of 5 Points (2.00 km))

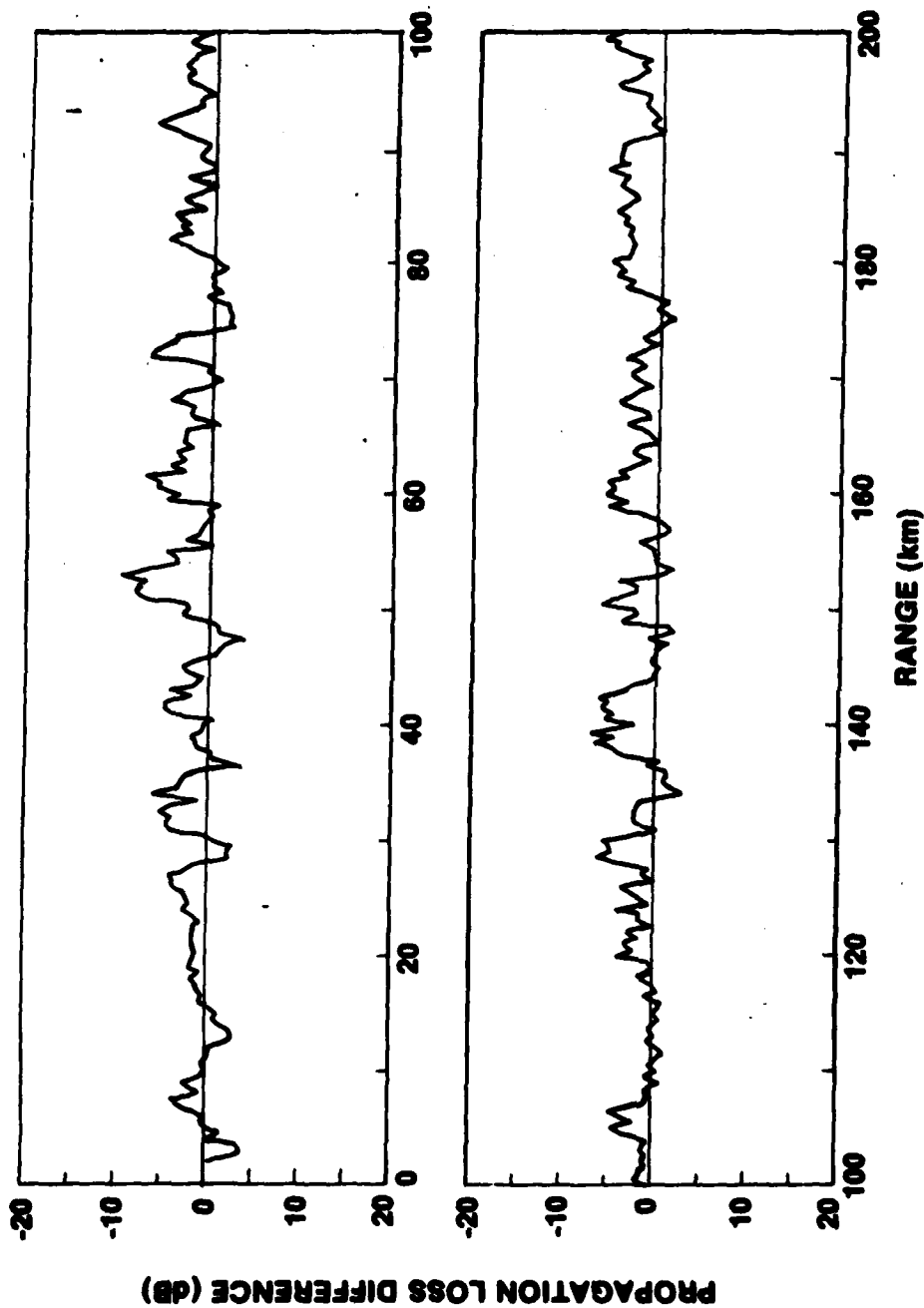


Figure 15. Difference Curves (Smoothed Raymode X (Coherent), Case II
Subtracted from Smoothed FFP (CW), Case II)

Table 1 shows mean and standard deviations of the difference curve for each model in each range interval. Numbers in parentheses represent the results of a second model submission. These resulted from followup contact with each modeler. Each modeler was given the results of the assessment of his model. He was also shown how his model compared with other models. Running time, core storage, a model description, references to his model, etc., were also provided. The modeler was then given the option of rerunning his model, possibly trading-off accuracy for running time. Four modelers availed themselves of the resubmission option.

Recall that the Cumulative Accuracy Measure for the mean and standard deviations is obtained by taking weighted averages of these quantities over all cases and range intervals. Since this example is for illustrative purposes, unit weights were assigned. The cumulative accuracy measures reduce to the grand mean and standard deviations shown in table 2. Each model's accuracy is now condensed to two numbers, both in decibels, giving the mean level of accuracy and the spread in accuracy over all cases and ranges. Note that all models were able to achieve values for grand means between 0.9 to 2.2 dB (upon consideration of only second submissions) and 2.1 to 5 dB for the standard deviation. This happy state of affairs would not be expected to persist for more challenging environmental scenarios.

Two facts regarding this accuracy assessment are worthy of note. First, the methodology results in a hierarchy ranging from the basic data to a single number. Thus a model's accuracy can be examined at many levels of detail. Further, this allows the results to be used for diagnostic purposes. The second point is the statement of a limitation: accuracy results should not be extended to other environmental scenarios, particularly those which are more complex.

In most cases, a second submission improved accuracy by 1 dB or less. In the case of Weinberg's⁴⁵ multipath expansion model, the larger improvement is due to two factors: (1) alteration of logic involving bottom bounce paths and (2) an error discovered in the sound speed profile input.

The cost of the modest accuracy improvements in terms of running time is provided in table 3. Note that the execution times are not directly comparable owing to the use of different computers. Examination of the first and second submissions reveals an approximate doubling of running time for Raymode X and Weinberg's multipath model. LORA's second submission was the addition of Cases I and II, but the basic program parameters were left unchanged.

Table 4 presents the core requirements for the models. Only one model, Raymode X, has less than 16K words. Four models require less than 32K; the remaining six models less than 64K words.

WAVEFORM PREDICTION MODELS

The major emphasis in modeling underwater acoustics has been with the prediction of propagation loss for an infinite CW point source. When information about the arrival structure or frequency dispersive characteristics of the waveform was desired, it was either obtained in a gross fashion from classical ray theory programs (reference 69) or, for low frequencies, by the use of stationary phase techniques in conjunction with normal mode theory⁷⁰ following the approach used by Pekeris.²²

Recently the alternative approach of direct numerical evaluation of the double integral expression for the pressure field via the FFT has been successfully implemented by DiNapoli.⁷¹ In this approach, the real part, \hat{P}_R , of the pressure field is given by the Fourier synthesis,

Table 1. Means and Standard Deviations of Differences Between the FFP (CW) and Model Results: Case II (in dB)

RANGE INTERVAL MODEL	DP		BB1		CZ		BB2		100 km		150 km		200 km	
	μ	σ	μ	σ	μ	σ	μ	σ	μ	σ	μ	σ	μ	σ
AP2	—	—	0.0	2.0	-0.5	1.9	-1.0	1.8	-1.6	2.7	-1.3	2.7	-1.9	2.6
NORMAL MODE	—	—	-1.2	2.1	-2.1	2.7	-0.8	3.1	-2.2	3.9	-2.3	3.2	-3.3	3.0
CONGRATS I COHERENT	—	—	(-1.2)	(1.5)	(-0.7)	(2.2)	(-1.9)	(2.7)	(-0.5)	(1.8)	(-1.5)	(2.5)	(-1.4)	(2.5)
CONGRATS II INCOHERENT	—	—	0.8	3.7	-0.8	2.0	-0.5	2.8	-1.1	1.4	-3.0	1.6	-4.4	2.0
INCOHERENT	—	—	(1.0)	(3.8)	(-0.2)	(2.1)	(-0.4)	(2.8)	(-0.8)	(1.0)	(-0.6)	(0.8)	(-0.8)	(1.5)
FACT/FNWC INCOHERENT	—	—	1.6	3.6	1.9	1.6	0.2	2.8	-0.3	1.2	0.7	1.1	1.0	1.4
FACT/NUSC COHERENT	—	—	-1.1	2.6	2.2	1.4	-0.2	1.7	-0.8	1.6	-0.5	1.2	-0.4	1.4
FACT/NUSC INCOHERENT	—	—	1.4	3.6	0.9	2.2	0.1	3.0	-2.2	2.0	-2.0	1.3	-1.9	1.5
FFP CW	—	—	—	—	—	—	—	—	—	—	—	—	—	—
FFP 1.3 OCTAVE	—	—	—	—	—	—	—	—	—	—	—	—	—	—
GORDON NORMAL MODE	—	—	0.6	2.0	0.4	2.2	-0.8	1.9	0.7	1.9	-0.3	2.6	-1.0	2.5
LORA COHERENT	—	—	(0.1)	(3.2)	(0.1)	(1.7)	(-0.4)	(3.1)	(-1.6)	(4.3)	(-2.5)	(3.6)	(-4.0)	(4.4)
LORA SEMICOHERENT	—	—	(0.2)	(2.9)	(0.8)	(2.0)	(0.2)	(2.4)	(0.0)	(1.0)	(-0.8)	(1.6)	(-1.8)	(1.9)
LORA INCOHERENT	—	—	(0.9)	(3.7)	(0.9)	(2.0)	(0.4)	(2.6)	(0.0)	(1.2)	(-0.8)	(1.7)	(-1.8)	(2.0)
NSWC NORMAL MODE	—	—	3.9	3.7	0.9	1.6	-0.2	1.4	-0.2	1.9	-0.1	2.0	-0.4	2.3
PL RAY SEMICOHERENT	—	—	(0.5)	(4.1)	(2.1)	(2.9)	(0.4)	(5.1)	(1.6)	(1.1)	(1.4)	(1.0)	(0.2)	(1.5)
PL RAY INCOHERENT	—	—	1.4	3.7	1.2	2.3	0.4	2.6	0.5	1.1	0.1	0.9	-0.8	1.5
RAYMODE I COHERENT	—	—	(-0.9)	(2.1)	(-1.5)	(2.4)	(-3.2)	(2.8)	(-2.0)	(2.0)	(-3.8)	(2.2)	(-2.4)	(1.9)
RAYMODE II INCOHERENT	—	—	(1.1)	(3.7)	(0.5)	(2.0)	(-0.8)	(2.7)	(-0.8)	(1.2)	(-2.0)	(1.3)	(-3.5)	(1.8)
RAYWAVE I INCOHERENT	—	—	2.9	3.0	1.8	2.8	2.2	3.5	1.4	2.1	0.9	1.7	0.7	1.8
RTRACK COHERENT	—	—	-0.6	2.7	-0.1	2.3	-2.1	3.7	-0.1	2.5	-0.5	1.9	-0.7	2.4
RTRACE INCOHERENT	—	—	—	—	—	—	—	—	—	—	—	—	—	—

Table 2. Averages of Means and Standard Deviations Over All Cases and Range Intervals (Standard of Comparison: FFP Model Results)

	$ \bar{\mu} $	$\bar{\sigma}$
AP2 NORMAL MODE	1.1	2.4
CONGRATS V COHERENT	2.4 (1.3)	3.5 (2.2)
CONGRATS V INCOHERENT	1.8 (0.9)	2.5 (2.1)
FACT/FNWC SEMICOHERENT	1.2	2.6
FACT/NUSC COHERENT	1.0	2.5
FACT/NUSC INCOHERENT	1.2	2.4
FFP CW	-	-
FFP 1/3-OCTAVE		
GORDON ^a NORMAL MODE	0.6	2.3
LORA ^b COHERENT	2.0 (1.6)	5.0 (4.5)
LORA ^b SEMICOHERENT	1.4 (1.2)	3.2 (2.9)
LORA ^b INCOHERENT	1.5 (1.0)	3.0 (2.8)
NSWC NORMAL MODE	1.0	2.8 ^c
PLAY SEMICOHERENT	1.0 ^c (1.3)	2.6 ^c (2.5)
PLAY INCOHERENT	1.3 ^c (1.2)	2.2 (2.3)
RAYMODE X COHERENT	3.1 (2.2)	2.7 (2.5)
RAYMODE X INCOHERENT	1.5 (0.9)	2.4 (2.3)
RAYWAVE II INCOHERENT	2.0	2.5
RTRACE COHERENT	0.9	3.5
RTRACE ^d INCOHERENT	1.9	2.5

^a CASES I-III ^b CASES III-IV ^c CASES II-IV ^d CASE III

Table 3. Model Running Times

MODEL	COMPUTER	AVERAGE RUN TIME PER CASE (s)	NO. OF POINTS PER PREDICTION (TO 200 km)	REMARKS
AP2	CDC 6600	60.6	400	Run time is frequency dependent.
CONGRATS V*	UNIVAC 1108	42.3 (70.0)	200	
FACT/FNWC	CDC 6500	25.0	216	Includes calculations besides those needed for propagation loss.
FACT/NUSC	UNIVAC 1108	2.5	200	
FFP	UNIVAC 1108	373.0	2371	Run time is frequency dependent.
GORDON NORMAL MODE	UNIVAC 1108	84.8 ^b	400	Run time proportional to frequency; f = 200 Hz not run.
LORA*	UNIVAC 1108	28.7 (21.2)	219	First submission: f = 37.5; 67 Hz not run. Run time is frequency independent.
NSWC NORMAL MODE	CDC 6500	702.0	400	Run time is strongly frequency dependent.
PLRAY	CDC 6600	? (24.0)	400 (200)	First submission: f = 37.5 Hz not run.
RAYMODE X*	UNIVAC 1108	19.2 (41.7)	400	Run time is frequency dependent.
RAYWAVE II	UNIVAC 1108	50.7	200	
RTRACE	CDC 3600	45.0	400	

* For these models, it is assumed that the various types of phase addition used were part of the same computer run and that the run time so compared to a run with only coherent phase addition is negligibly different.

Table 4. Words of Computer Storage Required

MODEL	COMPUTER STORAGE (DECIMAL WORDS)
RAYMODE X	14115
NSWC NORMAL MODE	18940
AP2	20000
PLRAY	20480
FACT (NUSC)	21855
LORA	35000
RAYWAVE II	37000
FFP	51572
CONGRATS V	51760
GORDON NORMAL MODE	53000
RTRACE	58100
FACT (FNWC)	60000

$$\hat{p}_R(r, z, t) = \int_{-\infty}^{\infty} \mathcal{P}(r, z, f) \Omega(f) e^{-i2\pi ft} df$$

where

$\Omega(f)$ is the Fourier transform of the input source waveform and (r, z, f) is the transfer function of the medium which can be expressed in terms of the Fourier-Bessel transform previously examined for CW propagation. The impulse response of the medium is then given by

$$h(r, z, t) = \int_{-\infty}^{\infty} \mathcal{P}(r, z, f) e^{-i2\pi ft} df.$$

Let the continuous variables t and f be evaluated at the discrete points t_k and f_p where with $\Delta t \Delta f = 1/M$, $t_k = t_0 + k\Delta t$, $f_p = f_0 + p\Delta f$; $(k, p) = 0, 1, 2, \dots, M-1$. The constant t_0 is usually set equal to the approximate arrival time of the beginning of the waveform and f_0 would correspond to the lowest frequency present after filtering. Since Δf is predetermined from sampling theory, information about the waveform will be obtained from t_0 to approximately $t_0 + (\Delta f)^{-1}$. Generally, the time duration of the received waveform will increase with increasing range. Thus Δf is chosen small enough so that the time duration of the received waveform is adequate at the largest range of interest. As might be anticipated, the required computer storage and execution time increases as the frequency resolution, Δf , decreases, resulting in a significant data management problem.

The pressure field waveform is obtained upon evaluation of

$$\hat{P}_R(r, z, t_k) = \Delta f e^{-12\pi f_0 t_k} \sum_{m=0}^{2M-1} E_p(r, z, f_p) e^{-12\pi p k / 2M}$$

where, in order to obtain a real answer, the input is arranged according to

$$E_p(r, z, f_p) = \Omega(f_p) \varphi(r, z, f_p) e^{-12\pi p \Delta f t_0}$$

$$E_{M+p}(r, z, f_p) = E_{M-p}^* \quad , \quad p = 1, 2, 3, \dots, M-1$$

where the * indicates the complex conjugate and, additionally,

$$E_0 = \text{Re}\{\Omega(f_0) \varphi(r, z, f_0)\} \quad E_M = \text{Re}\{\Omega(f_M) \varphi(r, z, f_M) e^{-12\pi M \Delta f t_0}\} .$$

If the FFP, equation (38), is used to obtain the transfer function, the evaluation of the double FFT

$$\hat{P}_R(r_n, z, t_k) = A r_n^{-1/2} \sum_{p=0}^{2M-1} \Omega(f_p) e^{-12\pi p \Delta f t_0} \sum_{m=0}^{L-1} E_{m,p} e^{i2\pi mn/L} e^{-12\pi p k / 2M}$$

where

$$A = \Delta f \Delta \xi \frac{2}{\pi i}^{1/2} e^{i(\xi_0 r_n - 2\pi f_0 t_k)} \quad , \quad E_{m,p} = G(z, z_s; \xi_m, f_p) \xi_m^{1/2} e^{i m r_0 \Delta \xi}$$

provides the received pressure waveform as a function of range and time.

As an illustration of the above procedure, consider the typical arctic profile shown in figure 16. The rough under ice cover effectively filters out high frequencies at significant ranges from the source. Limit the frequency range to $0 \leq f \leq 250$ Hz. With $\Delta f = 0.12207 \text{ sec}^{-1}$, $\Delta t = 0.002 \text{ sec}$, and $M = 2048$, the time duration of the predicted waveform will be 8.192 seconds. This is adequate for ranges less than a few hundred kilometers. The value of t_0 is set equal to $t_0 = r_n / (1475)$; this is roughly the average arrival time of the deep RSR paths which come in first. The bottom was assumed to be a semiinfinite half space fluid layer with a constant sound speed of 1600 m/s. Its density and that of the water column were set to unity. The treatment of the bottom is, of course, unrealistic and justifiable only in that the example is solely for illustrative purposes.

The FFP must then be run at each of the above discrete frequencies in order to obtain the input E_p . The parameters used for this calculation were

$$\begin{aligned} \Delta \epsilon &= 9.964727793 \times 10^{-6} & \epsilon_0 &= .02372488 & L &= 8192. \\ \Delta r &= 76.9705 \text{ m} & r_0 &= \Delta r \\ z_s &= 100 \text{ m} & z &= 100 \text{ m} \end{aligned}$$

which provide sampling of all significant wavenumbers.

SOUND SPEED (m/s)

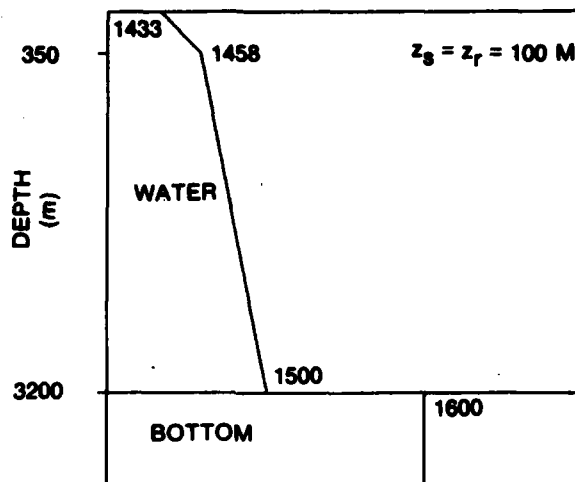


Figure 16. Typical Arctic Profile

The impulse response at $r_n \approx 100$ km is shown in figure 17. The three groups of spikes near the end of the figure from right to left correspond to bottom bounce energy associated with increasing angles of incidence. Three spikes, which correspond to the four rays interacting with the bottom, are evident within each group. The middle spike represents two rays whose travel time difference is so small that they cannot be resolved with the frequency resolution used. Excellent agreement with ray theory travel times is found to exist between each group and also within each group.

With the exception of the beginning, the remainder of the figure represents RSR rays which are trapped within the water column. The pattern of low amplitude arrival followed by arrivals of successively higher amplitude and then abrupt termination is typical of that commonly observed in the deep sound fixing and ranging (SOFAR) channel. In the case of the Arctic this has its axis at the ocean surface. Finally, the spikes at the beginning correspond to a combination of the deepest penetrating RSR arrivals and bottom bounce rays incident on the bottom between critical and grazing.

Kutschale^{72,73} has also examined this same problem with the FFP technique. In one case study, he compared the predicted frequency dispersion in that portion of the waveform, which would correspond to the first mode, with the analogous experimental results. That comparison is reproduced in figure 18 where it can be readily seen that excellent agreement was found. This agreement would not be expected to persist at higher frequencies where nondeterministic effects would be more significant.

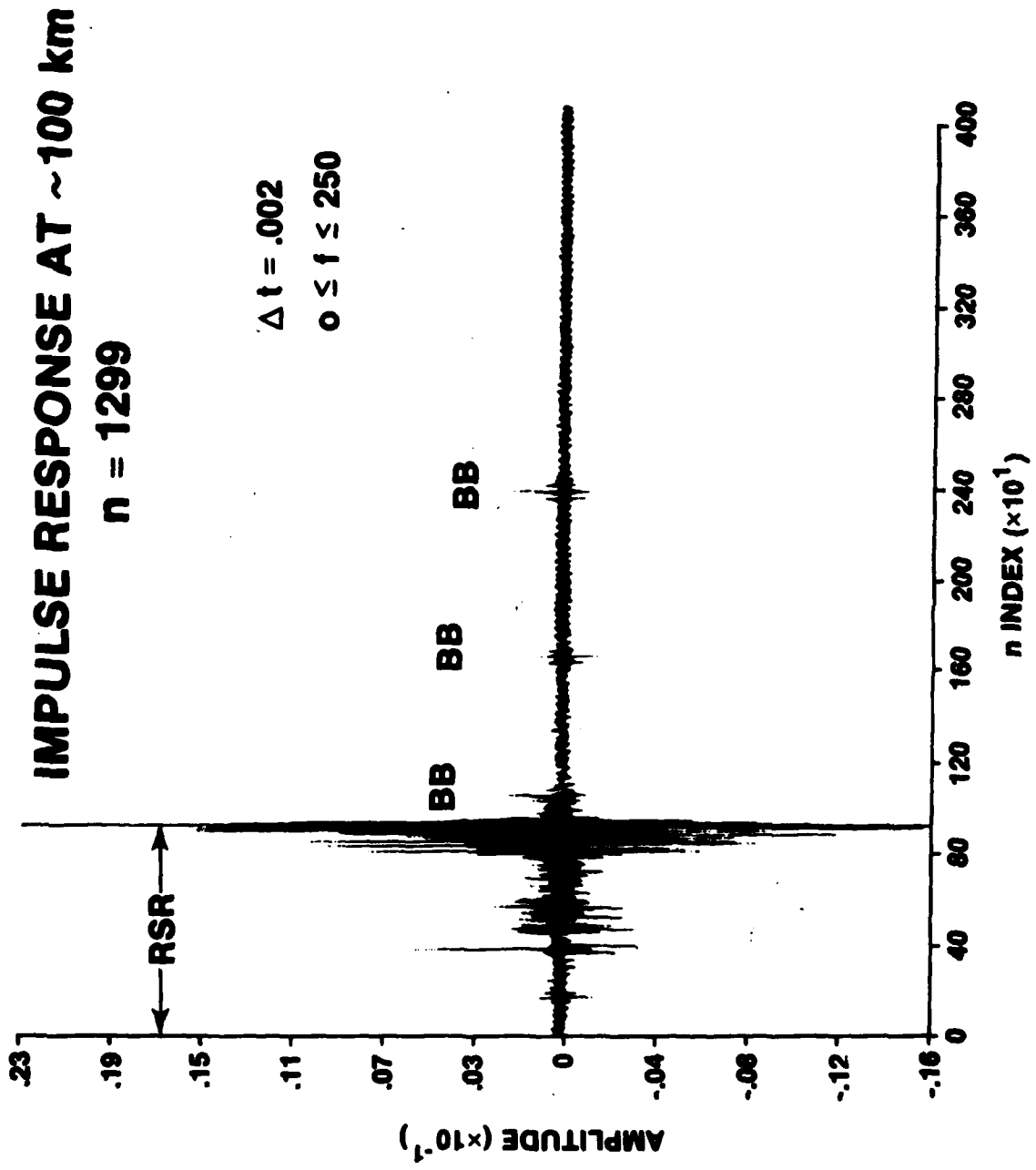


Figure 17. Impulse Response

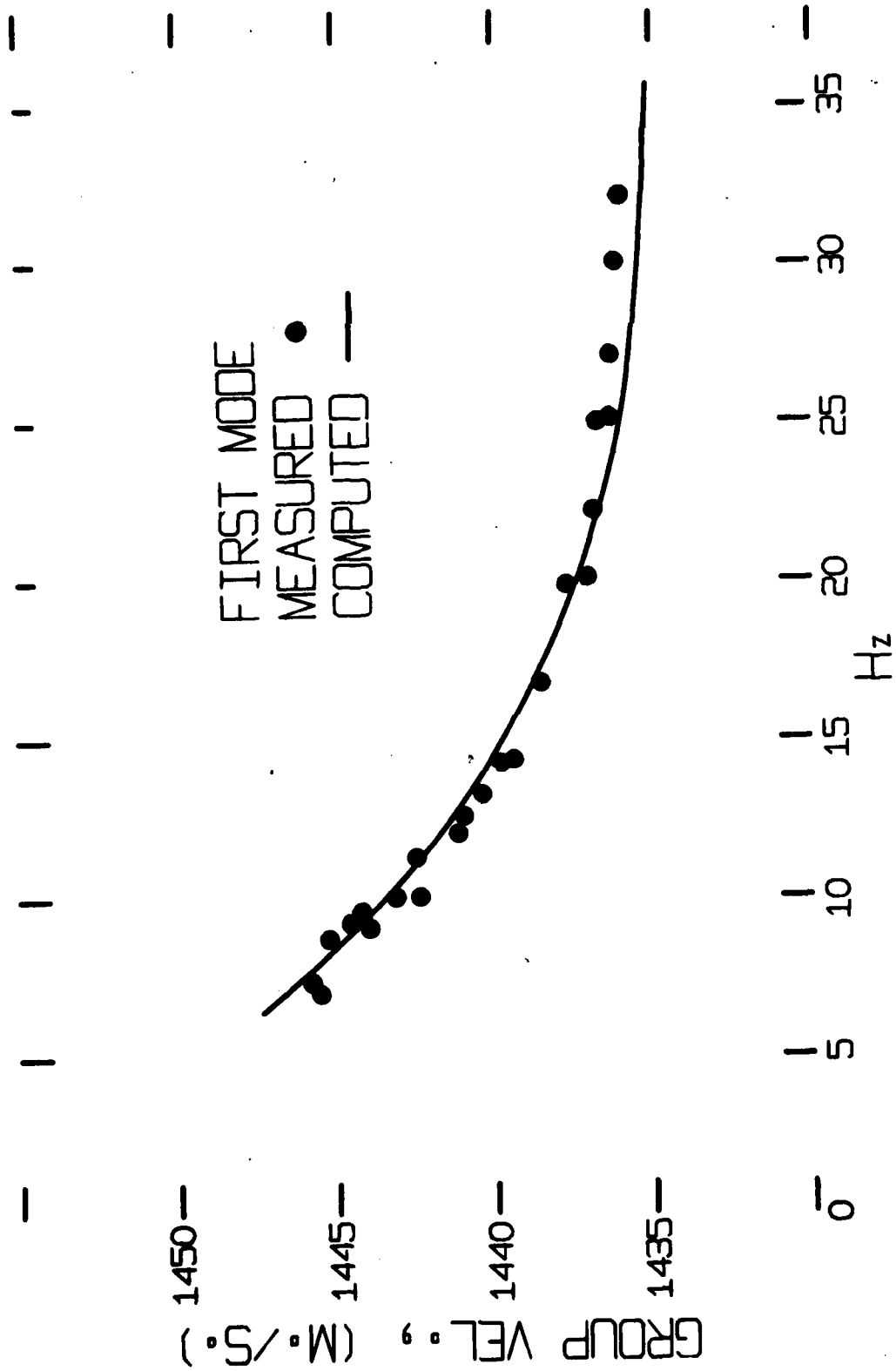


Figure 18. Dispersion of First Mode

2. RANGE DEPENDENT MODELS

INTRODUCTION

Computer models for the range dependent problem exist but are still in the developmental stage of evolution. In some instances, the validity of the solution is understood but its numerical implementation for underwater acoustic scenarios poses severe practical problems with existing computer technology. Alternate solutions are available which, to some extent, obviate the implementation problems. It is difficult, however, to precisely translate the required mathematical approximations into conditions of applicability of the solution. A limited amount of comparisons with experimental data has occurred. Often, however, this is not a totally satisfying process due to the incompleteness of the associated environmental data. For these reasons, a definitive appraisal of these models is best left for the future. It is felt that a brief survey of active areas of research would be more appropriate. This survey is provided below.

SPLIT STEP ALGORITHM FOR PARABOLIC EQUATION

The conditions under which the solution to the range dependent Helmholtz equation is well approximated by the parabolic approximation are discussed in reference 74 and in Chapter 2 of reference 75. Here attention is focused on the inherent approximations made in solving the parabolic equation by the split-step algorithm introduced by Hardin and Tappert⁷⁶ in 1973.

The parabolic equation may be written as

$$\frac{\partial U(r,z)}{\partial r} = i \{A(r,z) + B(z)\} U(r,z), \quad (94)$$

where the operators A and B are given by

$$A(r,z) = (k_0/2)(n^2(r,z)-1); \quad B(z) = (1/2k_0)(\partial^2/\partial z^2). \quad (95)$$

To obtain the split-step solution at $r = r_0 + \Delta r$ assume that

$$U(r,z) = \exp \left\{ i \int_{r_0}^{r_0+\Delta r} A(r,z) dr + i \int_{r_0}^{r_0+\Delta r} B(z) dr \right\} U(r_0,z), \quad (96)$$

which is only partially true since the quantity $[A(r,z) + B(z)]$ does not commute with its integral. Next assume that the index of refraction is a slowly varying function of range so that

$$U(r_0+\Delta r, z) = \exp[i\Delta r A + i\Delta r B] U(r_0, z). \quad (97)$$

The exponential operator can be approximated (split) in various ways. Originally Tappert⁷⁶ assumed

$$U(r_0 + \Delta r, z) = [\exp(i\Delta r A) \exp(i\Delta r B)] U(r_0, z) \quad (98)$$

and later (see reference 77)

$$U(r_0 + \Delta r, z) = [\exp(i\Delta r B/2) \exp(i\Delta r A) \exp(i\Delta r B/2)] U(r_0, z). \quad (99)$$

If the splitting given by equation (98) is assumed, it can be shown that the error incurred by assuming commutativity of the operators A and B is

$$[\exp(i\Delta r A)\exp(i\Delta r B) - \exp i\Delta r(A+B)] U(r, z) = +\frac{(\Delta r)^2}{2} \left\{ n \frac{\partial U}{\partial z} \frac{\partial n}{\partial z} + \frac{nU}{2} \frac{\partial^2 n}{\partial z^2} + \frac{U}{2} \left(\frac{\partial n}{\partial z} \right)^2 \right\} + \dots$$

In order to obtain the split-step algorithm, let $V \equiv [\exp(i\Delta r B)]U(r_0, z)$. Since $V = \mathcal{F}^{-1}[\mathcal{F}(V)]$ one has that

$$[\exp(i\Delta r B)]U(r_0, z) = \mathcal{F}^{-1} \{ \exp(-i\Delta r s^2 / 2k_0) \hat{U}(r_0, s) \},$$

where

$$\mathcal{F}[U(r_0, z)] = \hat{U}(r_0, s) = \int_{-\infty}^{\infty} U(r_0, z) e^{-izs} dz. \quad (100)$$

Then from equation (98), the split-step solution is

$$U(r_0 + \Delta r, z) = e^{ik_0 \Delta r (n^2 - 1)/2}$$

The Fourier integral transform indicated by \mathcal{F} is numerically evaluated with the FFT at each range step, i.e.,

AD-A082 380

NAVAL UNDERWATER SYSTEMS CENTER NEW LONDON CT NEW LO--ETC F/G 17/1
COMPUTER MODELS OF UNDERWATER ACOUSTIC PROPAGATION.(U)
JAN 80 F R DINAPOLI, R L DEAVENPORT

UNCLASSIFIED

NUSC-TR-5867

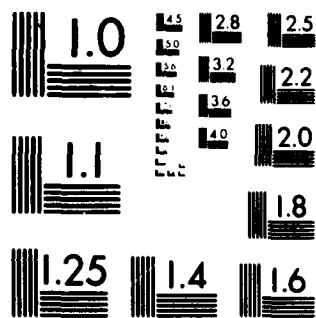
NL

2

1

1

END
DATE
FILMED
4 80
DTIC



MICROCOPY RESOLUTION TEST CHART
NATIONAL BUREAU OF STANDARDS 1963 A

$$\mathcal{F}^{-1}\{e^{-i\Delta r s^2/2k_0} \mathcal{F}[U(r_0, z)]\}$$

The solution can thus be marched out in range in a stable manner. In the evaluation of equation (100), attenuation is added to the medium below the depth of interest to ensure that the field decays to zero for large depths.

Consider the following three assumptions:

$$1. [A+B, \int (A+B)dr] = 0$$

(needed for equation (96) to be valid)

$$2. (ik_0/2) \int_{r_0}^{r_0+\Delta r} [n^2(r, z)-1]dr = (ik_0/2)[n^2(r, z)-1]\Delta r \quad (101)$$

(needed for equation (97) to be valid)

$$3. \exp[i\Delta r(A+B)] = \exp(i\Delta rA) \exp(i\Delta rB).$$

A feeling for their composite effects can be obtained by determining $\partial U/\partial r$ from equation (98) and then comparing the result with equation (94). From equation (98) one obtains

$$\frac{\partial U(r, z)}{\partial r} = [iA(r, z) + i\Delta r \frac{\partial A}{\partial r}]U(r, z) + [e^{i\Delta rA(r, z)} iB(z) e^{i\Delta rB(z)} U(r_0, z)] \quad (102)$$

The second term may be simplified upon rewriting equation (98) to obtain

$$e^{i\Delta rA} iB e^{i\Delta rB} U(r_0, z) = (e^{i\Delta rA} iB e^{-i\Delta rA}) U(r, z) \quad (103)$$

The term in parentheses can be written by the Baker-Hausdorff expansion⁷⁸ with the commutator $[A,B] = AB - BA$ as

$$\exp(i\Delta r A)(iB) \exp(-i\Delta r A) = iB - \Delta r [A,B] - i(\Delta r)^2/2! [A,[A,B]] + \dots$$

Then equation (102) may be written as

$$\frac{\partial U(r,z)}{\partial r} = i[A(r,z) + B(z)] U(r,z) + i\Delta r k_0 n (\partial n/\partial r) U(r,z) + \{-\Delta r [A,B] - i(\Delta r)^2/2! [A,[A,B]] + \dots\} U(r,z),$$

and the error (difference in differential equations) incurred by using the split-step solution,

$$ik_0 \Delta r n \frac{\partial n}{\partial r} U + \Delta r \left[n \frac{\partial n}{\partial z} \frac{\partial U}{\partial z} + \frac{nU}{2} \frac{\partial^2 n}{\partial z^2} + \frac{U}{2} \left(\frac{\partial n}{\partial z} \right)^2 \right] - \frac{ik_0 U}{2} \left(n \Delta r \frac{\partial n}{\partial z} \right)^2 + \dots, (104)$$

is seen to depend on the step size, Δr , the frequency, and the gradient of the index of refraction. Thus whenever significant energy from the field interacts with the bottom where $(\partial n/\partial z)$ is large, the Δr needed to make the error acceptable may lead to prohibitive computer execution times.

The result, equation (104), was also obtained by Jensen and Krol⁷⁹ who assume $n \approx 1$ and ignore higher order terms in the Baker-Hausdorff expansion. Their work also contains additional analysis regarding applicability of the split-step algorithm and comparison of execution times between the split-step solution and other models for several cases.

PARABOLIC DECOMPOSITION METHOD

Papadakis and Wood⁸⁰ seek an exact solution, $\varphi(z, z_s; r)$, to the Helmholtz equation for range dependent problems as an integral of the solutions of two parabolic equations. Specifically, with cylindrical symmetry and a separable index of refraction given by $n^2(z, r) = n_z^2(z) + n_r^2(r)$, one has

$$\varphi(z, z_s; r) = \int_0^{\bar{z}} G_1^*(t, r) G_2(t, z, z_s) dt, \quad (105)$$

where the asterisk denotes the complex conjugate and G_1 and G_2 satisfy the parabolic equations:

$$-2ik \frac{\partial G_1}{\partial t} + \frac{1}{r} \frac{\partial}{\partial r} \left(r \frac{\partial G_1}{\partial r} \right) + k^2 [n_1^2(r) + 1] G_1 = \frac{-2s(t)\delta(r)}{r} \quad (106)$$

$$2ik \frac{\partial G_2}{\partial t} + \frac{\partial^2 G_2}{\partial z^2} + k^2 [n_2^2(z) - 1] G_2 = \delta(t)\delta(z) \quad (107)$$

This approach reduces to the parabolic approximation usually obtained, which involves the solution of a single parabolic equation multiplied by a function dependent upon range. To see this, let $n_1(r)$ be zero. Then

$$G_1(r, t) = [H(t) / (4\pi t)] e^{-i\frac{k}{2}\left(\frac{r^2}{t} + t\right)}$$

where $H(t)$ is the unit step function. A stationary phase evaluation of equation (105) with the stationary phase point at $t = r$ yields

$$\mathcal{P}(z, z_s; r) = \frac{e^{i(kr + \pi/4)}}{2\sqrt{\pi kr}} G_2(r, z, z_s)$$

For arbitrary $n_1^2(r)$, G_1 is, in general, not known and would have to be approximated. The solution for \mathcal{P} could then be obtained by stationary phase techniques. Alternatively G_1 and G_2 could both be found numerically (see the discussion in *Finite Differences*) and the solution for \mathcal{P} obtained by quadrature. In this instance, attention would not have to be limited to an index of refraction which is slowly varying. Complex boundary value problems could be accommodated.

Finally, if the index of refraction is an arbitrary function of depth and range and nonseparable, the representation (105) remains valid. However, G_1 depends on r , z , and t . This case is also discussed in Chapter 2, reference 75 under *Corrected Parabolic Approximation*. Research on evaluating equation (105) for this case is in progress.

FINITE DIFFERENCES

The application of finite difference schemes to range dependent problems in underwater acoustics has received limited attention. Smith⁸¹ used finite difference to solve the coupled time dependent fundamental equations. McDaniel⁸² has investigated a finite difference solution of the parabolic wave equation and compared it with the split-step algorithm solution. The appeal of finite difference schemes lies in their ability to solve complicated boundary value problems which would be intractable with other approaches. Their shortcomings are primarily the excessive demands made upon computer

memory and execution time. It should be noted, however, that the exact nature of these demands within the context of underwater acoustic propagation has yet to be generally defined. Work along this line has recently been initiated by Lee and Papadakis.⁸³ A brief summary is provided below.

The solution of the elliptic wave equation given in terms of the parabolic decomposition integral, equation (105), is to be solved numerically. If the variation in both range and depth is rapid, the associated parabolic equations, (106 and 107), would be solved by finite differences. On the other hand if, for example, the range variation is slow, an asymptotic solution for that parabolic equation may be used. In any event, finite difference solutions of parabolic equations must be obtained. Consider as an example the parabolic equation

$$U_r = a(r,z) U + b(r,z) U_{zz} = \left(a + b \frac{\partial^2}{\partial z^2} \right) U = LU \quad (108)$$

The conventional development of implicit schemes can be expressed by

$$e^{-kL/2} U_m^{n+1} = e^{kL/2} U_m^n$$

and approximated by

$$(1 - kL/2) U_m^{n+1} = (1 + kL/2) U_m^n \quad (109)$$

where m is the depth index for a step size of h and n is the range index associated with the range step size k .

Introducing second order central difference operator,

$$D_z^2 = \frac{\delta_z^2}{h^2} (1 - \rho(k, h)) \quad ,$$

where ρ is a parameter chosen for optimum efficiency yields

$$-b_m^{n+1} \frac{(1-\rho)k}{2h^2} U_{m+1}^{n+1} + \left[1 + b_m^{n+1} \frac{k}{h^2} (1 - \rho) - \frac{ka_m^{n+1}}{2} \right] U_m^{n+1}$$

$$-b_m^{n+1} \frac{(1-\rho)k}{2h^2} U_{m-1}^{n+1} = b_m^n \frac{(1-\rho)k}{2h^2} U_{m+1}^n$$

$$+ \left[1 - b_m^n \frac{k}{h^2} (1-\rho) + \frac{ka_m^n}{2} \right] U_m^n + b_m^n \frac{(1-\rho)k}{2h^2} U_{m-1}^n .$$

The above may be written in matrix form, viz, $AU^{n+1} = BU^n + V_1^n + V_2^{n+1}$ where A and B are tridiagonal matrices and V_J ($J = 1, 2$) contain information about the boundary conditions. Appropriate selections for ρ will result in the familiar Crank-Nicolson and Douglas schemes.

The initial local truncation error is of order $O(k^3 + kh^2)$ for range independent problems and of order $O(k^2 + kh^2)$ for range dependent problems. The finite difference methods can be shown to be consistent and the stability condition is

$$\frac{1-b(1-\rho)k/h^2(1-\cos(Jh)) - ka/2}{1+b(1-\rho)k/h^2(1-\cos(Jh)) + ka/2} \leq 1 \quad J = 1, 2 .$$

Unconditional stability results if all $a, b, k, h > 0$. The convergence of the finite difference scheme can be shown by examining the norm inequalities $\|t.s.-n.s.\| \ll \|t.s.-f.s.\| + \|f.s.-n.s.\|$, where

t.s. stands for the theoretical solution of equation (108)

n.s. stands for the numerical solution of equation (108)

f.s. stands for the finite difference solution of equation (108).

The convergence is established by applying the consistency criteria to the first norm on the right hand side and applying the error control to the second norm.

A second approach involves the use of finite difference schemes developed to solve ordinary differential equations. Let the U_{zz} term in equation (108) be discretized by a second order central difference. Then

$$(U_m)_r = a_m U_m + \frac{bm}{h^2} (U_{m+1} - 2U_m + U_{m-1}) ,$$

which leads to a system of ordinary differential equations,

$$\frac{dU_m}{dr} = \left(a_m - \frac{2b}{h^2} \right) U_m + \frac{bm}{h^2} (U_{m+1} + U_{m-1}) .$$

They may be written in matrix form as $U' = AU + g(r,z,U)$. A family of nonlinear multistep (NLMS) methods,⁸⁴ as well as linear multistep (LMS) methods⁸⁵ have been developed to solve such systems. The conditions for consistency and stability for both the NLMS and LMS methods are well known and these methods are convergent. In addition to the existence of well developed numerical programs for such methods, powerful step-size adjustment techniques based upon the use of predictor-corrector algorithms automatically adjust the step size to maintain a prescribed accuracy.

To provide a feeling for the execution time, consider equation (108) with $b(r,z) = 1$, $a(r,z) = r^2 - z^2$ and the boundary conditions

$$U(0,z) = 1, U(r,0) = 1, U(r,1) = e^{-r}$$

for which the exact solution is $U(r,z) = e^{-r^2}$. The answers, as obtained on a PDP 11/70 computer, for a range of 1609 meters and a depth of 804.5 m are given below.

Method	k(m)	h(m)	Time(s)	Solution
Finite Difference	1.609	160.9	77	.6066E + 00
O.D.E.*	1.609	160.9	92	.6067E + 00
Exact				.6065E + 00

*Ordinary differential equation.

RANGE-DEPENDENT NORMAL MODE THEORY

Kanabis⁸⁶ has developed a computer model for the range dependent problem which has its foundations in normal mode theory. The rate of change in the stratification with range is not limited to be *slowly varying* since the effect of mode conversion is approximately included. For this reason, large changes in the sound speed profile, water depth, and bottom composition with range may, in principle, be accommodated.

The total range interval is divided into segments in which the sound speed profile and bottom composition are arbitrary functions of depth but do not change with range over the subinterval. The *trapped modes* within any range interval are calculated as if the problem were range independent. These modes are then summed to give the total field at the junction of the next segment. Next it is assumed that this field may be adequately represented by a vertical distribution of appropriately weighted point sources. The trapped modes of the new range interval are calculated for each point source and summed to give the total field at the end of that section. In the early development (see reference 87) each range segment was rectangular. This resulted in a bottom height with a staircase behavior. The backscattering of energy from this bottom structure, as well as backscattering, which would result from the difference in impedance of the water column between segments, was neglected.

This approximation was subsequently improved upon (see reference 86). This model has undergone limited comparison with both experimental data and analytical test cases. As a result, it is difficult at this time to reach a conclusion regarding the adequacy of the approximations made. In addition, the determination of the number of required range segments seems best arrived at by running the model for an increasing number of range segments until convergence in the answer is observed.

RANGE-DEPENDENT RAY THEORY MODELS

Two methods for implementing range dependent ray theory are in common use.⁸⁸ The first method⁸⁹ allows the sound-speed representation to be arbitrary in depth but linear, quadratic, or cubic in range at fixed depth. The second method⁹⁰ is based upon segmenting the region between the profiles into triangular sectors in which two vertices of the triangle correspond to two points on one of the profiles. The third vertex corresponds to a point on the other profile. Along the connecting legs of the triangle the sound speed varies as $c(z,x) = c_0 + az + bx$. Both methods have their drawbacks. The first method is easy to automate but leads to ray-tracing difficulties because closed form expressions for the ray paths are not available. Additionally, this method can lead to totally unreasonable profiles at intermediate ranges between reasonable specified profiles. The second method is quite difficult to automate. It usually requires an oceanographer to determine the required connections. Aside from this problem, however, the linearity of the sound speed leads to a closed form expression for a ray's path within each triangular sector resulting in a relatively rapid trace.

FINITE ELEMENT APPROACH

Kalinowski⁹¹ has recently examined the applicability of the finite element method (FEM) solution to acoustic propagation problems in a range dependent environment. A synopsis of that survey has been provided by Kalinowski and is presented below.

The FEM solution (in its current form) was initially developed (reference 92) in the structural mechanics field of the aircraft industry. A complete historical treatment is provided by Oden.⁹³ The initial generalization to other fields⁹⁴ has been followed by papers^{95,97} in nonstructural applications such as fluid mechanics, acoustics, electromagnetic field theory, heat transfer, etc. FEM is well documented in introductory books,⁹⁸⁻¹⁰¹ as well as in more detailed theoretical developments.^{102,103} Further, reference 104 provides a collection of 7115 references on the subject.

The propagation of acoustic energy in the ocean involves interaction between the areas of acoustic wave propagation in fluids and stress wave propagation in solids. A good deal of work related to the finite element is found exclusively in the fluids area (either fluids alone or interacting with submerged structures), see references 95-97 and 105-106, or, exclusively, in the solids area (either solids alone or interacting with buried structures). See, for example, references 107-115 and numerous articles in the *Earthquake Engineering & Structural Dynamics Journal* and the *Bulletin of the Seismological Society of America*. However, very little finite element orientated work^{91,116,117} appears to have been published specifically in the area of acoustic wave propagation in the ocean in which the ocean bottom is treated as a coupled part of the solution (i.e., the bottom is modeled with more detail than implied by the usual approach of treating the fluid-bottom interaction with interaction with either a rigid or known impedance type boundary condition).

In references 91 and 117 a displacement formulation FEM is suggested for acoustic propagation problems. The formulation discusses modeling both the fluid and an irregularly shaped multilayered bottom with either rotationally symmetric ring elements or with planar elements. This technique allows for a sound speed profile which can vary in both range and depth; a nonflat ocean surface or bottom; both dilatational and shear waves in the bottom; dissipative loss in the bottom; a simply connected fluid domain (e.g., voids to represent a school of fish); 3-d directional sources modeled via a Fourier expansion of the field solution in angular harmonics; and a methodology adaptable to existing general purpose programs (e.g., Nastran¹¹⁶). A sample solution taken from reference 91 is provided later in this section.

Although not specifically stated as such, in reference 116 a Galerkin type variational scheme is employed which leads to an FEM type formulation. The fluid domain is treated as rotationally symmetric and bounded by a flat free surface and an arbitrarily shaped (but rigid) bottom. The main contribution of this work is an accurate procedure for handling the infinite domain (i.e., *transparent boundary*) at the truncation end of the finite element mesh.

The Finite Element Method

As previously pointed out, the finite element method has been firmly established for the past 20 years. Consequently, its development is given briefly for completeness.* Consider the case in which the response of the continuum is expressed by the solution to the partial differential equation(s),

$$[A(\phi)] = 0, \quad (110)$$

which applies to a domain Ω where boundary conditions

$$[B(\phi)] = 0 \quad (111)$$

are satisfied on the boundary Γ . $[A]$ and $[B]$ are general partial differential operators and $\{\phi\}$ are function(s) representing the continuous field solution.† Often, $[B(\phi)]$ is defined as a mixed boundary value problem (i.e., $[B] = [B_1(\phi)]$ on Γ_1 and $[B] = [B_2(\phi)]$ on Γ_2 where $\Gamma = \Gamma_1 + \Gamma_2$). The specific meaning of $\{\phi\}$ depends on the formulation selected by the analyst (a specific example for a fluid domain is $\phi =$ pressure in the fluid and $\phi =$ field displacements in a solid ocean bottom).

*Reference 119 gives a concise description of the FEM. It is condensed here with some notational differences and with emphasis on the aspects of these methods relevant to the ocean-bottom interaction problem.

†The standard notation for matrices and column vectors, respectively, is employed throughout the finite element section.

The unknown response function(s) $\{\phi\}$ is approximated $\{\hat{\phi}\}$ by a series of prescribed shape functions, $[N(\bar{x})]$, and associated unknown multiplying factors $\{a\}$, where

$$\{\hat{\phi}(\bar{x})\} = [N(\bar{x})] \{a\}. \quad (112)$$

The column vector $\{a\}$ has I components, $[a_1, a_2, \dots, a_I]^T$. The specific structure of equation (112) is displayed more clearly with a specific example. Let $\{\hat{\phi}\}$ denote two dependent functions of a particular problem (like displaced components in a solid). The more detailed form of equation (112) then becomes

$$\{\hat{\phi}(\bar{x})\} = \begin{Bmatrix} 1\hat{\phi}(\bar{x}) \\ 2\hat{\phi}(\bar{x}) \end{Bmatrix} = \begin{bmatrix} N_1(\bar{x}) & 0 & N_2(\bar{x}) & 0 & \dots & N_J(\bar{x}) & 0 \\ 0 & N_1(\bar{x}) & 0 & N_2(\bar{x}) & \dots & 0 & N_J(\bar{x}) \end{bmatrix} \begin{matrix} 1^{a_1} \\ 2^{a_1} \\ 1^{a_2} \\ 2^{a_2} \\ \vdots \\ 1^{a_J} \\ 2^{a_J} \end{matrix}$$

where $I = 2J$.

The problem unknowns in the FEM are represented by discrete $\{a\}$ values rather than the continuous $\{\hat{\phi}(\bar{x})\}$ function. The $\{a\}$ values are determined as solutions to a set of *approximating* equations which have integral forms like

$$F_j(a_j) \equiv \int_{\Omega} G_j(\hat{\phi}) d\Omega + \int_{\Gamma} g_j(\hat{\phi}) d\Gamma = 0 \quad (113)$$

$j = 1, 2, \dots, I$

where the generation of $F_j(a_j)$ is obtained by alternate formulations to be defined shortly. The domain Ω and boundary Γ are subdivided into K finite element zones (see figure 19), where Ω_k^E, Γ_k^E denote the domain and boundary of a typical k^{th} finite element. The integrals appearing in equation (113) are then composed of the sum of the K element contributions

$$\int_{\Omega} G_j(\hat{\phi}) d\Omega = \sum_{k=1}^K \int_{\Omega_k^e} G_j(\hat{\phi}) d\Omega$$

$$\int_{\Gamma} G_j(\hat{\phi}) d\Gamma = \sum_{k=1}^K \int_{\Gamma_k^e} g_j(\hat{\phi}) d\Gamma,$$

where the Σ operators refer to the *standard assembly rules* of structural forms (see references 97 and 100).

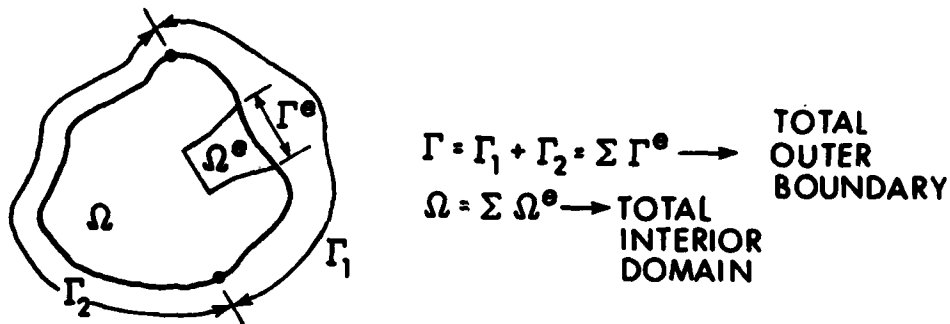


Figure 19. Definition of Interior Domain and Boundary

Although not absolutely necessary, the usual condition imposed is that the trial shape functions, $N_i(x)$, be narrowly based (i.e., for an arbitrary i , $N_i(x)$ are given zero values everywhere, except in elements containing the unknown, a_j). The narrow based trial functions leads to a set of banded (often symmetric) set of simultaneous equations for the unknown $\{a\}$.

Thus, substituting shape function expansions given by equation (112) into equation (113) (and performing the explicit spatial integrations, numerically if necessary) yields a set of simultaneous equations for the unknowns $\{a\}$. The above restriction only affects the bandedness of the resulting set of simultaneous equations. It is not a strict requirement of the FEM technique.¹²⁰ The differences between various finite element approaches arise from the choice of the shape functions, $N_i(x)$, selected and also by the manner in which the approximating equations, equation (113), are derived. Specific integral formulations of equation (113) are constructed from (1) weak formulations of the Galerkin type or least square or collocation types or (2) through the introduction of perhaps the most popular (although not always applicable) *variational principles*. In the least square and variational principle formulations, the development of the $F_j(a_j)$ in equation (113) involves the minimization of the functional, $I(\hat{\phi})$,

$$F_j(a_j) = \frac{\partial I(\hat{\phi})}{\partial a_j} = 0 \quad j=1,2,\dots,I \tag{114}$$

over the problem variables $\{a\}$, where $I(\hat{\phi})$ is of the form

$$I(\hat{\phi}) = \int_{\Omega} H(\hat{\phi}) d\Omega + \int_{\Gamma} h(\hat{\phi}) d\Gamma . \quad (115)$$

The evaluation of the $F_j(a_j)$ expression (113) usually leads to a linear set of algebraic equations of the form*

$$[K] \{a\} = \{f_j\} . \quad (116)$$

For either the variational principle or the least square formulation, it follows from equation (114) that the $G_j(\hat{\phi})$, $g_j(\hat{\phi})$ are related to $H(\hat{\phi})$, $h(\hat{\phi})$ by

$$G_j(\hat{\phi}) = \frac{\partial H(\hat{\phi})}{\partial a_j} ; \quad g_j(\hat{\phi}) = \frac{\partial h(\hat{\phi})}{\partial a_j} .$$

The matrix $[K]$ (known as the generalized stiffness matrix of the system for structural applications) is obtained from the volume integrals in equation (113). The problem loading, $\{f_j\}$, is determined from the surface integrals in equation (113). From a computational viewpoint, it is desirable to have the resulting $[K]$ banded and symmetric. However, not all FEM formulations yield this feature.

The volume integration in equation (113) generates the generalized stiffness matrix, $[K]$. Attention is focused on the various forms for the kernel, $H(\hat{\phi})$, that are employed for a specific problem. Briefly stated, the problem is that of solving the steady state acoustic response in a fluid domain governed by the Helmholtz equation,

$$\nabla^2 \phi(\bar{x}) + k^2 \phi(\bar{x}) = 0 , \quad (117)$$

where the fluid pressure, p , is related to the velocity potential, ϕ , by the relation $\phi = -i\omega q p$, with ρ = fluid density, $k = \omega/c$, ω = circular frequency, and c = a piecewise constant (within an element Ω_k sound speed). Reference 122 employs a variational principle, where

$$G_j(\hat{\phi}) = \frac{\partial H(\hat{\phi})}{\partial a_j} = \frac{\partial}{\partial a_j} \int_{\Omega} \nabla \hat{\phi} \cdot \nabla \hat{\phi} - k^2 \hat{\phi}^2 , \quad (118a)$$

that leads to the development of equation (116). In another approach, reference 115 employs a Galerkin variational form, where

$$G_j(\hat{\phi}) = - \int_{\Omega} \nabla \hat{\phi} \cdot \nabla \psi_j + k^2 \hat{\phi} \psi_j , \quad (118b)$$

(with $\psi_j(\bar{x})$ as a shape function having the form of the shape functions $N_j(\bar{x})$) and leads to another alternate development of equation (116). Finally, reference 123 employs a least square approach, where

$$G_j(\hat{\phi}) = \frac{\partial H(\hat{\phi})}{\partial a_j} = \frac{\partial}{\partial a_j} \int_{\Omega} (\nabla^2 \hat{\phi} + k^2 \hat{\phi})^2 , \quad (118c)$$

*In certain cases such as transient solutions⁹⁸ or with special *continuous coordinate* finite element formulations,¹²¹ equation (116) is replaced by an ordinary differential equation in $\{a\}$.

which leads to still another alternate form of equation (116).

Merits/Shortcomings of FEM

The merits and shortcomings of numerical solutions employing FEM, which are summarized in references 91 and 119, are given below with special emphasis on the ocean-bottom interaction problem.

Merits of FEM. 1. Representation of both the ocean (fluid) and bottom (solid) with finite elements is easily done. The total fluid and bottom domain are modeled with individual finite elements (each having their own physical constants). Therefore, the representation of solid media with multimaterial properties (e.g., layers) or representation of the fluid with variable sound speed profile in one, two, or three directions is achievable. The boundaries of the media can be irregular allowing sea mounds etc., to be modeled. A demonstration problem employing some of these features is presented below.

2. Nonlinearities (e.g., a nonlinear representation of the bottom media stress-strain law) potentially can be included in the formulation. This, however, is accomplished at the expense of having to treat the time variation as a transient rather than steady state problem. Thus transient ordinary differential equations in $\{a\}$ must be solved.

3. Owing to the locally based shape functions, the final equations for the discretized unknowns are banded (and usually symmetric). This offers certain computational advantages with relation to speed of solution and computer storage capacity.

4. The unknown parameters $\{a\}$ are physically identifiable (e.g., displacement and pressure variables for the ocean-bottom interaction problems).

Shortcomings of FEM. 1. The number, I , of unknown parameters in $\{a\}$ is large in that both the volume domain, Ω , and surface domain, Γ , are discretized. This is a particularly strong disadvantage for the ocean problems, especially if a total three-dimensional representation is considered. Practically speaking, 2-d planar or rotationally symmetric domains are considered to keep the number of degrees-of-freedom manageable. Theoretically, however, the method is totally applicable to the general three-dimensional case.

2. Representation of the infinite domain presents the problem that only approximate truncation boundary conditions are normally employed. The closely related boundary solution methodology (BSM) and boundary integral methodology (BIM) offer relief from element modeling. However, this is often at the expense of requiring the media to be homogeneous.^{91,117,119}

3. For steady state problems, as many as eight elements per wavelength are potentially needed to adequately model the domain.^{108,124} However, reference 116 appears to require less fine modeling (e.g., two elements per wavelength) with its particular approach.

4. Singularities that arise under concentrated loads are troublesome to model, e.g., the representation of a point (or line) source radiating from some location in the ocean.

TRANSPARENT BOUNDARY SIMULATION TECHNIQUES

Aside from the obviously large number of degrees-of-freedom required to model a problem, the chief disadvantage is the proper treatment of the infinite domain truncation. A typical planar or axis-of-revolution finite element model for an ocean-bottom problem typically involves four separate boundaries of an overall elongated region bounded by four surfaces (e.g., figure 20). The region is a

planar section for two-dimensional Cartesian coordinate problems or it is a cross section of a torus for rotationally symmetric (r-z cylindrical) problems.

The ocean surface boundary is perhaps the only clear cut boundary, when a zero pressure condition is imposed along this side. Depending upon the degree of bottom detail imposed by the modeler, the bottom boundary condition presents several choices. It may be considered rigid: (1) modeled with a prescribed impedance; (2) modeled with finite elements terminated by either of the two previously mentioned options; (3) modeled with finite elements and terminated with a prescribed impedance; or (4) modeled with finite elements that are terminated with a transparent boundary condition. The remaining two vertical surface boundaries cut through and truncate both the fluid and bottom domains. Each of these two boundaries has the problem of requiring the imposition of a proper radiation (i.e., transparent) boundary condition. In situations where the problem loading is such that a plane of symmetry exists (e.g., the sample problem considered later figure 20), a boundary condition demanding that the particle displacements be zero normal to the plane of symmetry clarifies one of the vertical boundaries. In various forms (in both the field of acoustics and the field of seismology), the remaining down range vertical boundary has received a good deal of attention in the literature. Other than in references 91 and 125 there appears no single reference that considers the most general case: that of having the vertical boundary made up of part fluid and part solid. Consequently, the transparent boundary treatment for each of these two types of media is briefly and separately considered. The reader is referred to in references 91 and 125 for a more detailed survey.

SOLID DOMAIN BOUNDARIES

Perhaps the simplest idea for handling the transparent boundary is given in reference 108. In that case, a plane wave type boundary condition of the form

$$\sigma_n = \rho c_n v_n \quad (119)$$

$$\sigma_t = \rho c_s v_t$$

is applied at the truncation of the solid finite elements, where σ_n , σ_t are the normal and tangential interface stresses, ρ is the solid media mass density, c_s , c_d are the dilatational and shear wave speeds, and v_n , v_t are the corresponding normal and tangential velocities at a typical point on the solid boundary surface. The conditions in equation (119) are exact if the incident radiating energy impinging on the surface is made up of plane waves of normal incidence to the surface. As pointed out in references 108 and 124 these conditions are still reasonably accurate, even when either of the incident waves is substantially off normal incidence. If one employs a displacement finite element approach (i.e., the unknown parameters $\{a\}$ are displacement quantities at the finite element grid work), the transparent boundary gives the appearance of having viscous dampers applied normal and tangential to the solid domain boundary point (where the ρc_n (or ρc_s) velocity coefficient multiplied by an appropriate area factor represents the value of the viscous damping constant). An application of this type of absorber is illustrated in figure 20. References 91, 108, 126 and 127 consider the accuracy of this type of boundary condition.

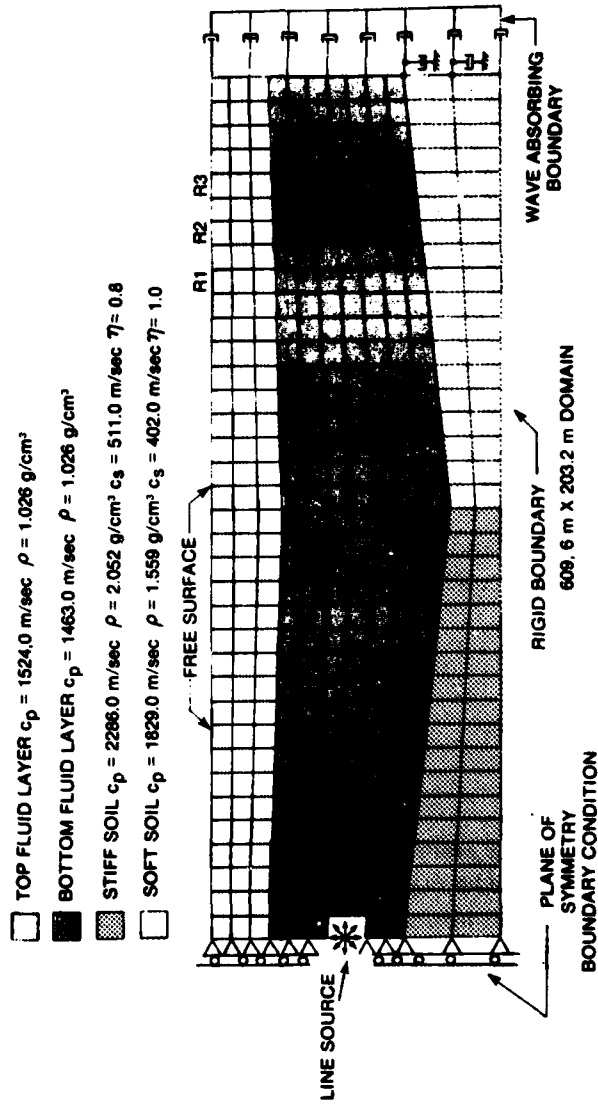


Figure 20. Ocean-Bottom Interaction Finite Element Method

More accurate methods of treating the transparent boundary exist but result in a more complicated formulation. Reference 128 considers a Rayleigh wave type viscous absorber similar to that in reference 108, except the right side of these equations are multiplied by known depth and frequency dependent parameters. A semianalytical consistent boundary concept involving *hyperclements* is considered in references 113 and 114 for rotationally symmetric domains and in references 109 and 112 for planar domains. These techniques are not easily utilized because they involve finding eigenvalues and associated eigen frequencies of the solid media beyond the mesh truncation. Reference 110 considers an approach analogous to that in references 109 and 112-114, except that *finite element substructuring* is employed. This enables one to treat a large domain of finite elements representing irregular material and irregularly shaped variation zones of the solid domain. Reference 121 considers an approach viewed in reference 114 as a generalization of the hyperclement. A main difference is that the solid domain is modeled with finite elements in all spatial coordinate directions except one, which, as in the usual FEM, is represented continuously rather than discretely. The result is that even for steady state problems, the final governing equations are differential equations (rather than algebraic equations) in the problem unknowns $\{a\}$. Finally, reference 119 considers treating the infinite domain by coupling FEM with either the boundary solution method or boundary integral method.

FLUID DOMAIN BOUNDARIES

In theory, one should be able to appropriately reduce the various schemes for the solids' case described above into the fluid application case by appropriately discarding the shear wave response portion of the solid media response. As an example of this, consider the viscous type boundary condition given by the first of equation (119). Reference 129 employed this type boundary condition for pressure element formulation and references 105 and 124 considered it for a displacement fluid element formulation. The accuracy of this type boundary absorber with relation to fluid applications is discussed in more detail in references 124, 116, and 91.

Considered next are other transparent boundary treatments which are not limiting cases of the solids' approaches already discussed. Reference 116 considers a *generalized radiation condition* of the form $\partial\phi/\partial r = T(\phi)$ which is incorporated into a Galerkin type variational formulation. In this formulation ϕ is the velocity potential and $T(\phi)$ is a Hankel function expansion representing outward radiating waves with coefficients determined as part of the solution methodology (e.g., for the equation (119) type of absorber, $T(\phi)$ reduces to $i\omega\phi$). *Infinite elements* are considered in references 130-132, which constitute the last (outmost) elements of the domain. The shape functions N_j are of the form

$$N_j = \tilde{g}_j(s) e^{-s/L} e^{iks}$$

where s is a spatial coordinate in the direction of the parametric coordinate extending to infinity, $\tilde{g}_j(s)$ is a Lagrange polynomial allowing for the usual amounts of shape change in the field of interest, $e^{-s/L}$ represents the wave decay with increasing s (where L is an approximate decay length constant), and e^{iks} represents the usual harmonic waveform variation. Reference 133 derives a *generalized outflow boundary condition* by the application of Fourier transforms in the region exterior to the

computational domain. Finally, techniques employing the boundary integral method are often used to handle the infinite fluid domain. However, these are primarily concerned with application of these techniques to radiation or scattering problems related to various types of solids^{105, 134-136} submerged in a constant sound speed fluid.

COMBINED SOLID-FLUID DOMAIN BOUNDARIES

The ocean-bottom interaction problem has not received much attention in finite element literature. Consequently, those wishing to apply FEM to this field must employ ingenuity in utilizing (or combining) the separate techniques (described earlier) for treating the solid domain alone and for treating the fluid domain alone.

As an example of making one such combination, consider the problem of solving for the pressure response in a variable sound speed, two-dimensional fluid region bounded by a free surface from above and by a multimaterial soil media (terminated by rock) from below (see figure 20). The input is a steady state line source whose axis is normal to the two-dimensional domain. For convenience in modeling, it is assumed that the source lies on a plane of symmetry enabling one to use an appropriate plane of symmetry boundary condition along one of the vertical faces. The remaining vertical face, at the opposite end of the model, is the one requiring the transmitting boundary condition. This boundary, shown at the right and in the finite element model (figure 20), contains part fluid and part solid media. The elementary viscous boundary condition of equation (119) is used for both the solid and fluid (the fluid case omits the unneeded viscous shear dampers). Wave speed parameters are assigned values according to the material they directly contact. The 430 element model is only used as a demonstration of the approach. Consequently, the size of the mesh modeling, particularly in the solid domain, is rather large.

The model is selected to emphasize the positive features of the finite element method. These features include the irregularly shaped bottom, the variable material bottom, inclusion of dissipative loss factor in the bottom, and a variable sound speed fluid domain (note fluid layers need not be flat and parallel with the global coordinate system). The generalization of the above sample problem to additional solid material variations and more complicated sound speed profiles is straightforward.

The finite element model is constructed from a displacement formulation approach for both the solid and fluid domain. An alternate approach more often used is to represent the fluid with *pressure type* finite elements, and only the solid domain with *displacement type elements*. The distinction between these basic type of elements is covered in more detail later. The FEM model satisfies the fluid-solid interface boundary condition of equal displacements normal to each point of interface contact. The physical constants of the sample problem such as mass density, ρ , dilatational sound speed, c_p , shear wave sound speed, c_s , and loss factor, η , are specified directly in figure 20. A 10 Hz line source pressure loading is represented by a set of nodal forces (applied at the open cut in the figure 20 mesh) which corresponds to a unit pressure at the initial wavefront (all other response pressure plots are referenced to this value).

In order to emphasize the importance of including the effect of bottom compliance on the down range pressure response, the problem was solved twice; once with a compliant soil sloping bottom (as shown in figure 20) and again with a rigid sloping bottom. The solution time on a Univac 1108 computer is approximately four minutes of computer program unit (CPU) time per incident frequency considered.

One method of displaying the pressure response is with contour plots. Since the solution is complex, plots reflecting both the real and imaginary parts of the solution (or, alternately, the amplitude and phase angle) are usually made. The amplitude phase angle contours are perhaps the most informative for the ocean-bottom interaction class of problems. Contour lines of constant pressure amplitude reveal the location of possible shadow zones. Lines of constant phase indicate wavefronts (lines normal to the constant phase contours are analogous to rays indicating the direction of wave propagation). The plot package used to generate the figure 21 results is not sophisticated in that contours approaching the boundary nodes are not as reliable as contours at or near interior nodes (due to the interpolation scheme employed at the boundary). Consequently, the contours are terminated at the nodes that are just inside the boundary nodes. Further, only pressure amplitude in the fluid (i.e., omitting the solid domain) is plotted.

For the phase angle plots, the 0° and -360° contours mathematically represent the same plotted line. As a result, this nonuniqueness creates some confusion to the contour plotter, particularly for closely packed contours. The computer plotted phase angle contours in figure 21b were considered unreliable in the shadow zone area. Consequently, the contours were sketched in by hand (dashed portion of contours only) based on conjecture and analogy with figure 21d.

Upon making a comparison of the corresponding rigid bottom and soil bottom plots the importance of modeling the compliance of the bottom in the problem formulation is clear. A closer look at the data reveals how some erroneous conclusions could be drawn from an improperly modeled bottom (e.g., if the bottom were approximated as rigid as a modeling simplification). Consider, for example, the point labeled D_1 in figures 21a and 21c. The rigid bottom pressure amplitude indicates point D_1 to be in a shadow zone in which the soil bottom pressure amplitude for the same point, all other things held constant, is twice as large. Conversely, comparing points D_2 (same range but roughly 44 meters deeper) in the same plots reveals the reverse situation. The rigid bottom pressure amplitude is twice as large as the corresponding soil bottom pressure amplitude.

As a final comment regarding the suitability of the standard viscous transparent boundary in the fluid domain, it is noted that in figure 21d normals to the wavefronts at the right end are very nearly perpendicular (90° is normal incidence) to the right side vertical face. This is the ideal situation for this viscous absorber to work. On the other hand, the figure 21b plot shows the wavefront normals are as far as 55° off normal. Reference 124 contains percent error versus angle of incidence plots indicating that at 55° approximately 97 percent of the energy is still absorbed by a plane wave. This plane wave would be obliquely incident upon a set of fluid viscous absorbers as employed in the figure 20 demonstration problem. In fact, according to reference 124, 90 percent of the incident energy is absorbed even at a shallow 30° angle of incidence. The phase angle contour plots approaching the mesh termination boundary thus provide a secondary use in aiding the modeler to check the validity conditions of the viscous absorbers. In fact, speculating further, it appears possible (although as yet untried) to alter the size of the damper according to the observed angle of incidence as determined from a contour phase angle plot. Portions of the boundary not meeting a prescribed tolerance regarding the deviation from the ideal normal incidence can have those particular absorbers adjusted by a prescribed amount (the amount depends on the angle of incidence) so that a second iteration computer can be made to improve the fluid portion transparent boundary performance.

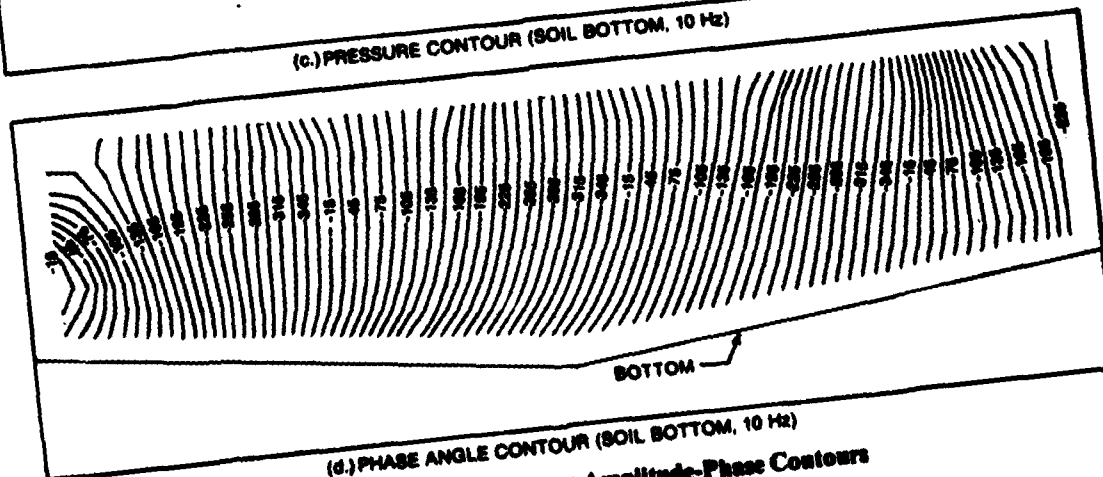
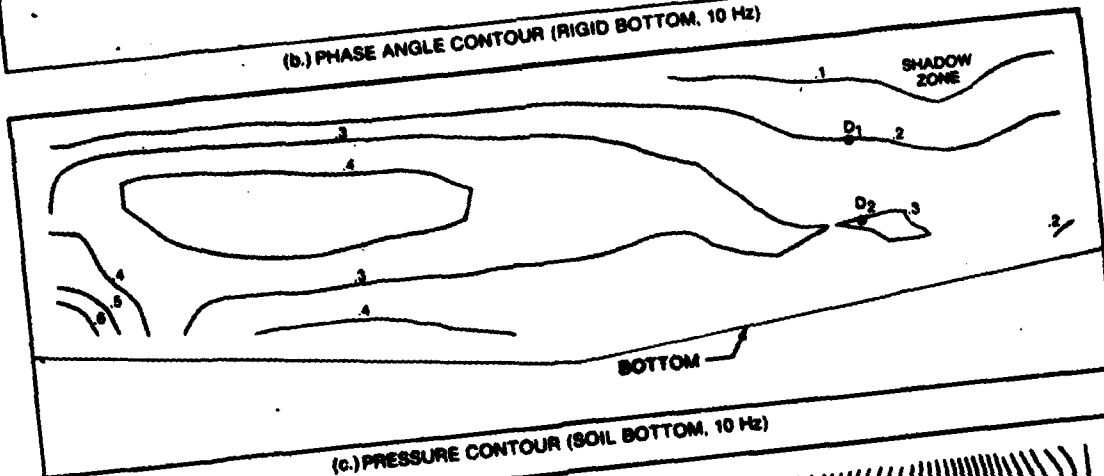
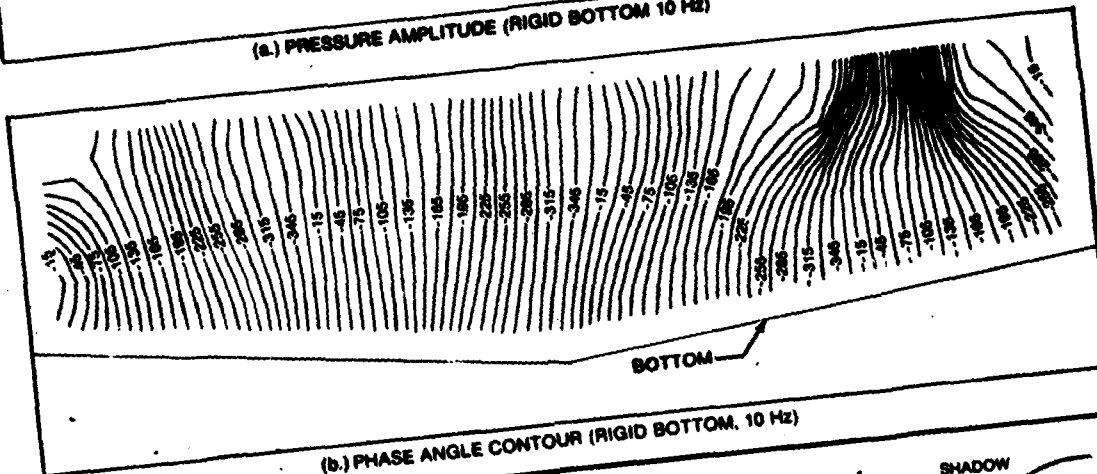
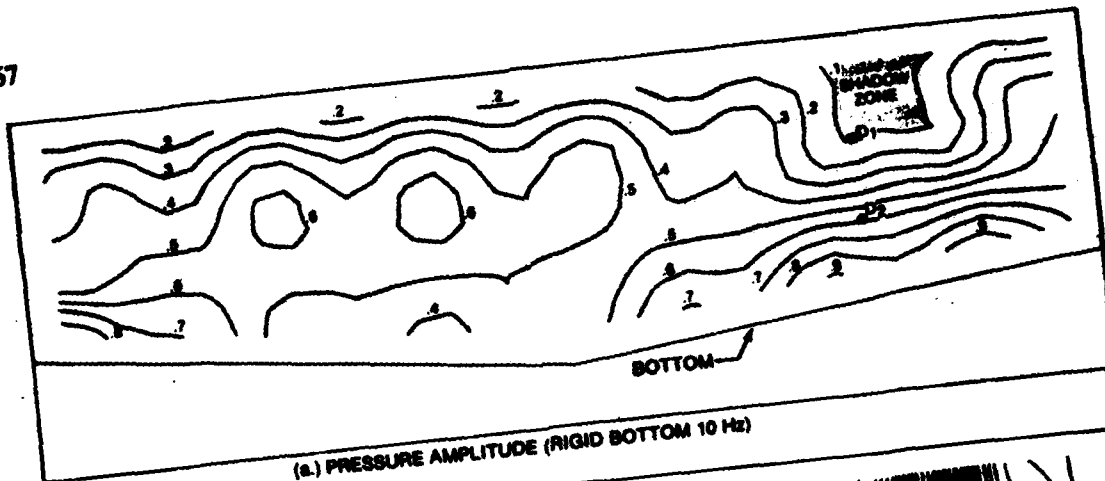


Figure 21. Finite Element Amplitude-Phase Contours

FLUID-FINITE ELEMENTS

The solid finite elements are well established and are treated in sufficient detail elsewhere.^{99,101,137} Conversely, the fluid elements deserve additional discussion in that the interface of solid and fluid elements require a certain degree of care. For the class of FEM problems which explicitly model the fluid, three approaches are used: (1) the pressure formulation for the fluid domain wherein there is one scalar (pressure) per discrete point in the FEM mesh;^{129,137,138} (2) the displacement formulation in which there are M unknowns per grid point, where M corresponds to the number of independent spatial coordinates (1, 2, or 3) needed to describe the response;^{105, 139-141} and (3) the mixed formulation where both pressure and the displacement vector (or equivalently by velocity potential ϕ and its divergence $\nabla \cdot \phi$) are taken as the problem unknowns.^{142,143} The displacement and pressure formulations have certain advantages over each other which are discussed in detail in^{91,144}.

Appendix A

SPECIAL CASES FOR $G(z, z_s)$ NOT CONSIDERED BY EQUATION (36)

Explicit results for the depth dependent Green's function are given for the case in which either the source or receiver is in the zero or N^{th} half space. These results are derived in the same manner used to obtain equation (36). However, that result does not reduce to the equations below because of an indexing inconsistency. In each case, it is assumed that $z > z_s$.

Case 1: $LS = 0, 1 < LR < N - 1$

$$G(z, z_s) = \left(\frac{e^{-i\beta_0 z_s}}{\beta_0} \right) \frac{[z_{LR+1}^{LR+1} Q_{LR}(d, b) + P_{LR}(d, b)]}{(z_1^1 - \bar{z}_0^1) / (i\omega\rho_0)} z_N^{LR} \Delta_{LS+1}^{LR} \quad (\text{A-1})$$

Case 2: $1 < LS < N - 2, LR = N$

$$G(z, z_s) = \frac{[\bar{z}_{LS}^{LS+1} Q_{LS}(e, b) + P_{LS}(e, b)] e^{i\beta_N(z-z_N)}}{(z_{LS+1}^{LS+1} - \bar{z}_{LS}^{LS+1})} z_N^N \Delta_{LS+1}^{N-1} \quad (\text{A-2})$$

Case 2a: $LS = N - 1, LR = N$

$$G(z, z_s) = \frac{[\bar{z}_{LS}^{LS+1} Q_{LS}(e, b) + P_{LS}(e, b)] e^{i\beta_N(z-z_N)}}{(z_N^N - \bar{z}_{N-1}^N)} z_N^N \quad (\text{A-3})$$

Case 3: $LS = 0, LR = N, (N > 1)$

$$G(z, z_s) = \left(\frac{e^{-i\beta_0 z_s}}{\beta_0} \right) \frac{e^{i\beta_N(z-z_N)}}{(z_1^1 - \bar{z}_0^1) / (i\omega\rho_0)} z_N^N \Delta_{LS+1}^{N-1} \quad (\text{A-4})$$

Case 4: $LS = LR = 0$

$$G(z, z_s) = \left(\frac{e^{-i\beta_0 z_s}}{\beta_0} \right) \frac{[z_1^1 \cos(\beta_0 z) - i\bar{z}_1^1 \sin(\beta_0 z)]}{(z_1^1 - \bar{z}_1^1) / (i\omega_0)} \quad (A-5)$$

Case 5: $LS = LR = N$

$$G(z, z_s) = \frac{[z_{N-1}^N \cos \beta_N (z_s - z_N) + i z_N^N \sin \beta_N (z_s - z_N)]}{(z_N^N - \bar{z}_{N-1}^N) / (i\omega_0)} \left(\frac{e^{i\beta_N (z - z_N)}}{\beta_N} \right), \quad (A-6)$$

where $d = r_{LS}^z$, $e = r_{LS}^s$, and $b = r_{LS}^{s+1}$.

Appendix B

AN ALTERNATIVE NUMERICAL EVALUATION SCHEME FOR BESSEL TRANSFORMS

The observation that the Fast Fourier Transform (FFT) algorithm could be used to evaluate Bessel transforms was first made by H. W. Marsh in 1967. The utilization of this approach requires that the Hankel function be replaced by its large argument (ξr) asymptotic expansion. Small values of r correspond to close proximity to the source. Small values of ξ may result from either a very low frequency or angles which are close to 90° as measured from the horizontal.

Recently, Tsang²¹ et al., evidently unaware of the work of Marsh, have proposed a different scheme for the evaluation of Bessel transforms which also utilizes the FFT algorithm. Their approach has the advantage of being exact for all values of ξr . Its major disadvantage is that it requires considerably more execution time if results are desired for more than one value of horizontal range. Their approach is used in this appendix to obtain results for the pressure field for small values of ξr which are then compared with Fast Field Program (FFP) answers.

First we summarize the Tsang approach. The Bessel transform for the pressure field is

$$\varphi(r, z_s, z) = \frac{S \omega}{2\pi} \int_0^{\infty} G(z, z_s; \xi) J_0(\xi r) \xi d\xi, \quad (B-1)$$

which is recast into the equivalent form,

$$\varphi(r, z_s, z) = \frac{S \omega}{2\pi} \int_0^{\infty} G(z, z_s; \xi) e^{-v\xi} J_0(\xi r) \xi d\xi,$$

where

$$G(z, z_s; \xi) = G(z, z_s; \xi) e^{v\xi}$$

and v is a theoretically arbitrary constant except for the restriction that $\text{Re}(v) > 0$. Next the Fourier Integral Transform pairs are introduced:

$$A(z, z_s; \lambda) = \int_{-\infty}^{\infty} G(z, z_s; \xi) e^{-12\pi\lambda\xi} d\xi \quad (B-2)$$

$$G(z, z_s; \xi) = \int_{-\infty}^{\infty} A(z, z_s; \lambda) e^{12\pi\xi\lambda} d\lambda .$$

Then the solution for the pressure field is

$$\varphi(r, z, z_s) = \int_{-\infty}^{\infty} A(z, z_s; \lambda) I(v, \lambda, r) d\lambda , \quad (B-3)$$

where

$$I(v, \lambda, r) = \int_0^{\infty} e^{-(v-12\pi\lambda)\xi} J_0(\xi r) \xi d\xi = \frac{(v-12\pi\lambda)}{[(v-12\pi\lambda)^2 + r^2]^{3/2}} .$$

Evaluation of equation (B-3) at the discrete points $\lambda_n = n \Delta\lambda$ yields

$$\varphi(r, z, z_s) = \Delta\lambda \sum_{n=-L/2}^{L/2} A(n\Delta\lambda) I(v, n\Delta\lambda, r) ,$$

where it has been tacitly assumed that contribution from the integrals corresponding to values of $|n| > L/2$ can be safely neglected. Assuming that $A(n\Delta\lambda)$ will be found from an FFT evaluation of equation (B-1), the pressure field may be written as

$$\begin{aligned} \varphi(r, z, z_s) \approx & \Delta\lambda A(0) \frac{v}{(v^2 + r^2)^{3/2}} + A \frac{L\Delta\lambda}{2} \frac{(v + i\pi L\Delta\lambda)}{(v + i\pi L\Delta\lambda)^2 + r^2} \quad (B-4) \\ & + \Delta\lambda \sum_{n=1}^{L/2-1} \left\{ A(n\Delta\lambda) I(v, r, n\Delta\lambda) + A(\sqrt{L-n^1}\Delta\lambda) I^*(v, r, n\Delta\lambda) \right\} , \end{aligned}$$

where the asterisk denotes the complex conjugate.

The above equation is valid for any r , but for each different r the equation must be recalculated.

LIST OF REFERENCES

1. J. E. Freehafer, "Physical Optics," *Propagation of Short Radio Waves*, D. E. Kerr, ed., McGraw-Hill Book Co., Inc., NY, 1951, vol. 13, MIT Rad. Lab. Ser., pp. 58-70.
2. L. B. Felsen and N. Marcuvitz, *Radiation and Scattering of Waves*, Prentice-Hall, Inc., Englewood Cliffs, NJ, 1973.
3. L. M. Brekhovskikh, *Waves in Layered Media*, Academic Press, Inc., NY, 1960.
4. I. Tolstoy, *Wave Propagation*, McGraw-Hill Book Co., Inc., NY, 1973.
5. J. R. Wait, *Electromagnetic Waves in Stratified Media*, Pergamon Press, Oxford, 1970.
6. D. G. Harkrider, "Theoretical and Observed Acoustic-Gravity Waves from Explosive Sources in the Atmosphere," *Journal of Geophysical Research*, vol. 69, 1964, pp. 5295-5321.
7. H. W. Kutschale, *Further Investigation of the Integral Solution of the Sound Field in Multilayered Media: A Liquid-Solid Half Space with a Solid Bottom*, Lamont-Doherty Geological Observatory of Columbia University, Technical Report Number CU-6-71, Palisades, NY, March 1972.
8. P. M. Morse and K. U. Ingard, *Theoretical Acoustics*, McGraw-Hill Book Co., Inc., NY, 1968, pp. 309-312.
9. H. Lamb, "On the Propagation of Tremors Over the Surface of an Elastic Solid," *Philosophical Transactions of the Royal Society*, London, vol. A203, 1904, pp. 1-42.
10. A. Sommerfeld, "Über die Ausbreitung der Wellen in der Drahtlosen Telegraphie," *Annalen der Physik*, vol. 28, 1909, pp. 665-736.
11. N. Marcuvitz, "Field Representations in Spherically Stratified Regions," *Communications on Pure and Applied Mathematics*, vol. 4, 1951, pp. 263-315.
12. H. F. Baker, "On the Integration of Linear Differential Equations," *Proceedings of the London Mathematical Society*, Series 1, vol. 35, 1902, pp. 333-378.
13. R. A. Frazer, W. J. Duncan, and A. R. Collar, *Elementary Matrices*, Cambridge University Press, London, 1960.
14. F. R. Gantmacher, *The Theory of Matrices*, Chelsea Publishing Company, NY, vol. 2, 1959, pp. 125-171.
15. F. Gilbert and G. E. Backus, "Propagator Matrices in Elastic Wave and Vibration Problems," *Geophysics*, vol. 31, 1966, pp. 326-332.
16. E. A. Coddington and N. Levinson, *Theory of Ordinary Differential Equations*, McGraw-Hill Book Co., Inc., NY, 1955.
17. H. W. Marsh and S. R. Elam, Internal Document, Raytheon Company, Marine Research Laboratory, New London, CT, 1967.

18. F. R. DiNapoli, *A Fast Field Program for Multilayered Media*, NUSC Technical Report 4103, Naval Underwater Systems Center, New London, CT, 1971.
19. F. R. DiNapoli and M. R. Powers, "Recursive Calculation of Products of Cylindrical Functions," NUSC Technical Memorandum No. PA-83-70, Naval Underwater Systems Center, New London, CT, 1970.
20. F. R. DiNapoli, "The Collapsed Fast Field Program (FFP)," NUSC Technical Memorandum No. TA11-317-72, Naval Underwater Systems Center, New London, CT, 1972.
21. L. Tsang, R. Brown, J. A. Kong, and G. Simmons, "Numerical Evaluation of Electromagnetic Fields Due to Dipole Antennas in the Presence of Stratified Media," *Journal of Geophysical Research*, vol. 79, 1974, pp. 2077-2080.
22. C. L. Pekeris, *Theory of Propagation of Explosive Sound in Shallow Water*, The Geological Society of America, Memoir 27, 1948.
23. H. W. Kutschale, *Rapid Computation by Wave Theory of Propagation Loss in the Arctic Ocean*, Lamont-Doherty Geological Observations of Columbia University Technical Report No. CU-8-73, 1973.
24. D. C. Stickler, "Normal-Mode Program with Both the Discrete and Branch Line Contributions," *Journal of the Acoustical Society of America*, vol. 57, 1975, pp. 856-861.
25. W. M. Ewing, W. S. Jardetzky, and F. Press, *Elastic Waves in Layered Media*, McGraw-Hill Book Co., Inc., NY, 1957.
26. C. L. Bartberger, "AP2 Normal Mode Program," Naval Air Development Center Report, Warminster, PA, in preparation, 1978.
27. I. Tolstoy, "Resonant Frequencies and High Modes in Layered Wave Guides," *Journal of the Acoustical Society of America*, vol. 28, 1956, pp. 1182-1192.
28. S. A. Schelkunoff, "Remarks Concerning Wave Propagation in Stratified Media," *Communications on Pure and Applied Mathematics*, vol. 4, 1951, pp. 117-128.
29. L. M. Brekhovskikh, *Waves in Layered Media*, Academic Press, Inc., NY, 1960, pp. 229-230.
30. F. W. Sluijter, "Arbitrariness of Dividing the Total Field in an Optically Inhomogeneous Medium Into Direct and Reversed Waves," *Journal of the Optical Society of America*, vol. 60, 1970, pp. 8-10.
31. J. R. Wait, "Comments on: On the Reflection Coefficient of a Plasma Profile of Exponentially Tapered Electron Density and Fixed Collision Frequency," *Institute of Electrical and Electronic Engineers Transactions on Antennas and Propagation*, vol. AP 18, 1970, pp. 297-298.
32. B. L. N. Kennett, "Reflections, Rays, and Reverberations," *Bulletin of the Seismological Society of America*, vol. 64, 1974, pp. 1685-1696.
33. F. W. Sluijter, "Generalizations of the Bremmer Series Based on Physical Concepts," *Journal of Mathematical Analysis and Applications*, vol. 27, 1969, pp. 282-302.

34. S. R. Santaniello, F. R. DiNapoli, R. K. Dullea, and P. Herstein, *A Synopsis of Studies on the Interaction of Low Frequency Acoustic Signals with the Ocean Bottom*, NUSC Technical Document 5337, Naval Underwater Systems Center, New London, CT, 1976.
35. O. M. Johannessen and L. E. Mellberg, *Layered Oceanic Microstructure, Its Effects on Sound Propagation*, NATO SACLANTCEN Technical Report 206, La Spezia, Italy, 1972.
36. P. Debye, "Das Elektromagnetische Feld um Einen Zylinder und die Theorie des Regenbogen," *Physikalische Zeitschrift*, vol. 9, 1908, pp. 775-778.
37. B. Van der Pol and H. Bremmer, "The Diffraction of Electromagnetic Waves From an Electrical Point Source Round a Finitely Conducting Sphere, With Application to Radiotelegraphy and the Theory of the Rainbow," *Philosophical Magazine*, vol. 24, 1937, pp. 825-863. (Also, H. Bremmer, *Terrestrial Radio Waves*, Elsevier Publishing Company, Amsterdam, NY, 1949, Chapters 8 and 9.)
38. J. R. Wait, "A Diffraction Theory for LF Sky-Wave Propagation," *Journal of Geophysical Research*, vol. 66, 1961, pp. 1713-1730.
39. D. V. Batorsky and L. B. Felsen, "Ray-Optical Calculation of Modes Excited by Sources and Scatterers in a Weakly Inhomogeneous Duct," *Radio Science*, vol. 6, 1971, pp. 911-923.
40. O. E. H. Rydbeck, "On the Propagation of Radio Waves," *Transactions of the Chalmers University of Technology*, vol. 34, 1944.
41. G. Gonzalez and L. A. Berry, "On the Saddle Point Evaluation of LF/VLF Path Integrals for a Vertical Electric Dipole," *Canadian Journal of Physics*, vol. 55, 1977, pp. 1092-1101.
42. L. A. Berry and M. E. Chrisman, "The Path Integral of LF/VLF Wave Hop Theory," *Radio Science*, vol. 69 D, 1965, pp. 1469-1480.
43. C. H. Chapman and R. A. Phinney, "Diffracted Seismic Signals and Their Numerical Solution," *Methods in Computational Physics*, B. A. Bolt, ed., vol. 12, Academic Press, NY, 1972, pp. 165-230.
44. C. H. Chapman, "Exact and Approximate Generalized Ray Theory in Vertically Inhomogeneous Media," *Geophysical Journal of the Royal Astronomical Society*, vol. 46, 1976, pp. 201-233.
45. H. Weinberg, "Application of Ray Theory to Acoustic Propagation in Horizontally Stratified Oceans," *Journal of the Acoustical Society of America*, vol. 58, 1975, pp. 97-109.
46. C. W. Spofford, *The FACT Model*, Maury Center for Ocean Science, Technical Report 109, Washington DC, 1974.
47. G. A. Leibiger, "Wave Propagation in an Inhomogeneous Medium With Slow Spatial Variation," Ph.D. Dissertation, Stevens Institute of Technology, Castle Point, Hoboken, N.J., 1968.
48. G. A. Leibiger, *The Acoustic Propagation Model RAYMODE: Theory and Numerical Treatment*, NUSC Technical Report, Naval Underwater Systems Center, New London, CT, in preparation.

49. M. A. Pederson and D. F. Gordon, "Normal Mode and Ray Theory Applied to Underwater Acoustic Conditions of Extreme Downward Refraction," *Journal of the Acoustical Society of America*, vol. 51, 1972, pp. 323-368.
50. C. Bartberger, *Normal Mode Solutions and Computer Programs for Underwater Sound Propagation*, Naval Air Development Center, Technical Report NADC-72002-AE, Warminster, PA, 1977.
51. E. C. Titchmarsh, *Introduction to the Theory of Fourier Integrals*, 2nd edition, Oxford University Press, Oxford, 1948.
52. H. Bremmer, *Terrestrial Radio Waves*, Elsevier Publishing Company, Amsterdam, NY, 1949.
53. H. M. Nussenzweig, "High-Frequency Scattering by an Inpenetrable Sphere," *Annals of Physics (NY)*, vol. 34, 1965, pp. 23-95.
54. F. Gilbert, "The Representation of Seismic Displacements in Terms of Travelling Waves," *Geophysical Journal of the Royal Astronomical Society*, vol. 44, 1976, pp. 275-280.
55. A. Ben-Menahem, "Mode-Ray Duality," *Bulletin of the Seismological Society of America*, vol. 54, 1964, pp. 1315-1321.
56. C. L. Pekeris, *Proceedings of the Symposium on Applied Mathematics*, American Mathematical Society, vol. 2, NY, 1950, pp. 71-75.
57. D. S. Ahluwalia and J. B. Keller, "Exact and Asymptotic Representations of the Sound Field in a Stratified Ocean," *Wave Propagation and Underwater Acoustics*, J. B. Keller and J. S. Papadakis, eds., Lecture Notes in Physics, vol. 70, Springer, Berlin, Heidelberg, New York, 1977.
58. N. A. Haskell, *Diffraction Effects in the Propagation of Compressional Waves in the Atmosphere*, Geophysical Research Papers No. 3, Air Force Cambridge Research Laboratories, Cambridge, MA, March 1950. Also, "Asymptotic Approximation for the Normal Modes in Sound Channel Wave Propagation," *Journal of Applied Physics*, vol. 22, 1951, pp. 157-168.
59. L. M. Brekhovskikh, "Focusing of Acoustic Waves by Means of Inhomogeneous Media," *Soviet Physics Acoustics*, vol. 2, 1956, pp. 124-133. (See also reference 3.)
60. R. B. Lauer and B. Sussman, *A Methodology for the Comparison of Models for Sonar System Applications*, vol. 1, Naval Sea Systems Command Technical Report SEA 06H1/036-EVA/MOST-10, 1976.
61. R. B. Lauer and B. Sussman, *A Methodology for the Comparison of Models for Sonar System Applications-Results for Low Frequency Propagation Loss in the Mediterranean Sea*, vol. II, Naval Sea Systems Command Technical Report SEA 06H1/036-EVA/MOST-11, in preparation.
62. D. F. Yarger, "The User's Guide for the Raymode Propagation Loss Program," NUSC Technical Memorandum 222-10-76, Naval Underwater Systems Center, New London, CT, 1976.
63. C. L. Bartberger, *PLRAY, A Ray Propagation Loss Program*, Naval Air Development Center Technical Report, Warminster, PA, in preparation.
64. D. F. Gordon, *Underwater Sound Propagation-Loss Program*, Ocean Systems Center, San Diego, CA, 17 May 1979.

65. D. W. Hoffman, *LORA, A Model for Predicting the Performance of Long-Range Active Sonar Systems*, Naval Undersea Center Technical Publication 541, San Diego, CA, 1976.
66. W. H. Watson and R. McGirr, "Raywave-II, A Propagation Loss Model for the Analysis of Complex Ocean Environments," Naval Undersea Center Technical Note 1516, San Diego, CA, 1975.
67. E. B. Wright, *Acoustic Transmission Loss by Single-Profile Ray Tracing, Program RTRACE*, Naval Research Laboratory Technical Report 7815, 1974.
68. I. M. Blatstein, *Comparisons of Normal Mode Theory, Ray Theory, and Modified Ray Theory for Arbitrary Sound Velocity Profiles Resulting in Convergence Zones*, Naval Ordnance Laboratory Technical Report 74-95, White Oak, Silver Spring, MD, 1974.
69. H. Weinberg, "A Continuous-Gradient Curve Fitting Technique for Acoustic-Ray Analysis," *Journal of the Acoustical Society of America*, vol. 50, 1971, pp. 975-984.
70. R. P. Porter and H. D. Leslie, "Energy Evaluation of Wide-Band SOFAR Transmission," *Journal of the Acoustical Society of America*, vol. 58, 1975, pp. 812-822.
71. F. R. DiNapoli, "The Inverse Fast Field Program (IFFP): An Application to the Determination of the Acoustic Parameters of the Ocean Bottom," NUSC Technical Memorandum 771160, Naval Underwater Systems Center, New London, CT, 1977.
72. H. W. Kutschale and F. R. DiNapoli, "Pulse Propagation in the Ocean, I: The Fast Field Program Method," *Journal of the Acoustical Society of America*, Fall Supplement 1, S18, vol. 62, 1977.
73. H. W. Kutschale and F. D. Tappert, "Pulse Propagation in the Ocean II: The Parabolic Equation Method," *Journal of the Acoustical Society of America*, Fall Supplement, S18, vol. 62, 1977.
74. F. D. Tappert, "The Parabolic Approximation Method," *Lecture Notes in Physics*, vol. 70, J. B. Keller and J. S. Papadakis, eds., Springer, Berlin, Heidelberg, New York, 1977.
75. J. A. DeSanto, "Theoretical Methods in Underwater Acoustics," *Topics in Current Physics, Underwater Acoustics*, J. A. DeSanto, ed., Springer-Verlag, Berlin, Heidelberg, New York, 1978.
76. R. H. Hardin and F. D. Tappert, "Applications of the Split-Step Fourier Method to the Numerical Solution of Nonlinear and Variable Coefficient Wave Equations," *Society for Industrial and Applied Mathematics Review*, vol. 15, 1973, p. 423.
77. F. D. Tappert and R. H. Hardin, "Computer Simulation of Long-Range Ocean Acoustic Propagation Using the Parabolic Equation Method," *Proceedings of the Eighth International Congress on Acoustics*, Goldcrest, London, vol. 2, 1974, p. 452.
78. R. M. Wilcox, "Exponential Operators and Parameter Differentiation in Quantum Physics," *Journal of Mathematical Physics*, vol. 8, 1967, pp. 962-982.
79. F. Jensen and H. Krol, *The Use of the Parabolic Equation Method in Sound Propagation Modeling*, NATO SAACLANTCEN Technical Report Sm 72, La Spezia, Italy, 1975.
80. J. S. Papadakis and D. Wood, *A Parabolic Decomposition of Helmholtz Equation*, NUSC Technical Report, Naval Underwater Systems Center, New London, CT, in preparation.

81. M. C. Smith, "Underwater Acoustic Propagation Prediction by the Alternating-Direction Implicit-Explicit Computational Method," *Journal of the Acoustical Society of America*, vol. 46, 1969, pp. 233-237.
82. S. T. McDaniel, "Parabolic Approximations for Underwater Sound Propagation," *Journal of the Acoustical Society of America*, vol. 58, 1975, pp. 1178-1185.
83. D. Lee and J. S. Papadakis, *Numerical Solutions of Underwater Acoustic Wave Propagation Problems*, NUSC Technical Report, Naval Underwater Systems Center, New London, CT, in preparation.
84. D. Lee, "Nonlinear Multistep Methods for Solving Initial Value Problems in Ordinary Differential Equations," Ph.D. Dissertation, Polytechnic Institute of New York, 1977.
85. P. Henrici, *Discrete Variable Methods in Ordinary Differential Equations*, John Wiley and Sons, Inc., NY, 1962.
86. W. G. Kanabis, *A Shallow Water Acoustic Model for an Ocean Stratified in Range and Depth*, NUSC Technical Report 4887-1, Naval Underwater Systems Center, New London, CT, 1975.
87. W. G. Kanabis, *Computer Programs to Calculate Normal Mode Propagation and Applications to Analysis of Explosive Sound Data in the BIFI Range*, NUSC Technical Report 4319, Naval Underwater Systems Center, New London, CT, 1972.
88. C. W. Spofford and H. M. Garon, "Deterministic Methods of Sound-Field Computation" the *Proceedings of the NATO Conference on Oceanic Acoustic Modeling*, W. Bachmann and R. B. Williams, eds., SACLANTCEN, La Spezia, Italy, 1975, pp. 40-1 to 40-43.
89. J. J. Cornyn, *Grass, A Digital-Computer Ray-Tracing and Transmission Loss-Prediction System*, NRL Report 7621, vol. I, Naval Research Laboratory, 1973.
90. H. P. Bucker, "The RAVE (Ray Wave) Method," the *Proceedings of the NATO Conference on Geometrical Acoustics*, B. W. Conolly and R. H. Clark, eds., SACLANTCEN, La Spezia, Italy, 1971, pp. 32-36.
91. A. J. Kalinowski, *The Shock and Vibration Digest*, vols. 10 and 11, 1978.
92. M. J. Turner, R. W. Clough, H. C. Martin, and L. J. Topp, *Journal of Aeronautical Science*, vol. 23, 1956.
93. J. T. Oden, *Finite Elements of Nonlinear Continuum*, McGraw-Hill Book Co., Inc., NY, 1972.
94. O. C. Zienkiewicz and Y. K. Cheung, "Finite Elements in the Solution of Field Problems," *The Engineer*, September 1965.
95. R. H. Gallagher, J. T. Oden, C. Taylor, and O. C. Zienkiewicz, *Finite Elements in Fluids - Vol. 1, Viscous Flow and Hydrodynamics*, John Wiley and Sons, Inc., NY, 1975.
96. R. H. Gallagher, J. T. Oden, C. Taylor, and O. C. Zienkiewicz, *Finite Elements in Fluids - Vol. 2, Mathematical Foundations, Aerodynamics and Lubrication*, John Wiley and Sons, Inc., NY, 1975.
97. J. T. Oden, O. C. Zienkiewicz, R. H. Gallagher, and C. Taylor, *Finite Element Methods in Flow Problems*, University of Alabama Huntsville Press, Huntsville, AL, 1974.

98. O. C. Zienkiewicz and Y. K. Cheung, *The Finite Element Method in Structural and Continuum Mechanics*, McGraw-Hill Book Co., Inc., NY, 1967.
99. L. J. Segerlend, *Applied Finite Element Analysis*, John Wiley and Sons, Inc., NY, 1976.
100. K. H. Huebner, *The Finite Element Method for Engineers*, John Wiley and Sons, Inc., NY, 1975.
101. R. D. Cook, *Concepts and Applications of Finite Element Analysis*, John Wiley and Sons, Inc., NY, 1974.
102. J. T. Oden and J. N. Reddy, *An Introduction to the Mathematical Theory of Finite Elements*, John Wiley and Sons, Inc., NY, 1976.
103. G. Strang, G. Fix, *An Analysis of the Finite Element Method*, Prentice-Hall, Inc., Englewood Cliffs, NJ, 1973.
104. D. Norrie and Gerard de Vries, *Finite Element Bibliography*, IFI/Plenum Data Company, NY, 1976.
105. A. J. Kalinowski, "Fluid-Structure Interaction," in *Shock and Vibration Computer Programs, Review and Summaries*, Pilkey and Pilkey, eds., SVM-10, The Shock and Vibration Information Center, 1975.
106. L. H. Chen and Pierucci, "Underwater Fluid-Structure Interaction Parts I and II," *The Shock and Vibration Digest*, April-May 1977.
107. R. L. Kuhlmeyer and J. Lysmer, *Journal of Soil Mech. Found Div.*, ASCE, 1972.
108. J. Lysmer and R. L. Kuhlmeyer, Proceedings Paper 6719, *Journal of Engr. Mech. Div.*, ASCE, 95, no. EM4, August 1969.
109. J. Lysmer and L. Drake, "A Finite Element Method for Seismology," *Methods in Computational Physics*, B. Bolt, ed., Academic Press, NY, 1972.
110. J. A. Gutierrez, *A Substructure Method for Earthquake Analysis of Structure-Soil Interaction*, Earthquake Engineering Research Center Report No. 76-9, April 1976.
111. J. Lysmer, *Bulletin of the Seismological Society of America*, vol. 60, no. 1, 1970.
112. J. Lysmer and G. Waas, *Journal of the Eng. Mech. Div.*, ASCE, February 1972.
113. E. Kausel, J. Roesset, G. Waas, *Journal of the Eng. Mech. Div.*, ASCE, October 1975.
114. E. Kausel and J. Roesset, *Journal of the Eng. Mech. Div.*, ASCE, August 1977.
115. P. Chakrabarti and A. K. Chopru, *Earthquake Engineering and Structural Dynamics*, vol. 2, 1973.
116. G. J. Fix and S. P. Marin, *Variational Method for Underwater Acoustics Problems*, ICASE Report 77-16, August 1977.

117. G. W. Platzman, *J. Physical Oceanography*, vol. 8, 1978, pp. 323-343.
118. *The NASTRAN User's Manual*, National Aeronautics and Space Administration SP-222(03), March 1976.
119. O. C. Zienkiewicz, D. W. Kelly, and P. Bettess, *International Journal for Numerical Methods in Engineering*, vol. II, 1977.
120. C. D. Mote, Jr., *International Journal for Numerical Methods in Engineering*, vol. 3, 1971.
121. E. A. Rukos, *International Journal for Numerical Methods in Engineering*, vol. 12, 1978.
122. M. Petyt, J. Lea, and Koopmann, *Journal of Sound and Vibration*, vol. 45, April 1976.
123. G. J. Fix and M. H. Gunzburger, *On the Use of Modern Numerical Methods in Acoustics*, ICASE Report (undated).
124. A. J. Kalinowski, *Shock and Vibration Bulletin*, vol. 48, 1977.
125. A. J. Kalinowski, *Application of the Finite Element Method to Acoustic Propagation in the Ocean*, NUSC Technical Report 5891, Naval Underwater Systems Center, New London, CT, 1978.
126. R. Dungar and P. J. L. Eledred, *Earthquake Engineering and Structural Dynamics*, vol. 6, 1978, pp. 123-138.
127. J. M. Rosset and M. M. Ettouney, *International Journal for Numerical and Analytical Methods in Geomechanics*, vol. 1, 1977.
128. R. Kuhlemeyer, "Vertical Vibrations of Footings Embedded in Layered Media," Ph.D. Dissertation, University of California, Berkeley, 1969.
129. O. C. Zienkiewicz and R. E. Newton, "Coupled Vibrations of a Structure Submerged in a Compressible Fluid," *Proceedings of the International Symposium on Finite Element Techniques*, Stuttgart, Germany, 1969.
130. P. Bettess and O. C. Zienkiewicz, *International Journal for Numerical Methods in Engineering*, vol. 11, 1977.
131. P. Bettess, *International Journal for Numerical Methods in Engineering*, vol. 11, 1977.
132. O. C. Zienkiewicz and P. Bettess, *2nd International Symposium on Computing Methods in Applied Science and Engineering*, Versailles, France, 1975.
133. B. Engquist and A. Majda, *Mathematical of Computation*, vol. 31, no. 139, July 1977.
134. J. T. Hunt, M. Knittel, C. S. Nichols, and D. Barach, *Journal of the Acoustical Society of America*, vol. 55, no. 2, February 1974.
135. J. T. Hunt, M. P. Knittel, and D. Barach, *Journal of the Acoustical Society of America*, vol. 55, no. 2, February 1974.

136. H. A. Schenck, *Journal of the Acoustical Society of America*, vol. 44, 1967.
137. O. C. Zienkiewicz, *The Finite Element Method in Engineering Science*, McGraw-Hill Book Co., Inc., London, 1971.
138. G. C. Everstine, E. M. Schroeder, and M. S. Marcus, "The Dynamic Analysis of Submerged Structures," *4th NASTRAN User's Colloquium*, Langley Research Center, 1975.
139. D. Shantaran, D. R. J. Owen, and O. C. Zienkiewicz, *Earthquake Engineering and Structural Dynamics*, vol. 4, 1976.
140. E. P. Sorensen, and D. V. Marcal, *A Solid Mechanics Approach to the Solution of Fluid-Solid Vibration Problems by Finite Elements*, Brown University Technical Report N00014-0007/13, May 1976.
141. L. Kiefling and G. C. Feng, *AIAA Journal*, vol. 14, February 1976.
142. G. J. Fix, M. D. Gunzburger, and R. A. Nicolaides, *On Mixed Finite Element Methods, I. The Kelvin Principle*, ICASE Report, December 1977.
143. G. J. Fix, M. D. Gunzburger, and R. A. Nicolaides, *On Mixed Finite Element Methods, II. The Least Squares Method*, ICASE Report 77-18, December 1977.
144. A. J. Kalinowski, "Transmission of Shock Waves Into Submerged Fluid Vessels," *Fluid Structure Interaction Phenomena in Pressure Vessel and Piping Systems*, by M. Wang and S. J. Brown, eds., ASME, NY.

INITIAL DISTRIBUTION LIST

Addressee	No. of Copies
COMSUBLANT	1
COMSUBPAC	1
COMSUBDEVRON 12	1
ASN (RE&S) (D. E. Mann)	1
OUSDR&E (W. J. Perry)	2
OASN (M. G. Cann, Dr. R. Høglund)	2
ONR, ONR-100, -102, -461 (Dr. L. Johnson), -480, -483 (Dr. M. Odegard)	9
-485, -222, -230, -486	9
CNO, OP-02, -090, -095, -098, -951, 951E, -952, -955, -96, -981	10
CNM, MAT-08T, -08T1, -08T2, -08T24, ASW-122, -10, -23, Special Projects	9
Office (PM-2) Trident, MAT-0801	9
NAV SURFACE WEAPONS CENTER, WHITE OAK LABORATORY (I. Blastein)	1
NRL (J. Desanto, F. Ingenito, O. I. Diachak, N. Rosenberg), Code 2625 (Library)	5
NORDA, 110 (Dr. R. Goodman), 320 (A. Anderson)	2
USOC, Codes 241, 240, 320, 340	4
SUBASE LANT	1
NAVOCEANO, Code 02	1
NAVELECSYSCOM, ELEX 00, PME-124 (CAPT H. Cox), ELEX 320	3
NAVSEASYSYSCOM, SEA-003, -06H14 (A. Francheschetti), -61R, -62R, -63R, -63R13, -63X, -631X, -631Y, -63R-2, 63R-23	11
NAVAIRDEVCCEN (C. Bartberger)	1
NOSC, Codes 573 (H. Bucker), 503 (D. Gordon, M. Pederson), 308 (J. Stewart)	4
NAVCOASTSYSLAB	1
NSRDC, Bethesda, Code 934 (D. Feit, B. Vogel)	2
SACLANT ASW RESEARCH CENTER (F. Jensen, W. Kuperman)	2
NAVPGSCOL	1
APL/UW, SEATTLE	1
ARL/PENN STATE, STATE COLLEGE (S. McDaniel)	1
DTIC	12
NATIONAL RESEARCH COUNCIL	1
WOODS HOLE OCEANOGRAPHIC INSTITUTION (G. Frisk, J. Ewing)	2
ENGINEERING SOCIETIES LIBRARY, UNITED ENGRING CTR	1
Asst. Dir. Land Resources, U.S. Geological Survey (J. Balsley)	1
Delft University of Technology, Physics Dept., Lorentzbug 1, Delft, The Netherlands (A. Berkant)	1
Forschungsanstalt der Bundeswehr, fuer Wasserschall-und Geophysik, Klausdorfer Weg 2-24, D-2300, Kiel 14 FRG (H. Schneider)	1
Weapons Research Establishment, Box 2151, G.P.O. Adelaide-5001, Australia (G. Gartrell)	1
Academy of Sciences of USSR, Leninskii, Prospect 14, Moscow 117071 (L. Brekhovskikh)	1
Defence Research Establishment Atlantic, P.O. Box 1012, Dartmouth, N.S. Canada B2Y3Z7 (H. Merlinger)	1
Defence Research Establishment Pacific, Victoria, B.C. VOSIBO, Canada, (D. Thomson)	1

INITIAL DISTRIBUTION LIST (Cont'd)

Addressee	No. of Copies
Southeastern Mass University, Electrical Engineering Dept., North Dartmouth, MA 02747 (G. Fain, L. Estes)	2
H. W. Marsh, Box 226, Penrose, NC 28766	1
Lamont-Doherty Geological Observatory, Palisades, NJ 07650 (H. Kutschale, P. Stoffa, R. Richards)	3
University of Denver, Dept. of Mathematics, Denver, CO 80210, (N. Bleistein)	1
Science Application Incorporated, McLean, VA 22101 (S. Spotford, D. Hanna)	2
ARL, Univ. of Texas, Austin, Texas 78712 (K. Hawker)	1
U. Miami, School of Marine & Atmospheric Sciences, 10 Rickenbacker Causeway, Miami, FL 33149 (F. Tappert)	1
EXXON Corporation, Houston, Texas 77001 (F. Levin)	1
AMOCO Production Company, P.O. Box 591, Tulsa, OK 74102 (J. Domenico)	1
N. Bojarski, Sixteen Pine Valley Lane, Newport Beach, CA 92660	1
TRACOR, Tracor Incorporated, 1601 Research Blvd. Rockville, MD 20850 (R. Urick)	1
University of Toronto, Dept. of Physics, Toronto, Ontario, Canada 1A7 (C. H. Chapman)	1
P. Stocklin, 25 Ledgewood Court, Norwich, CT 06360	1